Stepwise deprotonation-induced electronic state conversion in metal complexes

Ryo Saiki

February 2019

Stepwise deprotonation-induced electronic state conversion in metal complexes

Ryo Saiki

Doctoral Program in Nano-Science and Nano-Technology

Submitted to the Graduate School of
Pure and Applied Sciences
in Partial Fulfillment of the Requirements
for the Degree of Doctor of Philosophy in
Science

at the
University of Tsukuba

INDEX

CHAPTER 1 General Introduction
1.1 Aim of This Thesis…….....1
1.2 Bistable Molecules…….....2
1.2.1 Spin Crossover (SCO)…….....3
1.2.2 Electron-Transfer-Coupled Spin Transition (ETCST) ……...5
1.3 Multi-bistable Materials…….....6
1.4 Electronic State Conversions of Coordination Compounds by Protonation/deprotonation…….....8
1.5 Specific Physical Properties Based on Hydrogen Bonding Network….12
1.6 Contents……..14

CHAPTER 2 Effect of Ligand Modification in Iron Complexes
2.1 Introduction……19
2.2 Experiments……21
2.3 Results and Discussion……29
2,4 Conclusion……..42

CHAPTER 3 Electronic State Conversions of Iron Complexes with Brønsted Acid and Base
3.1 Introduction……45
3.2 Experiments……..47
3.3 Results and Discussion……53
3.4 Conclusion……..72

CHAPTER 4 An Antiferromagnetically Coupled Heterometal Cu_6Fe Wheel
4.1 Introduction……..……..75
4.2 Experiments……..……77
4.3 Results and Discussion……..……80
4.4 Conclusion……...88

CHAPTER 5 General conclusion.....91

List of Publications……92
Acknowledgement……93

CHAPTER 1

General Introduction

1.1 Aim of This Thesis

Development of chemical technology gives us a huge impact on our life. Chemistry makes new materials and we can't live in comfort without chemical products. The key scientific challenges of the 21st century are likely to lie in the areas of computational capacity, sustainable energy, human health, and global warming. Advances in chemistry will underpin the solutions to these problems. As the miniaturization of transistor and microchip technology approaches its limit, the concept of molecular electronics – that is, the development of molecules that can potentially be employed as the switchable components in information storage and calculation technologies – is proposed. On-off switching molecules have the potential to enhance the performance of computers by increasing the density of information storage, and thus are highly attractive materials, both from fundamental and applied perspectives. In reality, however, the integration of switchable molecules into addressable arrays is a major challenge, and remains a huge target in nanodevice fabrication. To solve these problems, metal complexes can be useful materials. Metal complexes are inorganic (metal ion) and organic (ligand) hybrid systems and the physical properties of metal ions can be changed by tuning the ligand design. In particular, transition metal complexes are a key target in molecular switch studies due to their cheapness, the abundance of first row transition metals, and their interesting and varied functions (control of magnetism, tuning of multi-redox and catalytic behavior). The potential combinations of metal ions and ligands are innumerable, and their structures and functionalities are probably equally so, making them exciting targets in both fundamental and applied research streams.

In the research field of nanoscience, next-generation intelligent molecular devices will rely on simple, nanoscale species that can exist in multiple distinct electronic states between which the molecule can be reversible interconverted under the application of external stimuli.[1] Switchable molecules such as bistable complexes that can exist in more than one state under identical conditions are excellent candidate systems for real life applications.[2] Obviously, flexible control of the electronic state of metal complexes is an important proposition in basic coordination chemistry. In accordance with these fundamental requirements, the purpose of this research is to employ a molecular design approach to the isolation of transition metal complexes that can exist in multiple stable electronic states. We will adopt ligands that can be reversibly protonated/deprotonated to

tune the local environment around the complexed transition metal ion, with the expectation that modification of the ligand protonation state will translate directly to the tuning of the electronic state of the transition metal ion. In this study, a novel ligand design strategy employing an asymmetric 'Brønsted ligand', which has acidic protons, can be used to isolate complexes with multiple independently accessible electronic states. According to this research purpose, two important factors were key: (1) the existence of acidic protons on the capping ligands; and (2) the use of iron ions that are known to form bistable (spin-crossover) systems, and can be relatively easily converted between oxidation states (Fe(II) and Fe(III)). Protonation/deprotonation of the ligand can directly affect the ligand field. Furthermore, iron ions can have various electronic states, such as divalent low-spin (S = 0), divalent high-spin (S = 2), trivalent low spin (S = 1/2) and trivalent high-spin (S = 5/2) in the octahedral hexa-coordinate geometry. This characteristic allows us to 'unlock' multiple electronic states in one molecule. Below is a more detailed explanation about the topics that underpin this research, including; bistable molecules (1.2), multi-bistable materials (1.3), electronic state conversion of complexes by protonation/deprotonation (1.4), and the manipulation of specific physical properties based on hydrogen bonding network (1.5).

1.2 Bistable Molecules

Bistable materials, which can be converted between two unique states by temperature, pressure, and light irradiation, have attracted continuous research interest due to their potential applications as components of future molecular memory and switching devices.[3]

Some organic molecules can exhibit changes in their molecular framework upon light irradiation, and when this conversion is reversible these systems can be considered examples of bistable materials. Representative molecules are diarylethene, spiropyran, and azobenzene. These molecules can be switched between open and closed frameworks (or *cis* and *trans*) by light. The transformation time is in the order of picoseconds, well within the timeframe form to be considered promising candidate components for future information processing or storage devices. Some metal complexes show drastic spin state conversion upon exposure to external stimuli such as light, temperature and pressure. Representative examples include spin crossover (SCO) complexes, electron transfer-coupled spin transition (ETSCT) clusters, and species that exhibit valence tautomerism (VT).[4] These systems can show magnetic hysteresis in their switching behavior, and are therefore attractive target components for memory storage systems. Herein SCO and ETCST complexes are discussed in detail.

1.2.1 Spin Crossover (SCO) Complexes

Transition metal ions have quintuply-degenerate d-orbitals in isolation, but when held in a six-coordinate octahedral coordination mode, the two d-orbitals that are orientated towards the ligands (e_g) are destabilized, causing them to split from the remaining three d-orbitals (t_{2g}), which are stabilized. The splitting of the d-orbitals (Δ_o, 10 Dq) is based on the electric repulsions between the d-electrons and the ligands. The electronic arrangements of six-coordinate octahedral complexes with d^n (n = 4 - 7) electrons depend on the relative strengths of Δ_o and the spin pairing energy P. When Δ_o is smaller than P, the electrons are arranged to maximize the sum of their spin angular momentum following Hund's rule (high spin (HS) state, Figure 1.1 (right)). In the reverse situation, Hund's rule is broken, and the electrons make pairs and occupy the t_{2g} orbitals, preferentially (low spin (LS) state, Figure 1.1 (left)). When Δ_o and P are close, some first row transition metal ions with d^4 to d^7 electronic configurations may show reversible spin-crossover (SCO) behavior between their HS and LS states upon exposure to external stimuli.

Iron (II) complexes are the most commonly reported thermal SCO materials and show dramatic magnetic changes between their paramagnetic HS state (S = 2) and diamagnetic LS state (S = 0) upon the application of external stimuli. In 1964, Bobonich reported the mononuclear Fe(II) complex $[Fe^{II}(phen)_2(NCE)_2]$ (phen = 1, 10-phenanthroline, E = S, Se), and three years later, its SCO properties were studied by magnetic measurements (Figure 1.2).[5] SCO phenomena can be observed from changes in the magnetic moment and coordination bond lengths between the iron ion and its coordinating donor atoms. In the HS state, the iron d-electrons occupy the anti-bonding e_g orbitals, thus the coordination bond distances between the iron ion and donor atoms are usually longer than those observed in the LS state. When temperature is used as an external stimuli, SCO complexes exist in their HS state at high temperatures and undergo spin conversion to their LS state upon decreasing temperature. In recent times the range of external stimuli employed to effect spin transition has significantly increased to include light, pressure, magnetic field, and guest absorption/desorption.[6]

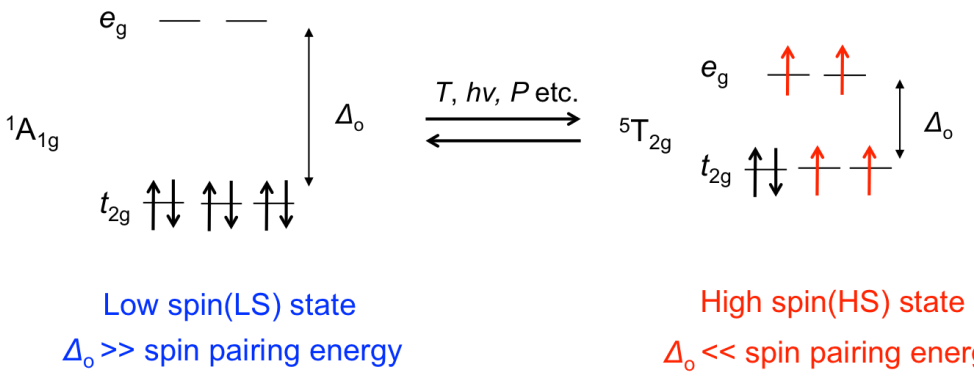

Figure 1.1: Low and high spin states of six-coordinate octahedral metal ions with d^6 electron configuration.

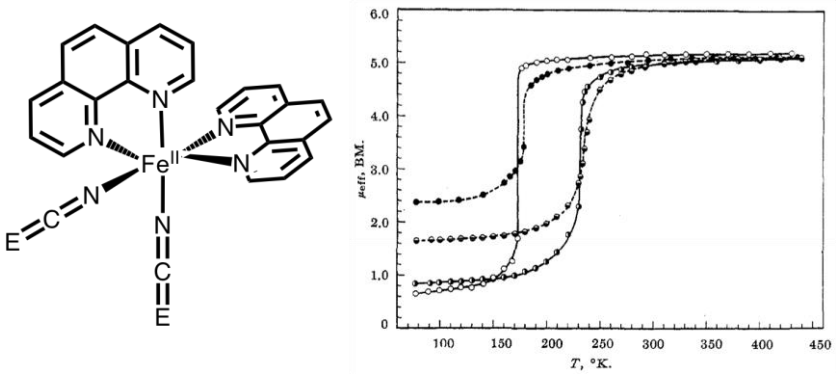

Figure 1.2: The structure of $[Fe^{II}(phen)_2(NCE)_2]$ and its thermal SCO behavior.

1.2.2 Electron-transfer-coupled Spin Transition (ETCST) Complexes

In 1996, Hashimoto *et al*. reported a Prussian blue analog 3D network complex $K_{0.2}Co^{III}_{1.4}[Fe^{II}(CN)_6] \cdot 9H_2O$.[7] This complex shows an increase in magnetic susceptibility upon irradiation with red light at low temperature (Figure1.3). This phenomenon is derived from excitation of the $Fe^{II} \rightarrow Co^{III}$ intervalence charge-transfer (IVCT) band and phase transition from a diamagnetic low temperature phase ($[Fe^{II}LS\text{-}CN\text{-}Co^{III}LS]$) to a ferrimagnetic high temperature phase ($[Fe^{III}LS\text{-}CN\text{-}Co^{II}HS]$). The reversible photomagnetism originates from the light-induced electron transfer between metal centers and the associated spin transition of the cobalt ions, which is described as Electron-Transfer-Coupled Spin Transition (ETSCT). More recently, thermally-responsive ETCST clusters and chain-like complexes have been reported, some of which have been found to exhibit multi bistable ETCST behavior, both under thermal and light excitation.[8] In 2011, Oshio *et al*. reported the Fe-Co tetranuclear complex $[Co_2Fe_2(CN)_6(tp^*)_2(dtbbpy)_4](PF_6)_2 \cdot 2MeOH$ (tp* = hydrotris(3,5-dimethylpyrazol-1-yl)borate, dtbbpy = 4,4'-di- *tert*-butyl-2,2'-bipyridine). This compound showed thermally induced multi-step ETCST and light induced ETCST at low temperature (Figure 1.4).[9]

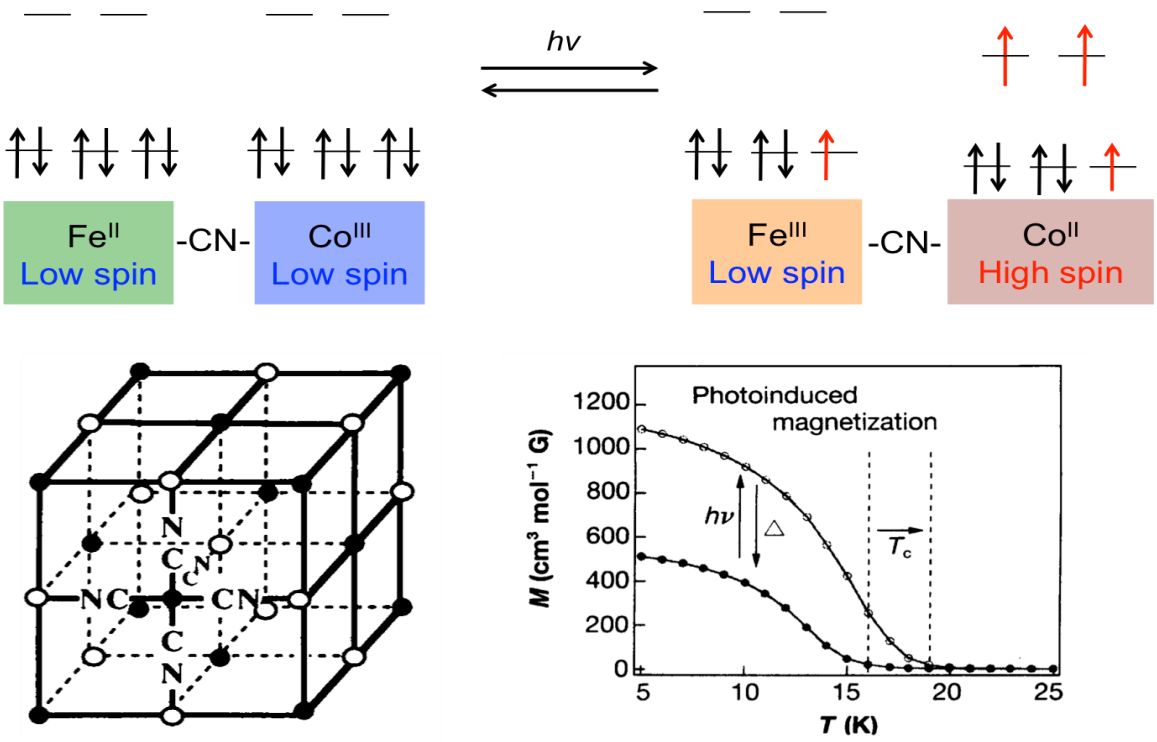

Figure 1.3: Diamagnetic and ferromagnetic spin state switching behavior of a cyanide-bridged Fe-Co ETCST complex (top). Framework and photomagnetism of $K_{0.2}Co^{III}_{1.4}[Fe^{II}(CN)_6] \cdot 9H_2O$ (bottom).

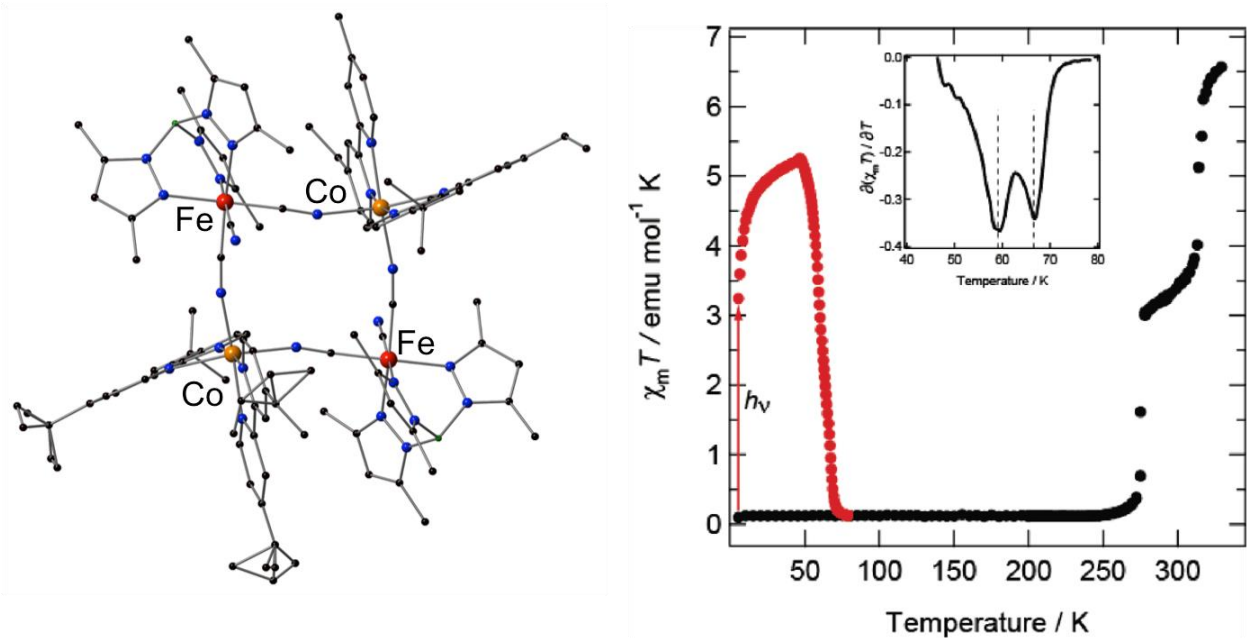

Figure 1.4: Structure (left) and magnetic data (right) of $[Co_2Fe_2(CN)_6(tp^*)_2(dtbbpy)_4](PF_6)_2 \cdot 2MeOH$

1.3 Multi-bistable Materials

Multi-bistable materials can be converted between more than three states (often with hysteresis) upon exposure to external stimuli. These materials have stable intermediate states, thus information storage capacity may be higher than can be achieved with simply bistable materials, and smaller, more information-dense data storage systems may be accessible. Multinuclear SCO complexes lend themselves to exhibiting multi-bistability. In 2005, Real *et al*. reported $\{[Fe(bztpen)]_2[\mu\text{-}N(CN)_2]\}(PF_6)_3$ (bztpen = *N*-benzyl-*N*,*N*',*N*'-tris(2-pyridylmethyl)ethylenediamine) which has two iron (II) SCO active sites.[10] It showed two-step thermal SCO behaviour, with the steps corresponding to transitions on the different iron centres (Figure 1.5). The fabrication of multinuclear complexes in which multiple switching centres are held in close proximity is a rational approach to the development of multi-bistable systems. [11]

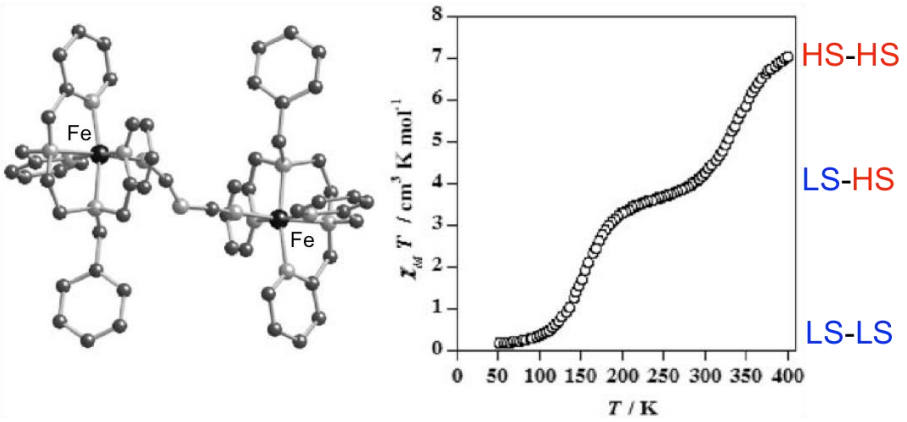

Figure 1.5: Structure of {[Fe(bztpen)]$_2$[μ-N(CN)$_2$]}(PF$_6$)$_3$ (left) and its magnetic data (right).

Another rational approach is through the co-crystallization of different bistable molecules. In 2010, Oshio *et al*. reported a co-crystallized compound [Fe^{II}(dpp)$_2$][Ni(mnt)$_2$]$_2$ · CH$_3$NO$_2$ (dpp = 2,6-di(1*H*-pyrazol-1-yl)pyridine, mnt = maleonitriledithiolate).[12] This is a co-crystallized compound containing an SCO-active complex cation [Fe^{II}(dpp)$_2$]$^{2+}$ and planar anion [Ni(mnt)$_2$]$^-$, which can switch between a diamagnetic dimer state and a paramagnetic monomer state. Both [Fe^{II}(dpp)$_2$]$^{2+}$ and [Ni(mnt)$_2$]$^-$ ions showed spin state conversion and five thermodynamically stable states were observed in the magnetic susceptibility measurements (Figure 1.6). The multi-step magnetic changes occurred due to SCO and [Ni(mnt)$_2$]$^-$ dimerization, as confirmed by X-ray structural analysis, Mössbauer spectra and heat capacity measurements.

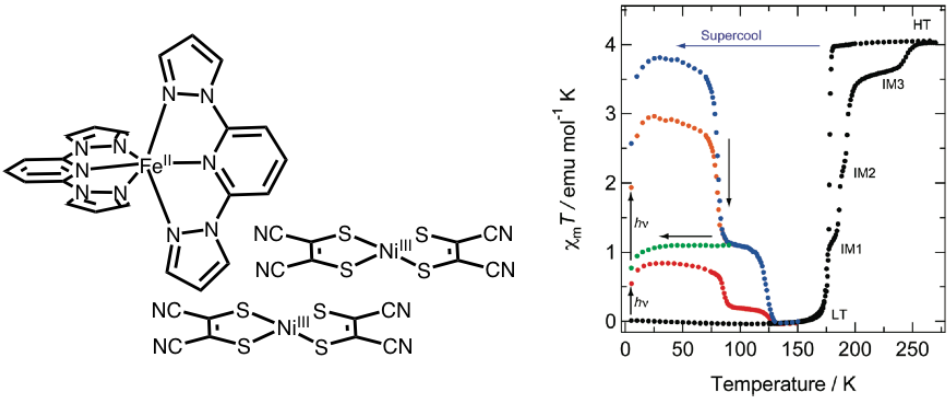

Figure 1.6: Structure of [Fe^{II}(dpp)$_2$][Ni(mnt)$_2$]$_2$ · CH$_3$NO$_2$ (left) and magnetic data (right).

To make multi-bistable systems using mulitinuclear complexes, complicated ligand design can often be a key aspect of the research. In contrast, while co-crystallization can remove the need for laborious ligand synthesis, optimization of the synthetic method can be difficult. It is therefore a key goal in molecular switching chemistry to isolate multi-bistable materials using only simple or cheap materials. Mononuclear complexes are typically amongst the easiest complexes to fabricate,

but almost all examples have a maximum of only two accessible states (for example, high spin and low spin). The development of mononuclear multi-bistable systems is therefore very challenging and important research. To this end, we proposed to employ Brønsted acid/base ligands as the capping groups for transition metal complexes. The fact that they can be adjusted between multiple protonation states means that their electronic state, and therefore the nature of their ligand field, can be modified by simple acid/base addition to the system. We proposed therefore that the combination of metal ion and Brønsted acid/base ligand will have the potential to display multistep spin state conversion.

1.4 Electronic State Conversions of Coordination Compounds by Protonation/deprotonation

The physical properties of metal complexes which have Brønsted acid/base ligands can be changed by controlling the pH of the environment. Ligand deprotonation causes drastic electronic state conversion derived from the increased basicity of the electron-rich ligand and the associated increase in ligand field strength.[13] In addition, deprotonation results in new intermolecular interactions originating from the loss of a hydrogen bond donor, gain of a hydrogen bond acceptor and possible inclusion of charge balancing counter ion(s).[14] There are a few reports of this approach being employed to fabricate bistable materials which can be triggered by chemical external stimuli. In 1986, Haga *et al.* reported a new Ru(II) complex $[Ru^{II}(bpy)_2(BiBzimH_2)]^{2+}$ ($BiBzimH_2$ = 2.2'-bibenzimidazole), which had benzimidazole moieties as Brønsted acid/base (Figure 1.7).[15] The complex exhibited stepwise deprotonation in acetonitrile/buffer mixture solution, and the redox potential shifted negatively as the ligand basicity increased. From differential-pulse voltammetric data and UV absorption spectra, the Ru(II) / Ru(III) (or Ru(III) / Ru(IV)) redox and protonated states were reversible. Therefore, this complex can exist in seven states in solution. The result is an example of multistep electronic state conversion by using both deprotonation and redox reactions.

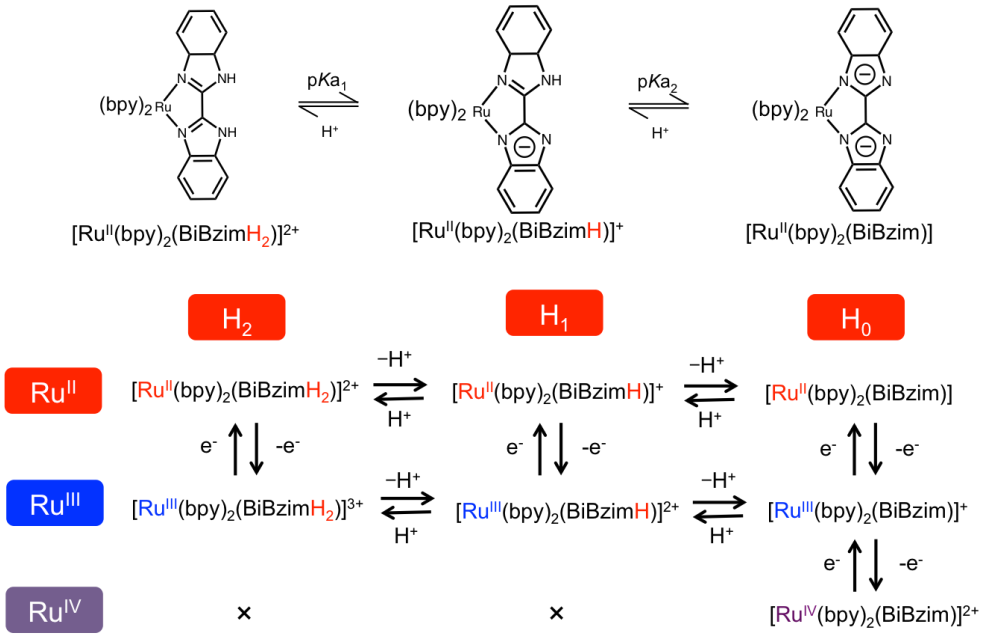

Figure 1.7: Structure of $[Ru^{II}(bpy)_2(BiBzimH_2)]^{2+}$ and electric state conversion by deprotonation and oxidation.

Deprotonation of ligands affect the spin states of metal cations. In 2004, Schikora *et al*. reported the iron (II) mononuclear complex $[Fe^{II}(bzimpy)_2](ClO_4)_2 \cdot 0.25H_2O$ (bzimpy = 2,6-bis(benzimidazol-2-yl)pyridine) and the observation of spin state switching by the deprotonation of benzimidazole.[16] Both this complex and the deprotonated complex $[Fe^{II}(bzimpy_{-1H})_2]$ showed SCO behavior above room temperature, but the SCO temperature was different (Figure 1.8) due to the changing ligand field upon deprotonation. The deprotonation of complex $[Fe^{II}(bzimpy_{-1H})_2]$ stabilizes the low spin state compared to $[Fe^{II}(bzimpy)_2]^{2+}$, causing an increase in SCO temperature.

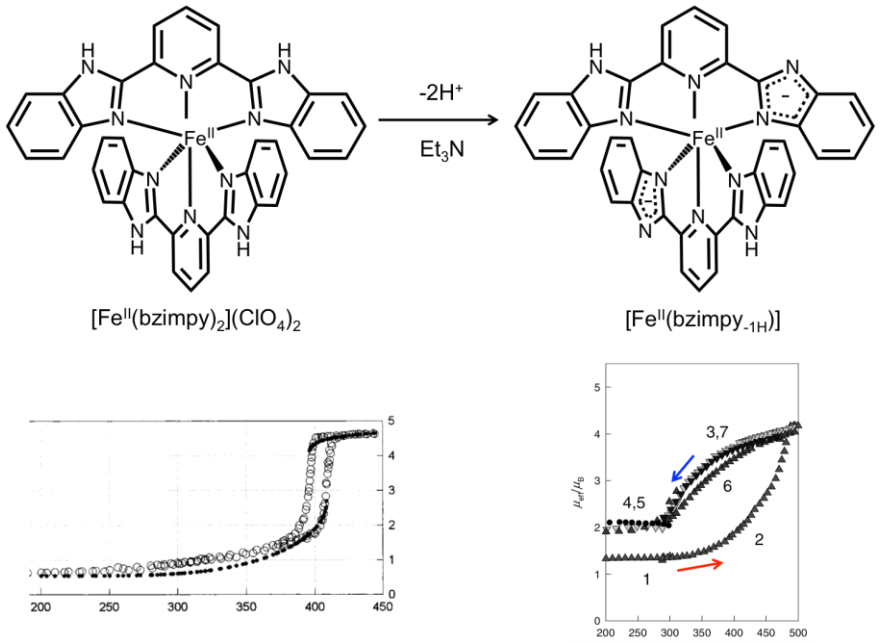

Figure 1.8: Structure of $[Fe^{II}(bzimpy)_2](ClO_4)_2$ and deprotonated $[Fe^{II}(bzimpy_{-1H})_2]$, (top) and magnetic data (bottom).

Multistep-deprotonation of metal complexes has been reported. In 2018, Clérac *et al*. synthesized a tetranuclear iron (II) grid $[Fe^{II}_4(H_2L)_4](BF_4)_8$, ($H_2L$ = Pyridine-2-carboxaldehyde [2-(3,4,5-Trimethoxyphenyl)pyrimidine-4,6-diyl]dihydrazone) with hydrazone moieties as Brønsted acid/base (Figure 1.9 (a)).[17] The complex could be deprotonated using triethylamine, and two intermediate states $[Fe_4(H_2L)_2(HL)_2](BF_4)_6$ and $[Fe_4(HL)_4](BF_4)_4$ were isolated. SQUID magnetometry indicated incomplete SCO behavior at different temperatures. In addition, from the UV-visible absorption measurements, a stepwise color change and red shift was observed upon deprotonation (Figure 1.9 (b)). There are also some reports on electronic state changes of grid-like complexes, and increases in the multistep SCO temperature were observed upon deprotonation.[18]

(a)

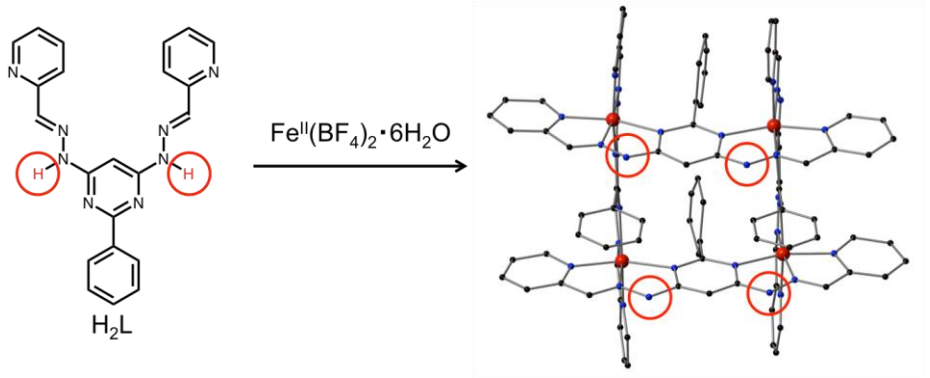

(b)

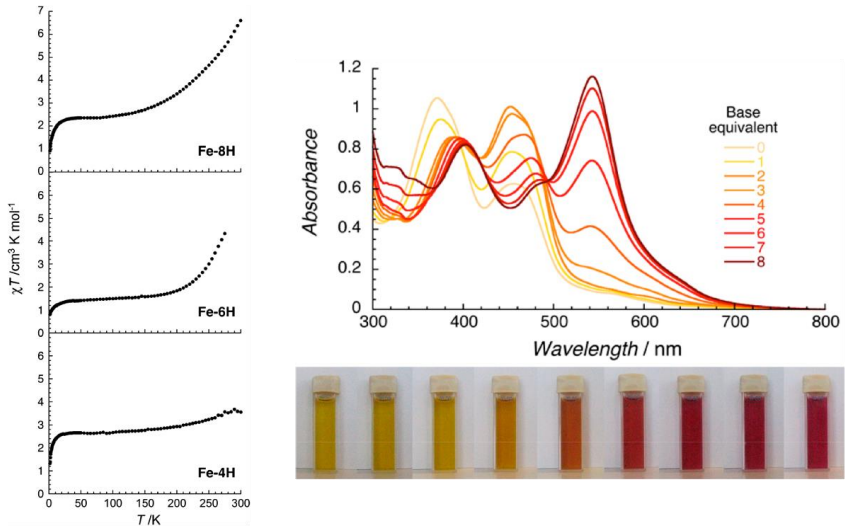

Figure 1.9: (a) Structure of ligand H_2L and $[Fe^{II}_4(H_2L)_4](BF_4)_8$. (Red circles mean Brønsted acid/base parts.) (b) Magnetic data of $[Fe_4(H_2L)_4](BF_4)_8$, $[Fe_4(H_2L)_2(HL)_2](BF_4)_6$ and $[Fe_4(HL)_4](BF_4)_4$ and base titration UV of $[Fe^{II}_4(H_2L)_4](BF_4)_8$.

1.5 Specific Physical Properties Based on Hydrogen Bonding Network

Intermolecular hydrogen bonding is a useful means to control supramolecular dimensionality. In recent times, proton transfer between neighboring molecules in the solid state has been employed to identify new switchable physical properties in crystalline materials. In 2005, Horiuchi *et al*. reported a eutectic compound containing both phenazine (proton donor) and chloranilic acid (proton acceptor).[19] The material is based on a hydrogen bonding network between donors and acceptors and showed ferroelectric behavior derived from proton transfer (Figure 1.10). This is the first example of the phenomenon and the high dielectric constant and Curie temperature near room temperature hint a new generation of molecular memory device. In the crystal, protons between donors and acceptors are disordered and show no polarization at high temperature. However, close to the phase transition temperature, the protons move and become ordered at the acceptor sites, causing an increase of ionicity and the appearance of polarization. Phase transition is not observed when the pK_a difference between proton donor and acceptor is too big. This type of ferroelectric effect has been reported for systems based on croconic acid and imidazole derivatives, among others.[20]

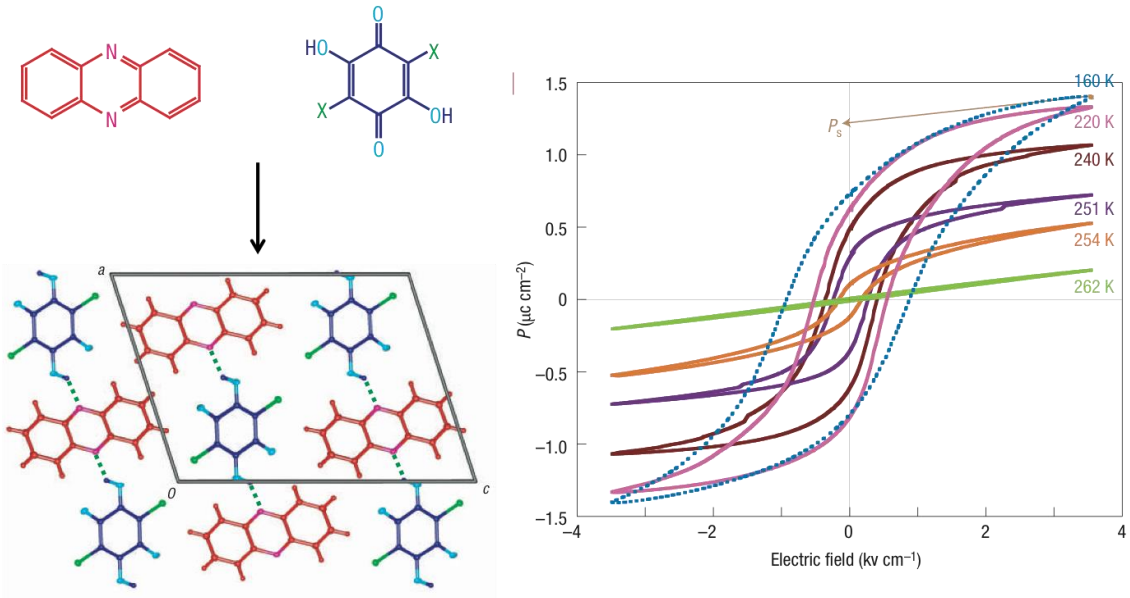

Figure 1.10: Structure of phenazine and chloranilic acid hydrogen bonding network (left) and its ferroelectric behavior (right).

In 2017, Tadokoro *et al*. reported the deprotonated Ru(III) complex $\{[Ru^{III}(Hbim)_3](MeOBn)_m\}_n$ (H_2bim = biimidazole, MeOBn = methyl benzoate). This complex was synthesized by the deprotonation of $[Ru^{II}(H_2bim)_3](PF_6)_2$.[21] Single crystal X-ray measurement showed the complex to form a 2D honeycomb network through hydrogen bonding network (Figure 1.11). In addition, solid-state cyclic voltammetry measurements showed two-step Ru^{III}/Ru^{II} redox processes. The potential difference originated from the number of ordered protons between complexes. In other words, this is an example of Proton Coupled Electron Transfer (PCET) complex in the solid state. In addition, the authors succeeded in synthesizing the mixed-valence complex $\{[Ru^{II}(H_2bim)(Hbim)_2][Ru^{III}(bim)(Hbim)_2][K(MeOBz)_6]\}_n$ as single crystals. The material was found to exhibit high proton conductivity in the solid-state.

In 2003, Matsumoto *et al*. reported the mixed-valence network $[Fe^{II}(H_3L)][Fe^{III}(L)](NO_3)_2$ consisting of the Fe(II) mononuclear complex $[Fe^{II}(H_3L)]^{2+}$ (H_3L = tris{[2-{(imidazole-4-yl)methylidene}amino]ethyl} amine) and its deprotonated Fe(III) complex $[Fe^{III}(L)]$. The material formed 2D sheets through a hydrogen bonded network through the ligand pyrazole moieties.[22] The homochiral structure contains both Λ and Δ enantiomers. Temperature dependent magnetic susceptibility measurement showed multi-step SCO behavior (Figure 1.12). In the solid state, both Fe(II) and Fe(III) sites were SCO active, leading to three stable states, Fe^{II}LS-Fe^{III}LS, Fe^{II}HS-Fe^{III}LS, and Fe^{II}HS-Fe^{III}HS. In addition, the Fe(II) sites showed Light-Induced Excited Spin State Trapping (LIESST) at very low temperature (λ = 514.5 nm).

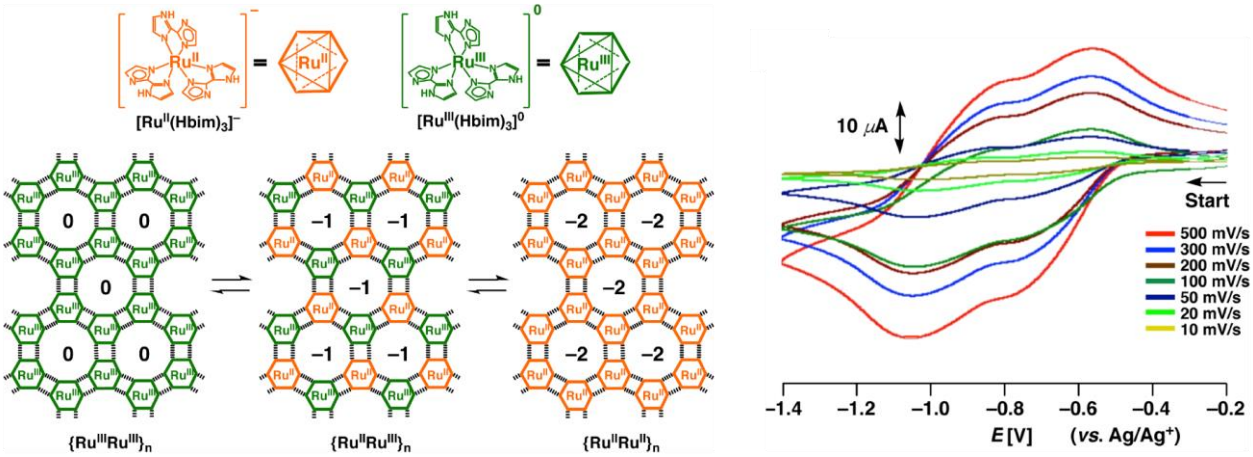

Figure 1.11: Hydrogen bonding network of $\{[Ru^{III}(Hbim)_3](MeOBn)_m\}_n$ and solid state CV.

(a)

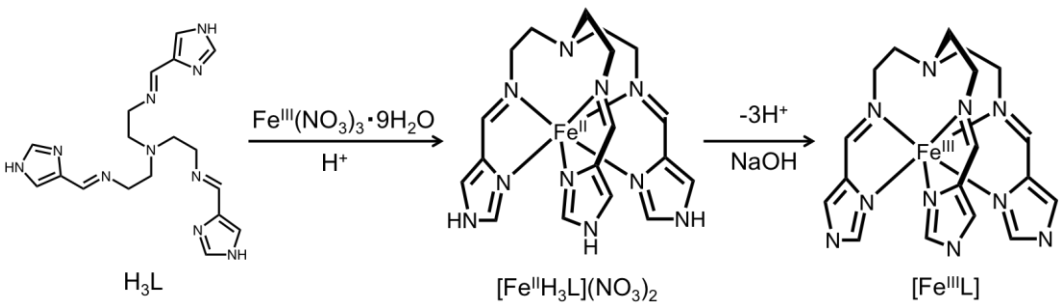

(b)

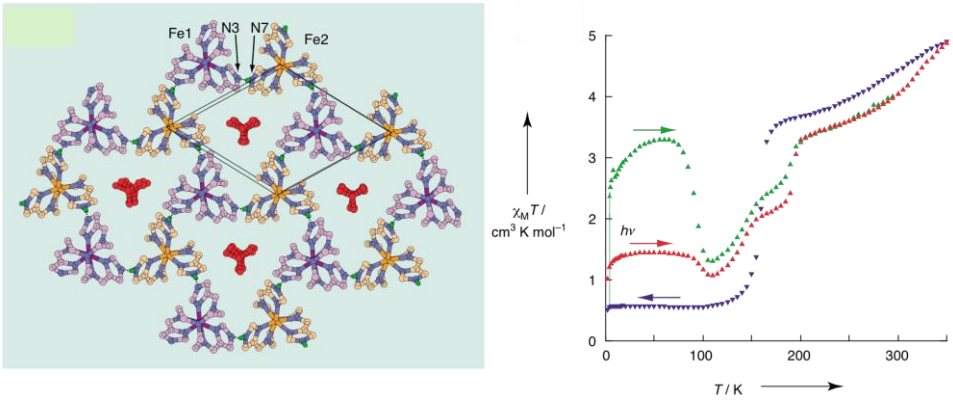

Figure 1.12: (a) Structure of H_2L, $[Fe^{II}(H_3L)]^{2+}$ and $[Fe^{III}(L)]$ (b) 2D network and magnetic data of $[Fe^{II}(H_3L)][Fe^{III}(L)](NO_3)_2$.

1.6 Contents

In this thesis, the syntheses, structures and physical properties of iron complexes with Brønsted ligands and Cu-Fe clusters are presented. In CHAPTER 1 (this chapter), the outline of the thesis and background of the important topics relating to the thesis are introduced. Molecular design of mononuclear iron complexes and the differences in the electronic states of the obtained complexes are presented in CHAPTER 2. In order to synthesize a mononuclear iron complex with N_6 coordination geometry, four asymmetric tridentate ligands ($H_2L^{1\text{-}4}$ Figure 1.13) were designed and their complexes were prepared and their physical properties investigated. In CHAPTER 3, the electronic state conversions of mononuclear iron complexes, $[Fe^{II}(H_2L^1)_2]^{2+}$, with Brønsted ligands were investigated. Five iron complexes with different electronic states were synthesized by trial and error of synthetic conditions. Their structural, magnetic, optical and electrochemical properties are presented. In CHAPTER 4, the protonation/deprotonation properties of a heptanuclear heterometallic cluster molecule, $[Cu^{II}_6Fe^{III}(HL^5)_6]$ with a multidentate pyrrole-based ligand are introduced.

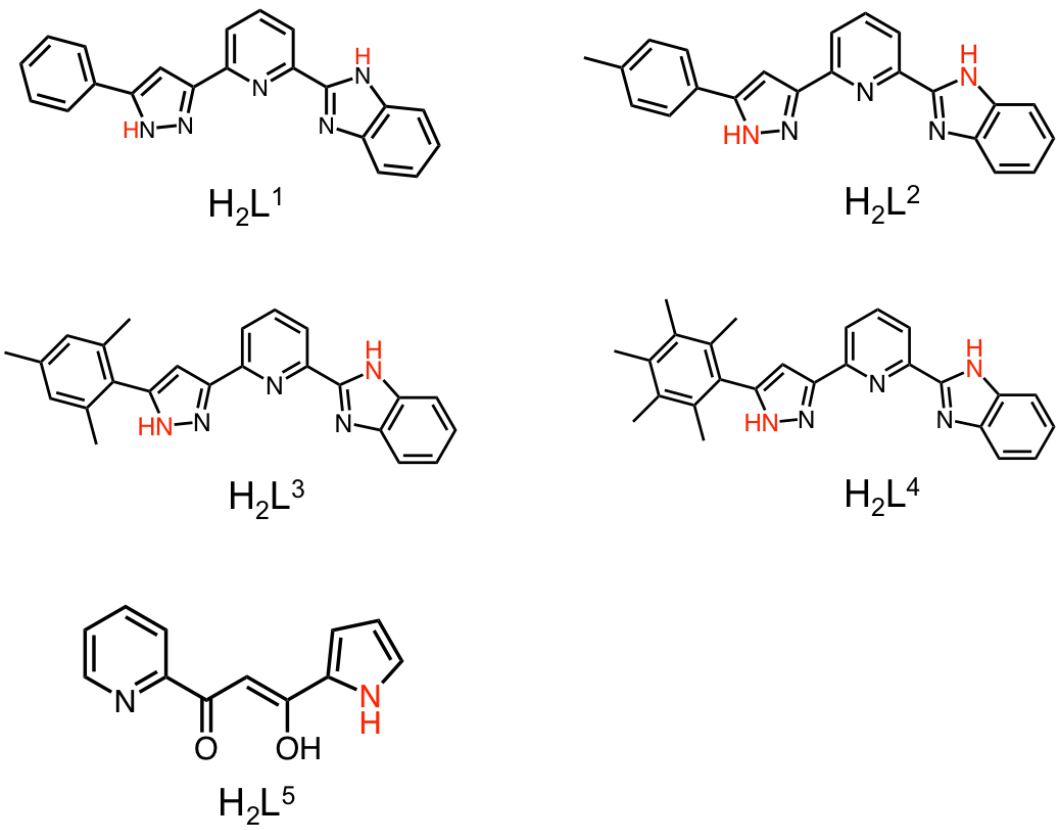

Figure 1. 13: List of ligands H_2L^{1-5}.

References

[1] (a) O. Kahn, C. J. Martinez, *Science*, **1998**, *279*, 44-48; (b) F. Prins, M. Monrabal-Capilla, E. A. Osorio, E. Coronado, H. S. J. van der Zant, *Adv. Mater.*, **2011**, *23*, 1545-1549; (c) G. Aromí, D. Aguilà, P. Gamez, F. Luis, O. Roubeau, *Chem. Soc. Rev.*, **2012**, *41*, 537-546; (d) O. Sato, *Nature Chem.*, **2016**, *8*, 644-656. (e) T. Tezgerevska, K.G. Alley and C. Boskovic, *Coord. Chem. Rev.*, **2014**, *268*, 23-40; (f) S. Sanvito, *Chem. Soc. Rev.*, **2011**, *40*, 3336-3355; (g) L. Bogani and W. Wernsdorfer, *Nat. Mat.*, **2008**, *7*, 179-186; (h) A.C. Fahrenbach, S.C. Warren, J. T. Incorvati, A.-J. Avestro, J.C. Barnes, J.F. Stoddart and B.A. Grzybowski, *Adv. Mat.*, **2013**, *25*, 331-348; (i) E. Ruiz, *Phys. Chem. Chem. Phys.*, **2014**, *16*, 14-22.

[2] (a) Huimin wen, Wengang Li, Jiewei Chen, Gen He, Longhua Li, Mark A. Olson, Andrew C.-H. Sue, J. Fraser Stoddart, Xuefeng Guo, *Sci. Adv.* **2016**, *2*, e1601113; (b) Youngsang Kim, Thomas J. Hellmuch, Dmytro Sysoiev, Fabian Pauly, Torsten Pietsch, Jannic Wolf, Artur Erbe, Thomas Huhn, Ulrich Groth, Ulrich E. Steiner, Elke Scheer, *Nano. Lett.* **2012**, *3*, 3736-3742; (c) Cina Foroutan-Nejad, Valery Andrushchenko, Michal Straka, *Phys. Chem. Chem. Phys.*, **2016**, *18*, 32673-32677; (d) Matthew J. Comstok, Niv Levy, Armen Kirakosian, Jongweon Cho, Frank Lauterwasser, Jessica H. Harvey, David A. Strubbe, Jean M.J. Frechet, Dirk Trauner, Steven G. Louie, Michael F. Crommine, *Phys. Rev. Lett.,* **2007**, *99*, 038301.

[3] (a) Rie Mikami, Minori Taguchi, Koji Yamada, Koji Suzuki, Osamu Sato, and Yasuaki Einaga, *Angew. Chem. Int. Ed.* **2004**, *43*, 6135-6139; (b) Wiktor Szymański, John M. Beierle, Hans A.V.Kistemaker, Willem A.Velema, Ben L.Feringa, *Chem. Rev.*, **2013**, *113*, 6114-6178; (c) Masahiro Irie, *Chem. Rev.*, **2000**, *100*, 1685-1716; (d) O. Sato, J. Tao, Y.-Z. Zhang, *Angew. Chem. Int. Ed.* **2007**, *46*, 2152-2187; (e) M. A. Halcrow, *Chem. Soc. Rev.* **2011**, *40*, 4119-4142; (f) D. J. Harding, P. Harding, W. Phonsri, *Coord. Chem. Rev.* **2016**, *313*, 38-61.

[4] (a) O. Sato, J. Tao, Y.-Z. Zhang, *Angew. Chem. Int. Ed*. **2007**, *46*, 2152-2187; (b) M. A. Halcrow, *Chem. Soc. Rev.* **2011**, *40*, 4119-4142; (c) D. J. Harding, P. Harding, W. Phonsri, Coord. *Chem. Rev*. **2016**, *313*, 38-61; (d) Z.-P. Ni, J.-L. Liu, M. N. Hoque, W. Liu, J.-Y. Li, Y.-C. Chen, M.-L. Tong, *Coord. Chem. Rev*. **2017**, *335*, 28-43; (e) Dunbar, K. R.; Achim, C.; Shatruk, M. In Spin-Crossover Materials-Properties and Applications; Wiley: Chichester, U.K., **2013**; pp 171−202; (f) Hendrickson, D. N.; Pierpont, C. G. *Top. Curr. Chem.* **2004**, *234*, 63; (g) Dei, A.; Gatteschi, D.; Sangregorio, C.; Sorace, L. *Acc. Chem. Res*. **2004**, *37*, 827; (h) Evangelio, E.; Ruiz-Molina, D. Eur. J. *Inorg. Chem*. **2005**, *2005*, 2957; (i) Tezgerevska, T.; Alley, K. G.; Boskovic, C. *Coord. Chem. Rev*. **2014**, *268*, 23.

[5] (a) W. A. Baker, H. M. Bobonich, *Inorg. Chem.* **1964**, *3*, 1184-1188; (b) König E., Madeja K., *Inorg. Chem.* **1967**, *6*, 48-55.

[6] (a) J. J. McGravey, I, J, Lawthers, *Chem. Soc. Chem. Commun.*, **1982**, 906-907; (b) Jean-Francois Létard, José Antonio Real, Nicolás Moliner, Ana B. Gaspar, Laurence Capes, Olivier Cador, and Olivier Kahn, *J. Am. Chem. Soc.* **1999**, *121*, 10630–10631; (c) Ester Breuning, Mario Ruben, Jean-Marie Lehn, Franz Renz, Yann Garcia, Vadim Ksenofontov, Philipp Gütlich, Elina Wegelius, Kari Rissanen, *Angew. Chem. Int. Ed.*, **2000**, *39*, 2504-2507; (d) Tao Liu, Hui Zheng, Soonchul Kang, Yoshihito Shiota, Shinya Hayami, Masaki Mito, Osamu Sato, Kazunari Yoshizawa, Shinji Kanegawa, Chunying Duan, *Nature Commun.* **2013**, *4*, 2826; (e) Natasha F. Sciortino, Kartin R. Scherl-Gruenwald, Guillaume Chastanet, Gregory J. Halder, Karena W. Chapman, Jean-Francois Létard, Cameron J. Kepert, *Angew. Chem. Int. Ed.*, **2012**, *51*, 10154-10158; (f) Shinya Hayami, Zhong-ze Gu, Motoo Shiro, Yasuaki Einaga, Akira Fujishima, Osamu Sato, *J. Am. Chem. Soc.* **2000**, *122*, 7126–7127; (g) Shojiro Kimura, Yasuo Narumi, Koichi Kindo,. *Physical. Review. B* **2005**, *72*, 064448; (h) Matthew G. Cowan, Juan Olguin, Suresh Narayanaswamy, Jeffery L. Tallon, Sally Brooker, *J. Am. Chem. Soc.* **2012**, *134*, 2892–2894; (i) I. A. Gass, S. R. Batten, C. M. Forsyth, B. Moubaraki, C. J. Schneider, K. S. Murray, *Coord. Chem. Rev.* **2011**, *255*, 2058-2067; (j) M. C. Muñoz, J. A. Real, *Coord. Chem. Rev.* **2011**, *255*, 2068-2093; (k) D. Aravena, Z. A. Castillo, M. C. Muñoz, A. B. Gaspar, K. Yoneda, R. Ohtani, A. Mishima, S. Kitagawa, M. Ohba, J. A. Real, E. Ruiz, *Chem. Eur. J.* **2014**, *20*, 12864-12873; (l) E. Coronado, M. Giménez-Marqués, G. Mínguez Espallargas, F. Rey, I. J. Vitórica-Yrezábal, *J. Am. Chem. Soc.* **2013**, *135*, 15986-15989; (m) M. J. Murphy, K. A. Zenere, F. Ragon, P. D. Southon, C. J. Kepert, S. M. Neville, *J. Am. Chem. Soc.* **2017**, *139*, 1330-1335; (n) D. Müller, C. Knoll, M. Seifried, J. M. Welch, G. Giester, M. Reissner, P. Weinberger, *Chem. Eur. J.* **2018**, *24*, 5271-5280; (o) M. Seredyuk, L. Piñeiro-López, M. C. Muñoz, F. J. Martínez-Casado, G. Molnár, J. A. Rodriguez-Velamazán, A. Bousseksou, J. A. Real, *Inorg. Chem.* **2015**, *54*, 7424-7432.

[7] O. Sato, T. Iyoda, K. Hashimoto, *Science,* **1996**, *272*, 704-705.

[8] (a) T. Yamauchi, A. Nakamura, Y. Morimoto, T. Hozumi, K, Hashimoto, S. Ohkoshi, *Physical. Review. B.* **2005**, *72*, 214425; (b) Abhishake Mondal, Yanling Li, Mannan Seuleiman, Miguel Julve, Loic Toupet, Marylise Buron-Le Cointe, Rodrigue Lescouezec, *J. Am. Chem. Soc.* **2013**, *135*, 1653–1656; (c) Yoshihiro Sekine, Masayuki Nihei, Hiroki Oshio, *Chem Lett.,* **2014**, *43*, 1029-1030; (d) Tao Liu, Yan-Juan Zhang, Shinji Kanegawa, Osamu Sato, *J. Am. Chem. Soc.* **2010**, *132*, 8250–8251; (e) Da-Peng Dong, Tao Liu, Shinji Kanegawa, Soonchul Kang, Osamu Sato, Cheng He, Chun-Yang Duan, *Angew. Chem. Int. Ed.*, **2012**, *124*, 5209-5213; (f) Noriaki Ozaki, Hiroko Tokoro, Yoshiho Hamada, Asuka Namai, Tomoyuki Matsuda, Souhei Kaneko, Shin-ichi Ohkoshi, *Adv. Funct. Mater.,* **2012**, *22*, 2089-2093; (g) Hoshino, N., Iijima, F., Newton, G. N., Yoshida, N., Shiga, T., Nojiri, H., Nakao, A., Kumai, R., Murakami, Y. Oshio, H. *Nature Chem.* **2012**, *4*, 921-926; (h) C. P. Berlinguette, A. Dragulescu-Andrasi, A. Sieber, J. R. Galán-Mascarós, H.-U. Güdel, C. Achim, K. R. Dunbar, *J. Am. Chem. Soc.* **2004**, *126*, 6222-6223; (i) D. Li, R. Clérac, O. Roubeau, E. Harté, C. Mathonière, R. Le Bris, S. M. Holmes, *J. Am. Chem. Soc.* **2008**, *130*, 252-258.

[9] Masayuki Nihei, Yoshihiro Sekine, Naoki Suganami, Kento Nakazawa, Akiko Nakao, Hironori Nakao, Youichi Murakami, Hiroki Oshio, *J. Am. Chem. Soc.* **2011**, *133*, 3592–3600.

[10] J N. Ortega-Villar, A. L. Thompson, M. C. Munoz, V. M. Ugalde-Saldıvar, A. E. Goeta, R. Moreno-Esparza, J. A. Real, *Chem.-Eur. J.*, **2005**, *11*, 5721-5734.

[11] (a) V. Ksenofontov, A. B. Gaspar, S. Reiman, V. Niel, J. A. Real and P. Gutlich, *Chem. Eur. J*., **2004**, *10*, 1291-1298; (b) N. Ortega-Villar, A. L. Thompson, M. C. Munoz, V. M. Ugalde- Saldívar, A. E. Goeta, R. Moreno-Esparza and J. A. Real, *Chem., Eur,. J*., **2005**, *11*, 5721-5734; (c) M. Nihei, M. Ui, M. Yokota, L. Han, A. Maeda, H. Kishida, H. Okamoto and H. Oshio, *Angew. Chem., Int. Ed*., **2005**, *44*, 6484-6487; (d) T. Matsumoto, G. N. Newton, T. Shiga, S. Hayami, Y. Matsui, H. Okamoto, R. Kumai, Y. Murakami, and H. Oshio, *Nature Commun.*, **2014**, *5*, 3865/1-3865/8; (e) M. Seredyuk, K. O. Znovjyak, J. Kusz, M. Nowak, M. C. Muñoz, J. A. Real, *Dalton Trans.* **2014**, *43*, 16387-16394;

[12] Nihei, M.; Tahira, H.; Takahashi, N.; Otake, Y.; Yamamura, Y.; Saito, K. & Oshio, H., *J. Am. Chem. Soc*., **2010**, *131*, 3553-3560.

[13] (a) L. L. Martin, R. L. Martin, A. M. Sargeson, *Polyhedron,* 1994*, 13*, 1969–1980. (b) J. A. Kitchen, J. Olguín, R. Kulmaczewski, N. G. White, V. A. Milway, G. N. L. Jameson, J. L. Tallon, S. Brooker, *Inorg. Chem.* **2013**, *52*, 11185-11199; (c) B. Schäfer, C. Rajnák, I. Šalitroš, O. Fuhr, D. Klar, C. Schmitz-Antoniak, E. Weschke, H. Wende, M. Ruben, *Chem. Commun.* **2013**, *49*, 10986-10988; (d) F. Lambert, C. Policar, S. Durot, M. Cesario, L. Yuwei, H. Korri-Youssoufi, B. Keita, L. Nadjo, *Inorg. Chem.* **2004**, *43*, 4178-4188; (e) Y.-H. Luo, M. Nihei, G.-J. Wen, B.-W. Sun, H. Oshio, *Inorg. Chem.* **2016**, *55*, 8147-8152; (f) M. Nihei, Y. Yanai, I. J. Hsu, Y. Sekine, H. Oshio, *Angew. Chem. Int. Ed.* **2017**, *56*, 591-594.

[14] (a) Veronica Jornet-Mollá, Yan Duan, Carlos Giménes-Saiz, Joao C. Waerenborgh, Francisco Romero, *Dalton Trans.,* **2016** *45*, 17918-17928. (b) M. Yamada, E. Fukumoto, M. Ooidemizu, N. Bréfuel, N. Matsumoto, S. Iijima, M. Kojima, N. Re, F. Dahan, J.-P. Tuchagues, *Inorg. Chem.* **2005**, *44*, 6967-6974; (c) P. Guionneau, *Dalton Trans.* **2014**, *43*, 382-393; (d) R.-J. Wei, R. Nakahara, J. M. Cameron, G. N. Newton, T. Shiga, H. Sagayama, R. Kumai, Y. Murakami, H. Oshio, *Dalton Trans.* **2016**, *45*, 17104-17107; (e) Y. Sekine, M. Nihei, H. Oshio, *Chem. Eur. J.* **2017**, *23*, 5193-5197; (f) K. Sugiyarto, D. Craig, A. Rae, H. Goodwin, *Aust. J. Chem.* **1994**, *47*, 869-890; (g) G. Brewer, L. J. Alvarado, C. T. Brewer, R. J. Butcher, J. Cipressi, C. Viragh, P. Y. Zavalij, *Inorg. Chim. Acta* **2014**, *421*, 100-109.

[15] Alan M Bond, Masa-aki. Haga, *Inorg. Chem.* **1986**, *25*, 4507-4514.

[16] (a) R. Boča, M. Boča, L. Dlhán, K. Falk, H. Fuess, W. Haase, R. Jaroščiak, B. Papánková, F. Renz, M. Vrbocá, R. Werner, *Inorg. Chem.* **2001**, 40, 3025-3033; (b) Roman Boča, Franz Renz, Miroslav Boča, Hartmut Fuess, Wolfgang Haase, Guido Kickelbick, Wolfgang Linert, Martina Vrbová-Schikora, *Inorg. Chem.Commun* **2005**, ***8***, 227-230.

[17] Sébastien Dhers, Abhishake Mondal, David Aguilá, Juan Ramírez, Sergi Vela, Pierre Dechambenoit, Mathieu Rouziéres, Jonathan R. Nitschke, Rodophe Clérac, Jean-Marie Lehn, *J. Am. Chem. Soc.* **2018**, *140*, 8218–8227.

[18] (a) Mario Ruben, Jean-Marie Lehn, Gavin Vaughan, *Chem. Commun.* **2003**, 1338-1339; (b) Takuya Shiga, Yamato Sato, Minami Tachibana, Hiroki Sato, Takuto Matsumoto, Hajime Sagayama, Reiji Kumai, Youichi Murakami, Graham N. Newton, Hiroki Oshio, *Inorg. Chem.*, **2018**, *57*, 14013-14017.

[19] Sachio Horiuchi, Fumiyuki Ishii, Reiji Kumai, Yoichi Okimoto, Hiroaki Tachibana, Naoto Nagaosa, Yoshinori Tokura, *Nature Materials,* **2005**, *4*, 163-166.

[20] (a) Sachio Horiuchi, Fumitaka Kagawa, Kensuke Hatahara, Kensuke Kobayashi, Reiji Kumai, Youichi Murakami, Yoshinori Tokura, *Nature Commun,* **2012**, *3*, 1-6; (b) Sachio Horiuchi, Yusuke Tokunaga, Gianluca Giovannetti, Silva Picozzi, Hirotake Itoh, Ryo Shimano, Reiji Kumai, Yoshinori Tokura, *Nature,* **2010**, *463*, 789-792; (c) Sachio Horiuchi, Reiji Kumai, Yoshinori Tokura, *Angew. Chem. Int. Ed.*, **2007**, *119*, 3567-3571.

[21] Makoto Tadokoro, Hiroyuki Hosoda, Tomonori Inoue, Akira Murayama, Koichiro Noguchi, Atsushi Iioka, Ryota Nishimura, Masaki Itoh, Tomoaki Sugaya, Hajime Kamebuchi, Masaaki Haga, *Inorg. Chem.* **2017**, *56*, 8513-8526.

[22] Yukinari Sunatsuki, Yuichi Ikuta, Naohide Matsumoto, Hiromi Ohta, Masaaki Kojima, Seiichiro Iijima, Shinya Hayami, Yonezo Maeda, Sumio Kaizaki, Françoise Dahan, Jean-Pierre Tuchagues, *Angew. Chem. Int. Ed.*, **2003**, *42*, 1614-1618

CHAPTER 2
Effect of Ligand Modification in Iron Complexes

2.1 Introduction

Bistable molecules attract significant interest due to their potential applications as components in molecular electronic and nanoscale devices.[1] Spin crossover (SCO) molecules are one such class of bistable material that lend themselves to potential molecular switching applications.[2] SCO behaviour can be tuned by modifying ligand field strength, complex nuclearity and intermolecular interactions. Many systematic studies on the SCO behaviour of molecular species have shown dependence of the bistability on anions, guest molecules, solvent molecules and substituent groups.[3] Anions affect the crystal packing and intermolecular electrostatic interactions, while solvent molecules can interact with spin crossover complexes through hydrogen bonds or CH-π interactions, resulting in perturbation of the electronic states of SCO-active iron complexes. Matsumoto *et al*. reported a series of two-dimensional SCO complexes, $[Fe^{II}H_3L^{Me}][Fe^{II}L^{Me}]X$ (H_3L^{Me} = tris-[2-(((2-methylimidazol-4-yl)methylidene)aminoethyl)amine], X^- = ClO_4^-, BF_4^-, PF_6^-, AsF_6^-, SbF_6^-), which show different SCO behaviour depending on the nature of the interlayer elastic interactions mediated by the anions.[4] The influence of counter ions and solvent molecules in cobalt SCO systems has been discussed in detail by Real *et al*.[5] However, the origin of the effects on the SCO behaviour mediated by anion and solvent molecules can be difficult to precisely define due to the complex nature of supramolecular systems. In contrast, ligand substituent groups directly affect the electlon-donating nature of the ligand, and the ligand field strength can be controlled based on precise molecular design. For example, tridentate 2,6-bis(pyrazol-1-yl)pyridine (bpp) ligands can be readily modified, and the nature of the substituent effect on the SCO properties of their complexes with iron is well understood,[6] and can be predicted by Hammett's rule.[7] Distinct differences in the SCO properties of $[Fe(bpp)]^{2+}$ analogues with different substitution groups were observed in solid and solution states.[8] Substituent groups also exert a secondary influence on complex SCO behaviour via their effect on complex topology and supramolecular packing structure. For example, $[Fe^{II}(qsal\text{-}X)_2]$ (qsal-X = 5-X-*N*-(8-quinolyl)salicylaldimines), X = F, Cl, Br, I) complexes exhibit different SCO behaviour, dependent on the nature of the supramolecular interactions

of their halogen substituents.[9] In order to obtain fine-tuned SCO systems, systematic studies on substituent effects on complex structure and magnetic properties remain a key approach.

In this work, new asymmetric tridentate ligands H_2L^{1-4} ((2-[5-(R-phenyl)-1*H*-pyrazole-3-yl] 6-benzimidazole pyridine) H_2L^1: R = phenyl, H_2L^2: R = 4-methylphenyl, H_2L^3: R = 2,4,6-trimethylphenyl, H_2L^4: R = 2,3,4,5,6-pentamethylphenyl, Scheme 2.1) were designed as supports for SCO materials. Four bis-chelate type iron complexes, $[Fe^{II}(H_2L^n)_2](BF_4)_2$ (**1**, n = 1; **2**, n = 2; **3**, n = 3; **4**, n = 4), were synthesized, and their structures and magnetic properties were investigated.

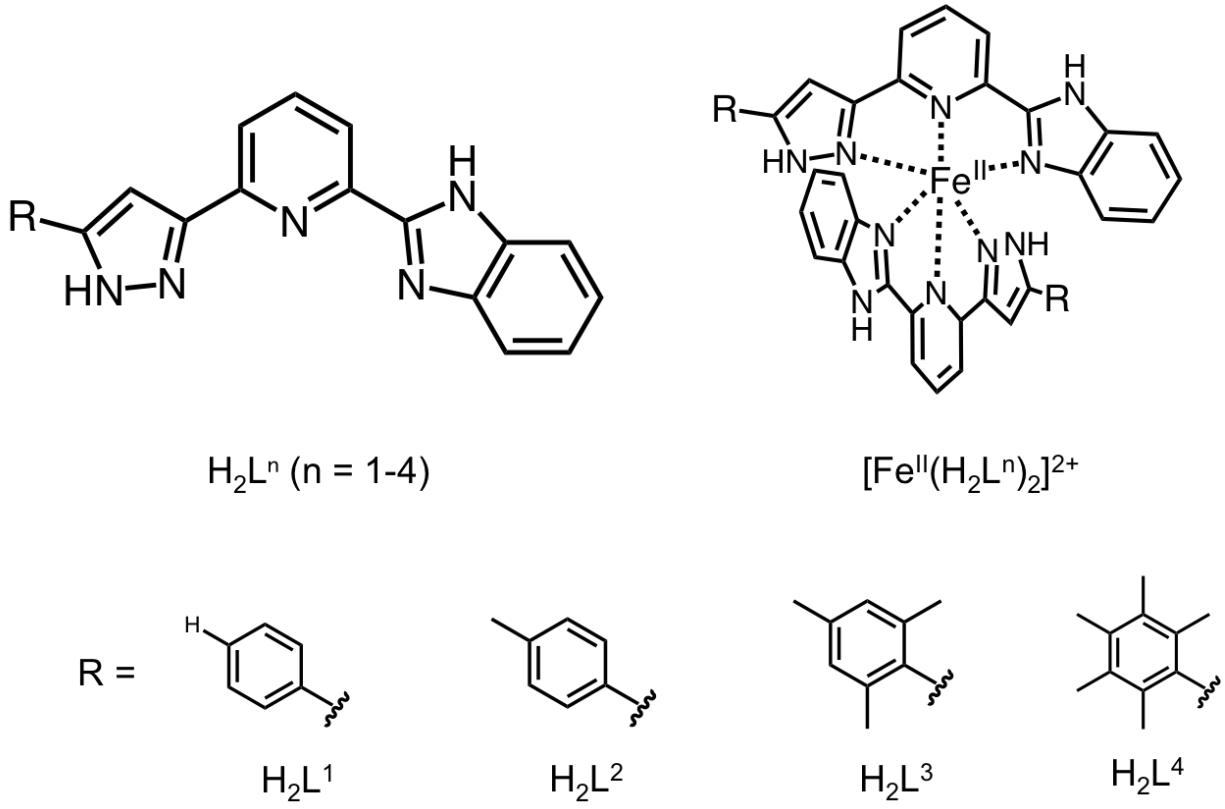

Scheme 2.1: Structures of ligands and complexes.

2.2 Experiments

Materials

All solvents and chemicals were reagent-grade, purchased commercially, and used without further purification unless otherwise noted.

X-ray Crystallography

Crystals were mounted on a glass capillary or a MiTeGen Dual-Thickness MicroMount, and data were collected at 100 K (Bruker SMART APEXII diffractometer coupled with a CCD area detector with graphite monochromated Mo-$K\alpha$ (λ = 0.71073 Å) radiation). The structure was solved using direct methods and expanded using Fourier techniques within the SHELXTL program. Empirical absorption corrections by SADABS were carried out.[10] In the structure analyses, non-hydrogen atoms were refined with anisotropic thermal parameters. Hydrogen atoms were included in calculated positions and refined with isotropic thermal parameters riding on those of the parent atoms. X-ray diffraction experiments at 20 K for complex **2'** after light irradiation using green laser (532 nm) were performed by using the synchrotron radiation source (λ = 1.0 Å) at Photon Factory BL-8A in High Energy Accelerator Research Organization (KEK), Japan.

Magnetic measurements

Variable-temperature magnetic susceptibility measurements were carried out on polycrystalline samples using a Quantum Design MPMS-XL SQUID magnetometer. Pascal's constants were used to determine the diamagnetic corrections.

Mössbauer spectra

Mössbauer experiments were carried out using a ^{57}Co/Rh source in a constant-acceleration transmission spectrometer (Topologic Systems) equipped with an Iwatani HE05/CW404 cryostat. The spectrometer was calibrated using standard *α*-Fe foil.

NMR measurements

^{1}H-NMR spectra were measured on a Bruker AVANCE400 spectrometer at room temperature. Chemical shifts in NMR were reported in ppm (δ), relative to the internal standard of tetramethylsilane (TMS). The signals observed were described as s (singlet), d (doublet), t (triplet), m (multiplets). The number of protons (n) for a given resonance is indicated as nH. Coupling constants are reported as *J* in Hz.

Elemental analysis

Elemental analyses were performed using a Perkin Elmer 2400 element analyzer.

The non-substituted tridentate ligand, H_2L^1, was synthesized by the following procedure described in Scheme 2.2. Ligands H_2L^{2-4} were synthesized following a protocol adapted from H_2L^1. Recrystallization methods, yield and characterization data were described as follows.

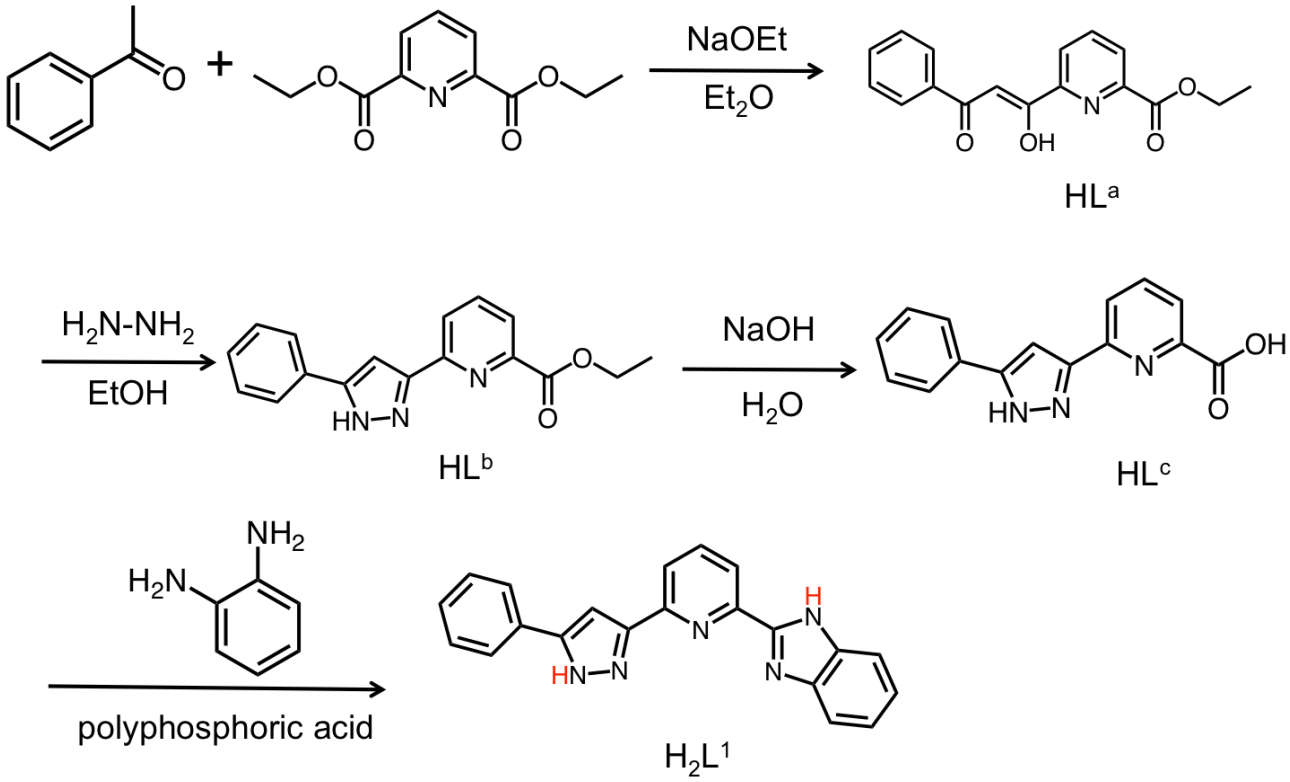

Scheme 2.2**:** Synthetic pathway of H_2L^1

Synthesis of 6-[1,3-dioxo-3-(2-phenyl)propionyl]pyridine-2-carboxylic acid ethyl ester (HL^a)

A solution of Na (3.18 g, 138 mmol) in 150 ml ethanol was stirred at room temperature. After stirring, sodium ethoxide was obtained as white solid by evaporation. To this solid, a solution of acetophenone (13.46 g, 112 mmol) and diethyl-2,6-pyridinedicarboxylate (25.00 g, 112 mmol) in diethyl ether were then added. Yellow solid was obtained after 2 h reflux. The solid was separated by filtration, and carefully washed with ether. After drying, the solid was added to 200 ml water and 20 ml of acetic acid was added with stirring. After 24 h stirring, yellow solid was obtained by filtration. Last, the white solid HL^a was obtained by recrystallization from ethanol (31.68 g, yield 95 %). ^{1}H NMR (400 MHz, $CDCl_3$): δ 1.51 (t, 3H), 4.54 (q, 2H), 7.28 (s, 1H), 7.53 (t, 2H), 7.60 (t, 1H), 7.71 (s, 1H), 8.04 (t, 1H), 8.11 (d, 2H), 8.26 (d, 2H), 8.35 (d, 2H).

Synthesis of 6-[5-phenyl-1*H*-pyrazol-3-yl-]-pyridine-2-carboxylic acid ethyl ester (HL^b)

A solution of hydrazine monohdrate (1.798 mL, 37.0 mmol) in 100 mL of ethanol was slowly added in a solution of HL^a (10 g, 33.6 mmol) in 300 mL of ethanol. The mixture was refluxed

for 1 h. After refluxing, the yellow solution was obtained. The solution was evaporated to remove ethanol and brown oil was obtained. Brown oil was dissolved in dichloromethane, and washed by water to remove impurities. After extraction, a pale yellow powder of HL^b was obtained by evaporation (6.61 g, yield 67 %). Anal. (calc.) for $C_{17.4}H_{16.4}N_3O_{0.3}$ ($C_{17}H_{15}N_3O_2 \cdot 0.2C_2H_5OH \cdot 0.1\ H_2O$): C,68.57 (68.67); H,5.33 (5.43); N,14.07 (13.81) %. ^{1}H NMR (400 MHz, $CDCl_3$): δ 8.35 (d, 2H), 8.26 (d, 2H), 8.11 (d, 2H), 8.04 (t, 1H), 7.71 (s, 1H), 7.60 (t, 1H), 7.53 (t, 2H), 7.28 (s, 1H), 4.54 (q, 2H), 1.51 (t, 3H). FT-IR (KBr, cm^{-1}): 3470 (s, $\nu_{N\text{-}H}$) 1713 (s, $\nu_{C=O}$).

Synthesis of 6-[5-phenyl-1*H*-pyrazol-3-yl-]-pyridine-2-carboxylic acid (HL^c)

A solution of 2 M NaOH in 100 mL of water was added in a solution of HL^b (3.01 g, 10.3 mmol) in 65 mL ethanol. After addition, the mixture was refluxed at 80 min and evaporated to remove ethanol. The white precipitate was solved in 300 mL H_2O and washed by dichloromethane to remove impurities. After extraction, the water layer was adjusted pH 8 by 12 M HCl, and stir 2 h at room temperature. White solid of HL^c was obtained by filtration and drying. The crude compound was used for synthesis of H_2L^1 (2.25 g, yield 82 %). Anal. (calc.) for $C_{15}H_{16}N_3O_{4.5}$ ($C_{15}H_{11}N_3O_2 \cdot 2.5H_2O$): C,58.21 (58.06); H,4.80 (5.20); N,13.61 (13.54) %. FT-IR (KBr, cm^{-1}): 3334 (s, $\nu_{N\text{-}H}$) 1701 (s, $\nu_{C=O}$).

Synthesis of 2-[6-[5-(phenyl)-1*H*-pyrazol-3-yl]-2-pyridinyl]-1*H*-benzimidazole (H_2L^1)

HL^c (2.10 g, 7.9 mmol) was added in polyphosphoric acid (25 g) at 180 ^{o}C and stirred 15 min. After stirring, *o*-phenylenediamine (0.854 g, 7.9 mmol) was added and stirred 7 h. The resulting dark green oil was added to water and a pale gray/green suspension was obtained. This mixture was adjusted to pH 10 by using 28 % ammonia solution. A dark beige solid was then obtained by filtration. The filtered solid was then re-dissolved in hot acetone and filtered once more to remove impurities. A beige microcrystalline powder of H_2L^1 was then obtained by evaporation of acetone. (1.68 g, yield 63 %) Anal. (calc.) for $H_2L \cdot 2H_2O$ ($C_{21}H_{19}N_5O_2$): C,67.55 (67.85); H,5.13 (5.16); N,18.75 (18.78) %. ^{1}H NMR (400 MHz, $CDCl_3$): δ 12.96 (s, 1H), 8.22 (d, 1H), 8.10 (t, 1H), 8.02 (d, 1H), 7.92 (d, 2H), 7.76 (d, 1H), 7.67 (d, 1H), 7.63 (s, 1H), 7.51 (t, 2H), 7.39 (t, 1H), 7.34 (t, 1H), 7.29 (t, 1H). FT-IR (KBr, cm^{-1}): 3201.8 (s, $\nu_{N\text{-}H}$) 1602.9 (s, $\nu_{C\text{-}H}$).

Synthesis of H_2L^2

A beige powder of H_2L^2 was obtained by evaporation of acetone. (yield 79.2 %) Anal. (calc.) for $H_2L^2 \cdot H_2O$ ($C_{22}H_{19}N_5O$): C,71.60 (71.53); H,5.36 (5.18); N,18.88 (18.96) %. ^{1}H NMR (400 MHz, DMSO): δ 8.22 (d, 1H), 8.09 (t, 1H), 8.01 (d, 1H), 7.80 (d, 2H), 7.76 (d, 1H), 7.67 (d, 1H), 7.58 (s, 1H), 7.31 (m, 4H), 2.37 (s, 3H). FT-IR (KBr, cm^{-1}): 3142.0 (s, $\nu_{N\text{-}H}$) 1600.9 (s, $\nu_{C\text{-}H}$).

Synthesis of H_2L^3

A beige powder of H_2L^3 was obtained by evaporation of acetone. (yield 37.0 %) Anal. (calc.) for $H_2L^3 \cdot 0.5H_2O$ ($C_{24}H_{22}N_5O_{0.5}$): C,74,21 (74.20); H,5.65 (5.71); N,18.22 (18.03) %. ^{1}H NMR (400 MHz, $CDCl_3$): δ10.9 (s, 1H), 8.38 (d, 1H), 7.93 (t, 1H), 7.85 (t, 1H), 7.47 (t, 1H), 7.28 (m, 2H), 7.26 (s, 1H), 6.97 (s, 2H), 6.90 (s, 1H), 2.32 (s, 3H), 2.16 (s, 6H).4 FT-IR (KBr, cm^{-1}): 3203.8 (s, ν_{N-H}) 1604.8 (s, ν_{C-H}).

Synthesis of H_2L^4

A brown powder of H_2L^4 was obtained by evaporation of acetone. (yield 41.2 %) Anal. (calc.) for ($H_2L^4 \cdot H_2O \cdot 0.8(CH_3)_2CO$) $C_{28.4}H_{31.8}N_5O_{1.8}$: C,72.18 (72.27); H,6.70 (6.79); N,14.97 (14.84) %. ^{1}H NMR (400 MHz, DMSO): δ12.89 (s, 1H), 8.21 (d, 1H), 8.05 (d, 2H), 7.74 (d, 1H), 7.60 (d, 1H), 7.27 (m, 2H), 2.26 (s, 3H), 2.22 (s, 6H). 2.01 (s, 6H), FT-IR (KBr, cm^{-1}): 3172.9 (s, ν_{N-H}) 1599.0 (s, ν_{C-H}).

Synthesis of $[Fe^{II}(H_2L^1)_2](BF_4)_2 \cdot 1.5(C_3H_7CN)$ (1)

$Fe(BF_4)_2 \cdot 6H_2O$ (100 mg, 0.297 mmol) in butyronitrile (5 ml) was added to H_2L^1 (201 mg, 0.598 mmol) in butyronitrile (30 ml) and stirred for 5 min at room temperature. After stirring, the red solution was filtered to remove impurities. The red block crystals of $[Fe^{II}(H_2L^1)_2](BF_4)_2 \cdot 3(C_3H_7CN)$ (**1'**) were obtained by slow evaporation for 2 days. Crystals were collected by vacuum filtration, affording $[Fe^{II}(H_2L)_2](BF_4)_2 \cdot 1.5(C_3H_7CN)$ (**1**) for physical measurements. (177 mg, yield 56.2 %) Anal. (calc.) for $C_{48}H_{40.5}N_{11.5}B_2F_8Fe$ (**1**$\cdot 1.5C_3H_7CN$): C,57.20 (57.19); H,4.05 (4.19); N,15.98 (15.94) %. FT-IR (KBr, cm^{-1}) 3284.8 (s, ν_{N-H}) , 1047.3 (s, ν_{B-F}).

Synthesis of $[Fe^{II}(H_2L^2)_2](BF_4)_2 \cdot 0.5(i\text{-}Pr_2O) \cdot 2(H_2O) \cdot 2(CH_3OH)$ (2)

Methanol solution (5 mL) of $Fe(BF_4)_2 \cdot 6H_2O$ (30.0 mg, 0.09 mmol) was added to a solution of H_2L^2 (63.2 mg, 0.18 mmol) in methanol (10 mL). The resulting red solution was filtered and allowed to diffuse with *i*-Pr_2O. After a few days, red plates of $[Fe^{II}(H_2L^1)_2](BF_4)_2 \cdot (i\text{-}Pr_2O) \cdot 2(CH_3OH)$ (**2'**) had formed. The crystals were collected by suction and air-dried, affording $[Fe^{II}(H_2L^1)_2](BF_4)_2 \cdot 0.5(i\text{-}Pr_2O) \cdot 2(H_2O) \cdot 2(CH_3OH)$ (**2**). Yield 55.9 mg (66.4 %). Anal. (calc.) for $C_{49}H_{53}N_{10}O_{4.6}B_2F_8Fe_1$: C, 54.41 (54.32); H, 4.76 (4.93); N, 13.18 (12.93) %. FT-IR (KBr, cm^{-1}): 3277.1 (s, ν_{N-H}), 1084 (s, ν_{B-F}).

Synthesis of $[Fe^{II}(H_2L^3)_2](BF_4)_2 \cdot 0.5(AcOEt) \cdot 0.5(H_2O) \cdot 1.5(CH_3OH)$ (3).

Methanol solution (5 mL) of $Fe(BF_4)_2 \cdot 6H_2O$ (34 mg, 0.10 mmol) was added to a solution of H_2L^3 (75.8 mg, 0.20 mmol) in methanol (10 mL). The resulting red solution was filtered and allowed to diffuse with AcOEt. After a few days, red plates of $[Fe^{II}(H_2L^3)_2](BF_4)_2 \cdot (AcOEt) \cdot 1.5(CH_3OH)$ (**3'**) were obtained. The crystals were collected by suction and air-dried, affording $[Fe^{II}(H_2L^2)_2](BF_4)_2 \cdot 0.5(AcOEt) \cdot 0.5(H_2O) \cdot 1.5(CH_3OH)$ (**3**). Yield 55.4 mg (56.1 %). Anal. (calc.) for $C_{49.5}H_{49}N_{10}O_2B_2F_8Fe_1$: C, 56.51 (56.87); H, 5.01 (4.72); N, 13.30 (13.40) %. FT-IR (KBr, cm^{-1}): 3280.9 (s, ν_{N-H}), 1051.2 (s, ν_{B-F}).

Synthesis of $[Fe^{II}(H_2L^4)_2](BF_4)_2 \cdot 2.5(H_2O) \cdot (i\text{-}Pr_2O)$ (4).

Methanol solution (5 mL) of $Fe(BF_4)_2 \cdot 6H_2O$ (34 mg, 0.10 mmol) was added to a solution of H_2L^4 (1.0 mg, 0.20 mmol) in methanol (10 mL). The resulting red solution was filtered and allowed to diffuse with i-Pr_2O. After a few days, red plates of $[Fe^{II}(H_2L^4)_2](BF_4)_2 \cdot 2(i\text{-}Pr_2O)$ (**4'**) were obtained. The crystals were collected by suction and air-dried, affording $[Fe^{II}(H_2L^4)_2](BF_4)_2 \cdot 2.5(H_2O) \cdot (i\text{-}Pr_2O)$ **(4).** Yield 33.4 mg (32 %). Anal. (calc.) for $C_{52}H_{55}N_{10}O_{2.5}B_2F_8Fe_1$: C, 57.51 (57.32); H, 5.20 (5.09); N, 12.55 (12.86) %. IR (KBr, cm^{-1}): 3280.8 (s, ν_{N-H}), 1057.0 (s, ν_{B-F}).

Table 2.1: Crystal parameters of **1'**

	100 K	270 K
Formula	$C_{42}H_{30}B_2F_8FeN_{10}$	$C_{42}H_{30}B_2F_8FeN_{10}$
M / g mol^{-1}	904.23	904.23
Crystal system	Monoclinic	Monoclinic
Space Group	*C*2/c	*C*2/c
a / Å	23.06 (4)	23.590 (5)
b / Å	12.49 (2)	12.299 (2)
c / Å	19.42 (4)	19.719 (4)
α / °	90	90
β / °	118.659 (18)	116.05 (3)
γ / °	90	90
V / Å^3	4908 (15)	5140 (2)
Z	4	4
d / g cm^{-3}	1.224	1.168
μ / mm^{-1}	0.376	0.359
λ / Å	0.71073	0.71073
*R*1 (*I* > 2σ(*I*))	0.0660	0.0643
*wR*2 (*I* > 2σ(*I*))	0.1382	0.1410

Table 2.2: Crystal parameters of **2'.**

	20 K	100 K	270 K	LIESST
Formula	$C_{51.5}H_{58}N_{10}$ $O_4B_2F_8Fe$	$C_{52}H_{56}N_{10}$ $O_3B_2F_8Fe$	$C_{52}H_{56}N_{10}$ $O_3B_2F_8Fe$	$C_{52}H_{57}N_{10}$ $O_{3.5}B_2F_8Fe$
M / g mol^{-1}	1110.55	1098.53	1098.53	1107.54
Crystal system	Monoclinic	Monoclinic	Monoclinic	Monoclinic
Space group	*C*2/c	*C*2/c	*C*2/c	*C*2/c
a / Å	31.8358 (9)	32.019 (3)	32.372 (12)	32.0647 (13)
b / Å	16.2318 (6)	16.3126 (14)	16.452 (6)	16.2520 (5)
c / Å	24.1500 (13)	24.246 (2)	24.557 (16)	24.1773 (17)
α / ^{o}	-	-	-	-
β / ^{o}	121.0380 (10)	121.2070 (10)	121.401 (4)	121.5440 (10)
γ / ^{o}	-	-	-	-
V / Å^3	10692.8 (8)	10831.7 (16)	11164 (9)	10737.5 (9)
Z	8	8	8	8
d / g cm^{-3}	1.380	1.347	1.307	1.370
μ / mm^{-1}	0.889	0.358	0.347	0.883
*R*1 ($I > 2\sigma(I)$)	0.0920	0.0860	0.0689	0.1078
R_w2 ($I > 2\sigma(I)$)	0.2535	0.2231	0.1892	0.2970

Table 2.3: Crystal parameters of **3'** and **4'**.

	Comp. **3'** (100 K)	Comp. **4'** (100 K)
Formula	$C_{53.5}H_{56}N_{10}$	$C_{64}H_{78}N_{10}$
	$O_{3.5}N_{10}B_2F_8Fe$	$O_2B_2F_8Fe$
M / g mol^{-1}	1124.55	1248.83
Crystal system	Triclinic	Monoclinic
Space group	$P\bar{1}$	$P2_1/n$
a / Å	12.496 (10)	18.389 (3)
b / Å	12.836 (10)	16.551 (3)
c / Å	17.661 (14)	22.333 (3)
α / °	85.769 (8)	-
β / °	73.318 (11)	112.772 (2)
γ / °	84.140 (11)	-
V / Å^3	2696 (4)	6267.2 (16)
Z	2	4
d / g cm^{-3}	1.385	1.324
μ / mm^{-1}	0.362	0.317
*R*1 ($I > 2\sigma(I)$)	0.1422	0.1335
R_w2 ($I > 2\sigma(I)$)	0.3343	0.2993

2.3 Results and discussion

Crystal structures

All complexes were determined by single-crystal X-ray measurement. The crystallographically determined structures of complexes are shown in Figure 2.1-4.

1' was synthesized as red block crystals in the mixture of H_2L^1 and Fe(II) tetrafluoroborate. **1'** crystallized in the *C*2/c space group and temperature dependent structural data were collected at 100 K and 270 K (Table 2.1). This is a mononuclear complex which is constructed from two ligands and one iron ion (Figure 2.1 (a)). The iron ion is coordinated by two tridentate binding sites of H_2L^1 (pyrazole, pyridine, benzimidazole), resulting in an N6 coordination environments. Four Brønsted moieties (pyrazoles and benzimidazoles) are all protonated, and there are two tetrafluoroborate ions per complex. Thus, the iron ion is divalent. The average bond length between the iron ion and the nitrogen atoms is 1.96 Å at 100 K, with a Σ value of 96.4°, it means the iron ion is low spin. As for the intermolecular interactions, there are weak hydrogen bonds between complex cations and counter anions (Figure 2.1 (b)). In addition, π-π-stacking interactions are observed between phenyl moieties. These interactions form 3D networks and are likely to result in a strong cooperative effect in the crystals. Increasing the measurement temperature from 100 K to 270 K, resulted in changes to the structure and the color of the solid. The space group is still same, *C*2/c, but the Fe-N average bond length and Σ-value increased to, 2.15 Å and 142.1° respectively. These values are characteristic for Fe(II) in its high spin state, so **1'** was spin crossover complex.

Complex **2'** crystallizes in the monoclinic space group *C*2/c (Figure 2.2). The cationic part of the complex consists of two H_2L^2 ligands and one Fe(II) ion, forming a bis-chelate type mononuclear structure. The Fe(II) ion exists in an octahedral coordination environment, coordinated by six nitrogen atoms from two H_2L^2 ligands. At 100 K, the average Fe-N distance is 2.097 Å, and the Σ value is 124.1°, which suggests a mixture of high and low spin states (Figure 2.2 top). The thermal ellipsoids of the benzimidazole group are elongated towards the direction of the benzimidazole plane, which implies a mixture of two coordination modes. From the data collected at 20 K with the synchrotron X-ray source, the coordinated benzimidazole group was solved in two positions, the occupancies of which were equal (Figure 2.2 center). The average Fe-N distances are 2.063 Å and 2.097 Å, and the Σ values are 110.6° and 138.3° for the low and high spin parts, respectively. The average dihedral angle between the pyrazole and trimethylphenyl moieties is 12.30°. Structural analysis of **2'** at 270 K was also performed, and confirmed that the iron ion has a high spin state based on coordination bond length (2.173 Å) and Σ value (140.0°). These data are consistent with partial spin crossover behavior.

Complex **3'** crystallizes in the triclinic space group $P\bar{1}$ (Figure 2.3). The structure of **3'** is similar to **2'**, but the solvent molecules and intermolecular interactions are different. At 100 K, the

average Fe-N distance is 2.129 Å, and the Σ value is 136.5°, indicating a mixture of low and high spin complexes. The lattice contains disordered trimethyl phenyl groups and BF_4^- anions. The average dihedral angle between the pyrazole and trimethylphenyl moieties is 70.39°. Hydrogen bonded interactions are operative between two pyrazole groups and methanol molecules, and two benzimidazole groups and BF_4^- anions respectively, forming a one-dimensional chain structure along the *b* axis (Figure 2.3). There are π-π stacking interactions between benzimidazole moieties, forming a dimer of iron complexes.

Complex **4'** crystallizes in the monoclinic space group $P2_1/n$ (Figure 2.4). The structure of **4'** is also similar to that of **2'**, but again, the solvent molecules and interactions with counter anions are different. The Fe (II) ion exists in an octahedral coordination environment, coordinated by six nitrogen atoms from two H_2L^4 ligands. At 100 K, the average Fe-N distance is 2.178 Å, and the Σ value is 142.3°, indicative of a Fe (II) ion in the high spin state. The average dihedral angle between pyrazole and trimethylphenyl moieties is 73.61°. Disordered BF_4^- anions are present in the lattice. One pyrazole moiety interacts with a solvent *i*Pr_2O molecule, while the other pyrazole group interacts with a BF_4^- anion. Two benzimidazole groups interact with BF_4^- anions. In the lattice, BF_4^- anions link mononuclear iron moieties, forming a one-dimensional network structure. There are two kinds of π-π stacking interactions; one between pentamethylphenyl and benzimidazole groups, and the other between two benzimidazole groups.

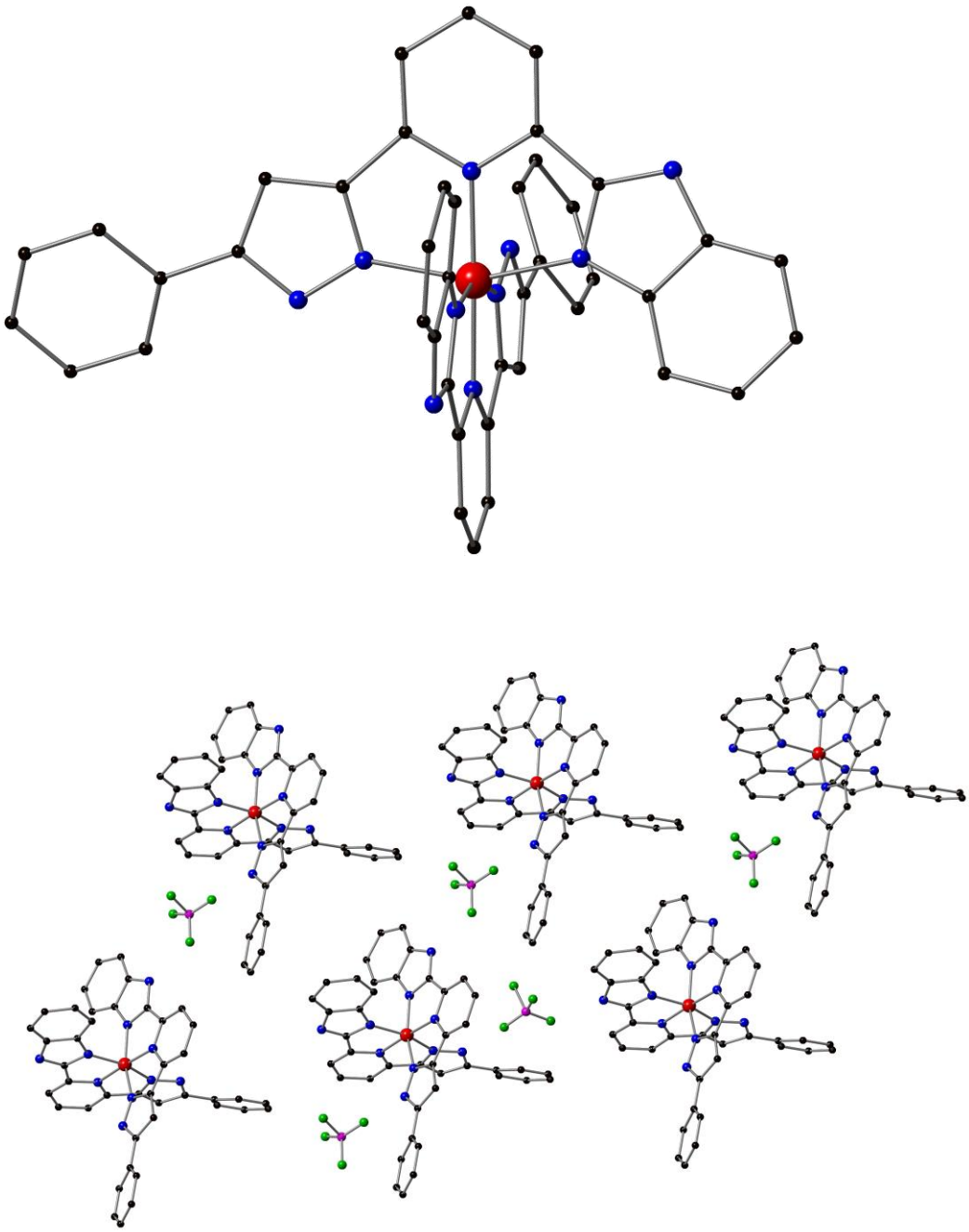

Figure 2.1: Molecular structure (top) and three-dimensional hydrogen bond network (bottom) of **1'** at 100 K. Hydrogen bonds were formed between complex cation and counter anion BF_4^- chain through network structure of **1'.** Colour code: C, black; N, blue; Fe(II), red.

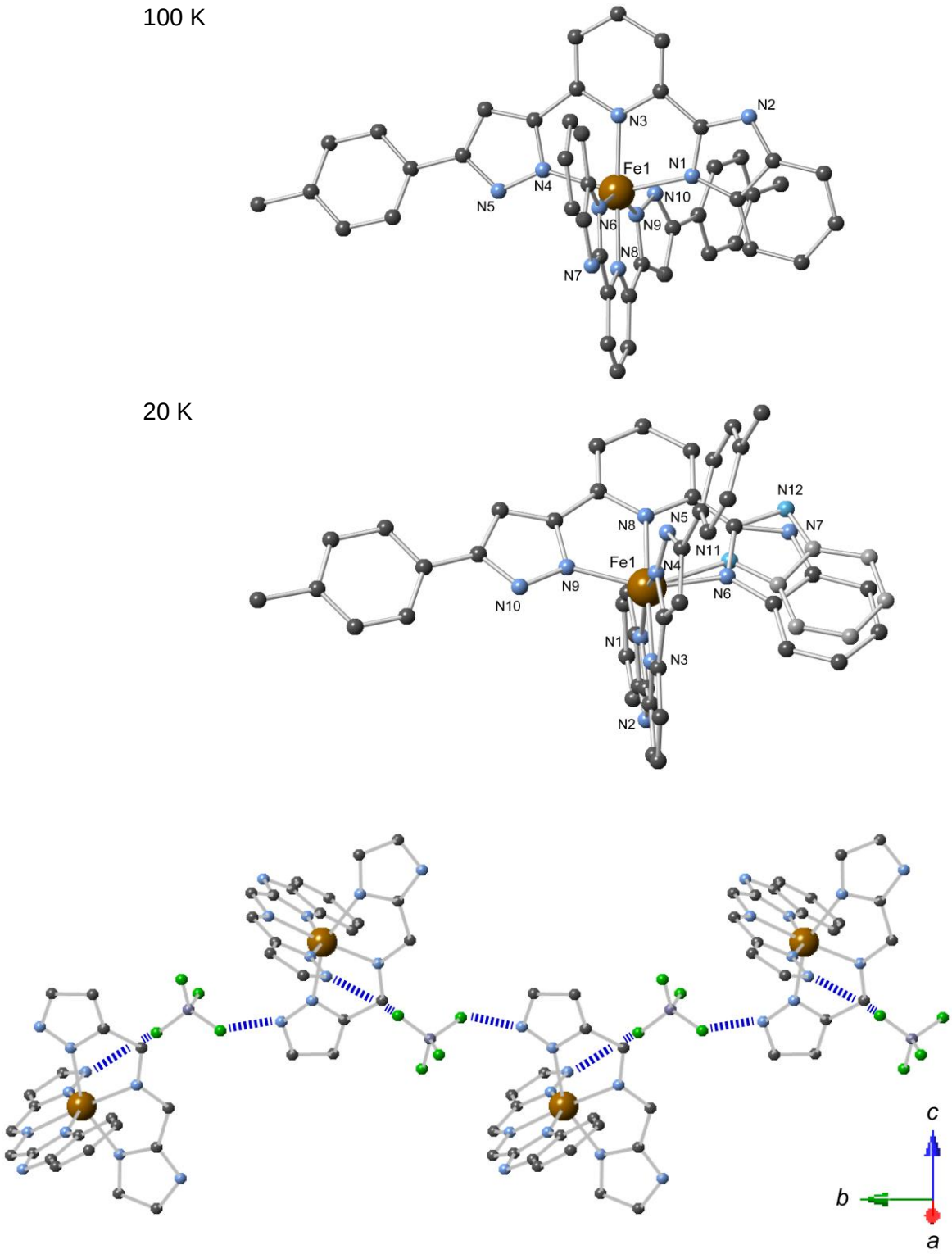

Figure 2.2: Molecular structure (top: 100 K, center: 20 K) and one-dimensional chain network structure (bottom) of **2'**. Carbon atoms of phenyl and pyridyl rings were omitted for clarity. Lattice solvents and non-interacting BF_4^- anions have been omitted. Color code: C, grey; N, light blue; Fe(II), brown.

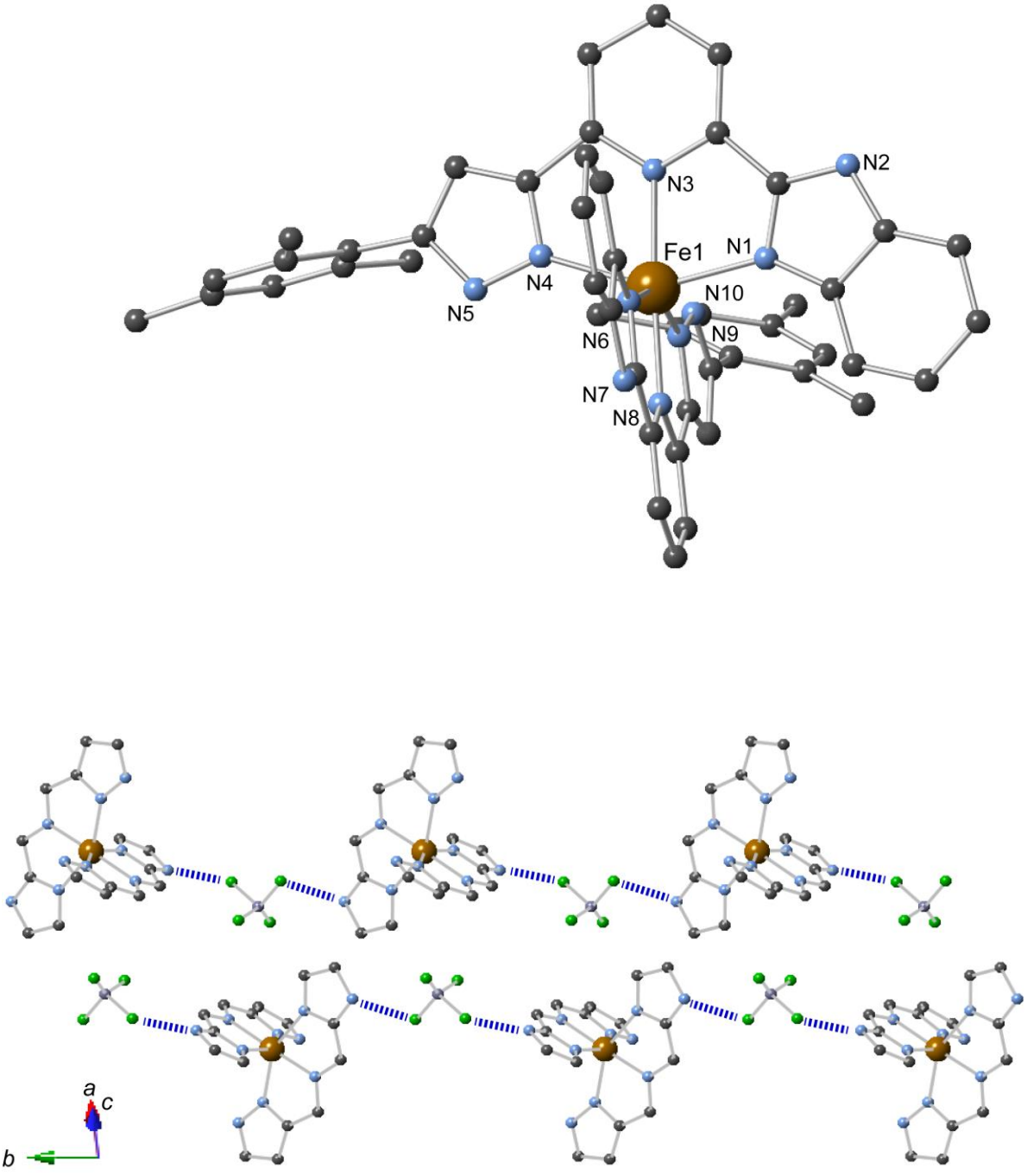

Figure 2.3: Molecular structure and one-dimensional chain network structure of **3'**. Carbon atoms of the phenyl and pyridyl rings were omitted for clarity. Lattice solvents and non-interacting BF_4^- anions have been omitted. Color code: C, grey; N, light blue; Fe(II), brown.

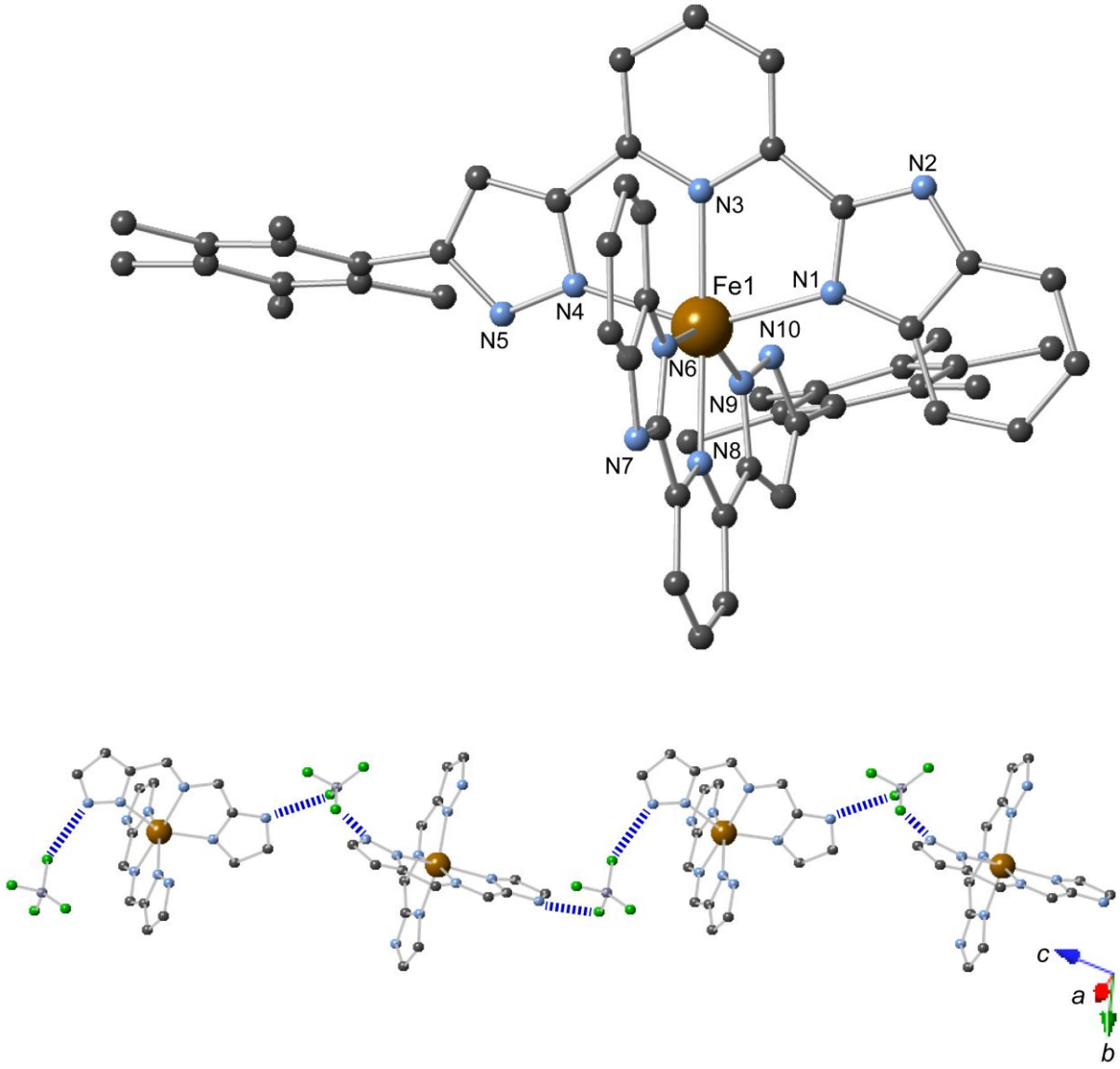

Figure 2.4: Molecular structure one-dimensional chain network structure of **4'**. Carbon atoms of phenyl and pyridyl rings were omitted for clarity. Lattice solvents and non-interacting BF_4^- anions have been omitted. Color code: C, grey; N, light blue; Fe(II), brown.

Magnetic properties of 1

DC magnetic susceptibilities of the crystalline sample of **1** were measured under an applied magnetic field of 10000 Oe. $[Fe^{II}(H_2L^1)_2](BF_4)_2$ displays rapid spin conversion at $T_{1/2}$ = 260.5 K. From 300 K to 260 K, the $\chi_m T$ of $[Fe^{II}(H_2L^1)_2](BF_4)_2$ was constant at 3.33 emu mol^{-1} K, which is close to the spin only value expected for four unpaired electrons, S = 2 (3.0 emu mol^{-1} K), suggesting that all Fe(II) centres were in the HS state (Figure 2.5). High temperature single-crystal X-ray structural analysis of **1'** 270 K supports this assignment. At low temperatures **1** is essentially diamagnetic, however it was also demonstrated that **1** shows a low-temperature photo-magnetic response based on conversion to the HS state through light-induced excited spin state trapping (LIESST) on irradiation with both green and red laser light (Figure 2.6). Temperature dependent Mössbauer spectroscopy of **1** at 270 K and 100 K are listed in Figure 2.7. At high temperature, the spectrum showed a quadrupole doublet, and parameters of isomer shift (δ) and quadrupole splitting (ΔE_Q) are δ = 0.96 mm s^{-1} with ΔE_Q = 1.80 mm s^{-1}, suggesting that all iron ions are in the Fe(II) HS state. At low temperature, however, the spectrum shifted and was fitted to give δ = 0.435 mm s^{-1} and ΔE_Q = 0.670 mm s^{-1}. These parameters are typical values of the Fe(II) LS state and suggest spin transition of complex **1**.

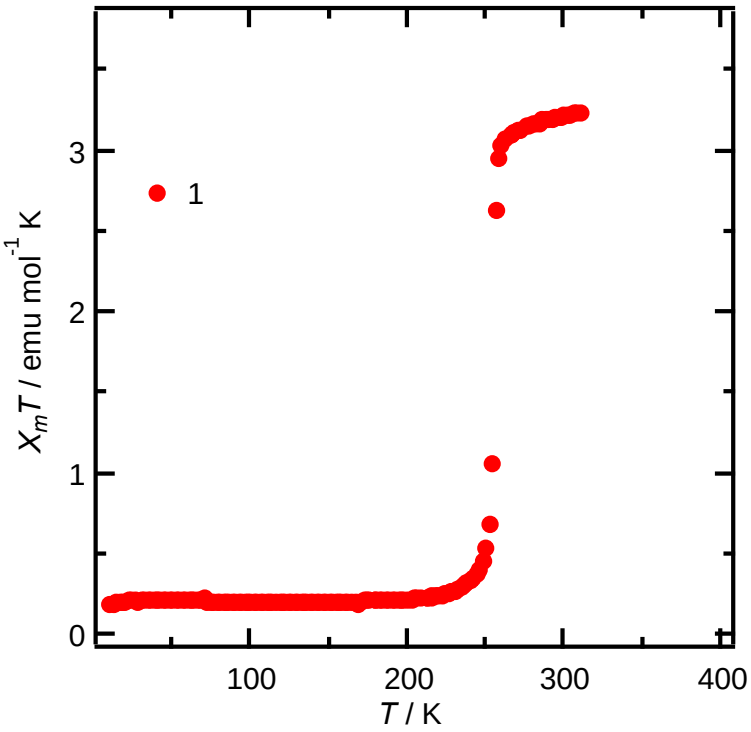

Figure 2.5: The thermal magnetic susceptibility data of **1**.

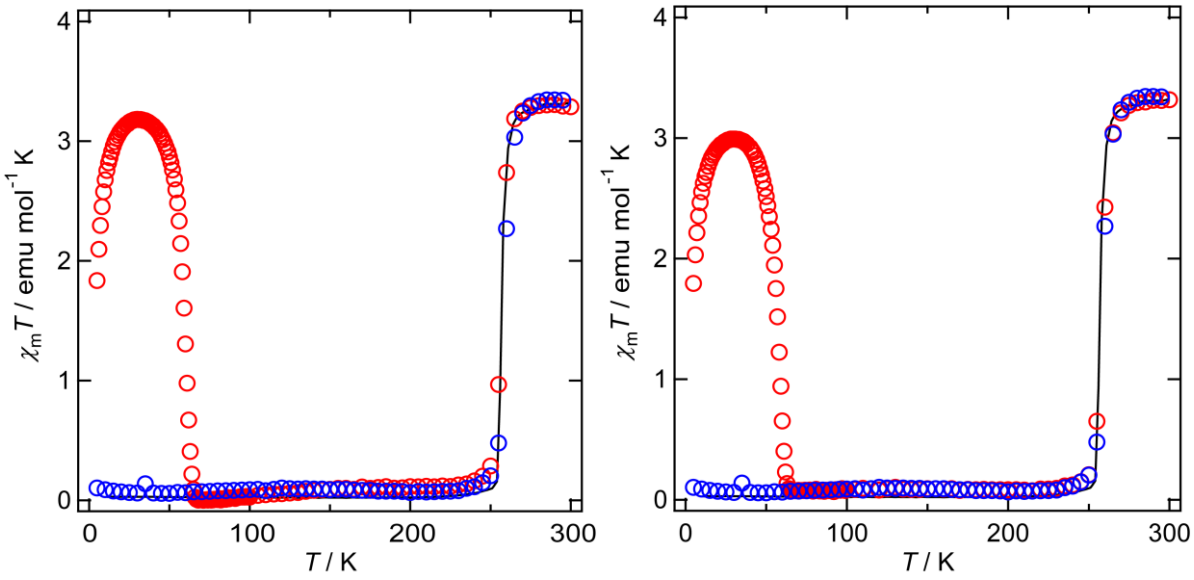

Figure 2.6: Light induced magnetic susceptibility data collected for **1**. (Left; 532 nm laser, Right; 808 nm laser). Red circle: heating, blue circle: cooling, solid line: bulk data.

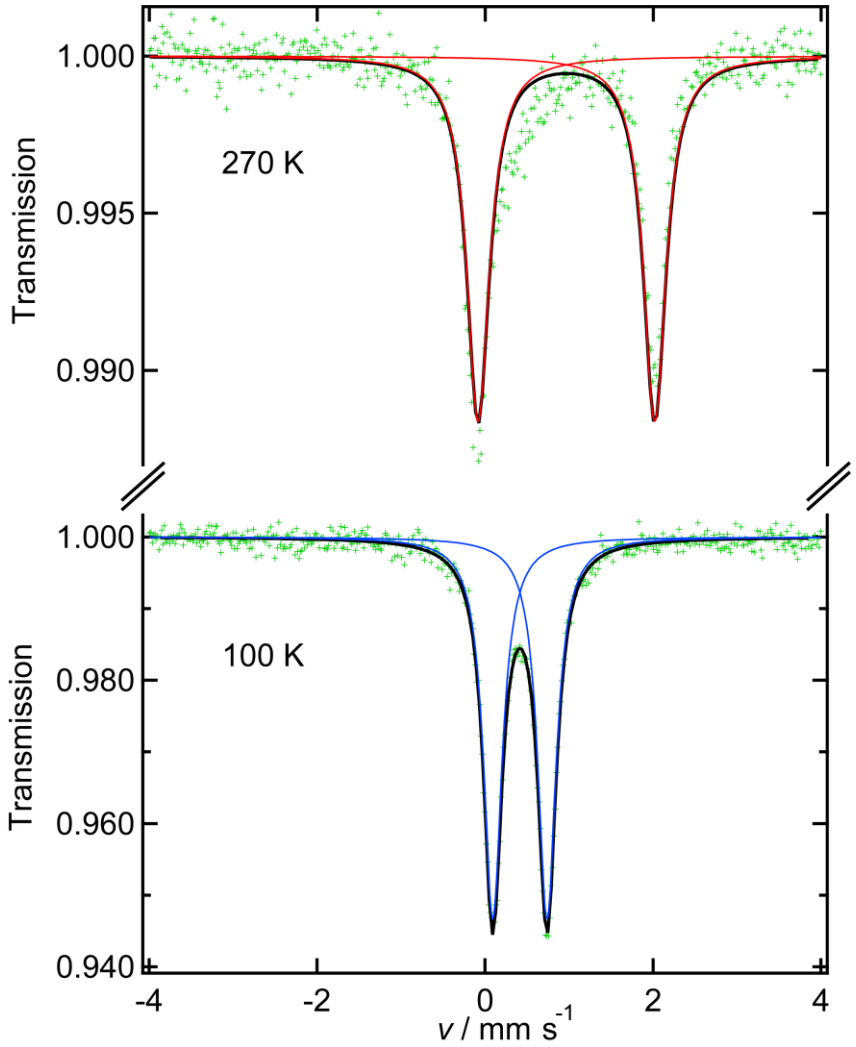

Figure 2.7: Mössbauer spectra of **1** at 270 K (top) and 100 K (bottom).

Table 2.4: Mössbauer parameters for **1**.

T / K	δ_{IS} (mm / s)	ΔE_Q (mm / s)	Spin state
270	1.119	2.870	Fe(II) HS
100	0.435	0.670	Fe(II) LS

Magnetic properties of 2-4

The magnetic susceptibilities of **2**-**4** were studied by SQUID magnetometor. The $\chi_m T$ vs. T plots for all complexes are shown in Figure 2.8. Complexes **2** and **3** show gradual SCO behavior, while complex **4** has a high spin state (S = 2) in the whole temperature range. The $\chi_m T$ values for **2** and **3** at room temperature are 3.11 and 3.37 emu mol^{-1} K, values consistent with magnetically isolated high-spin Fe(II) ions (S = 2). Spin crossover temperatures for **2** and **3** were determined by maxima on the $d\chi/dT$ plots, affording 200 K and 250 K, respectively. Below 100 K, the $\chi_m T$ values for **2** and **3** were almost constant (1.46 and 1.59 emu mol^{-1} K, respectively). The paramagnetic state indicates partial spin transition of the iron ions, in agreement with the structural data discussed above. Complexes **2**-**4** exhibit different magnetic behavior originating from the steric and packing effects of the ligands.

The densities of the crystals are 1.347, 1.385, and 1.324 g cm^{-3} for complexes **2'**, **3'** and **4'** respectively. One can also speculate that this may influence the magnetic behavior and that the lower density exhibited by **3'** may stabilize a high spin state in the lower temperature region. A detailed consideration of packing effects will require estimation of precise thermodynamic parameters and DFT calculations.[11] In order to elucidate this partial spin transition, Mössbauer spectra were measured for complex **2** at 20 K and 300 K (Figure 2.9-10). At 20 K, the data can be analysed as a mixture of high- and low spin iron(II) species. On the other hand, the data collected at 300 K reveals only high spin iron(II) species. These facts indicate the occurrence of partial spin crossover in **2**. The obtained fitting parameters for Fe(II) high- or low-spin species are reasonable values for low symmetry SCO complexes.[1]

LIESST experiments were conducted on complex **2**, and the magnetic data is shown in Figure 2.11. An increase in $\chi_m T$ values was observed after light irradiation with a green. Structural analyses after light irradiation were also performed at the KEK synchrotron and the high spin state of Fe(II) ion was confirmed based on average coordination bond lengths (2.127 Å) and Σ values (129.1°).

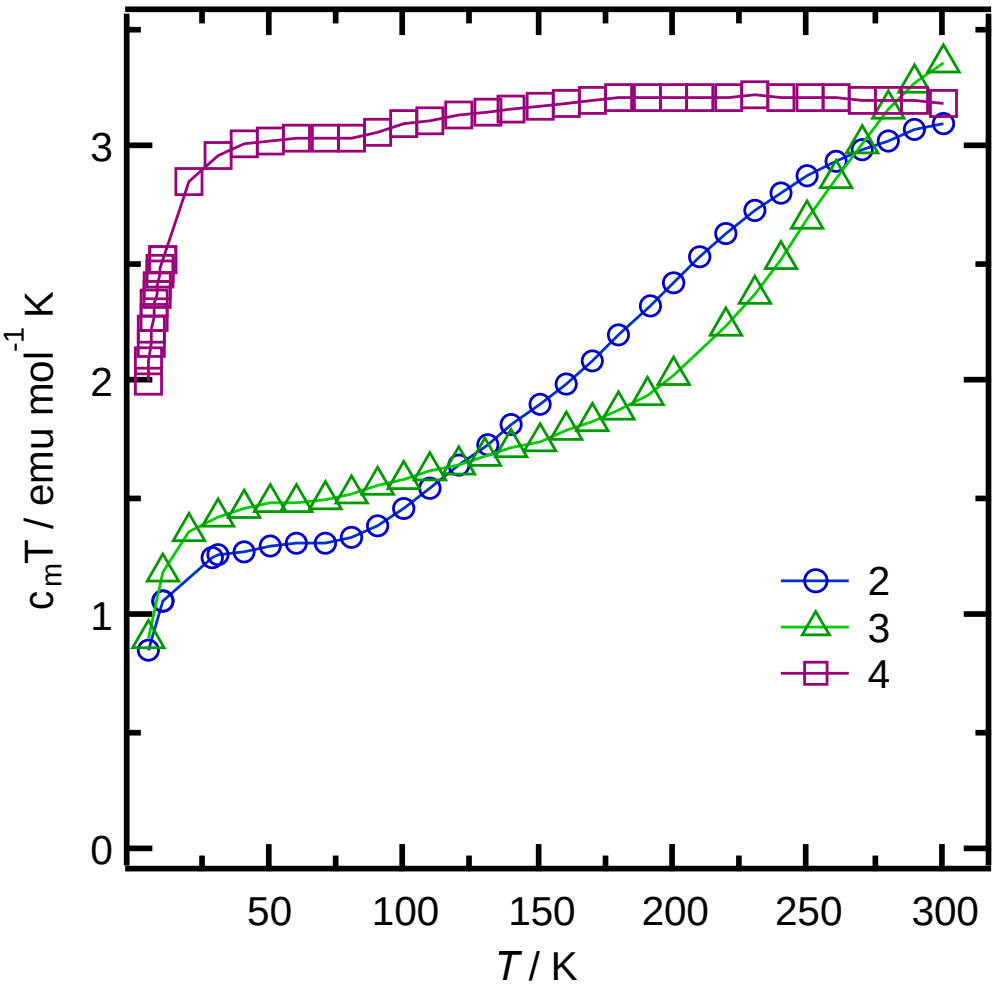

Figure 2.8: The thermal magnetic susceptibility data of **2**, **3**, and **4**.

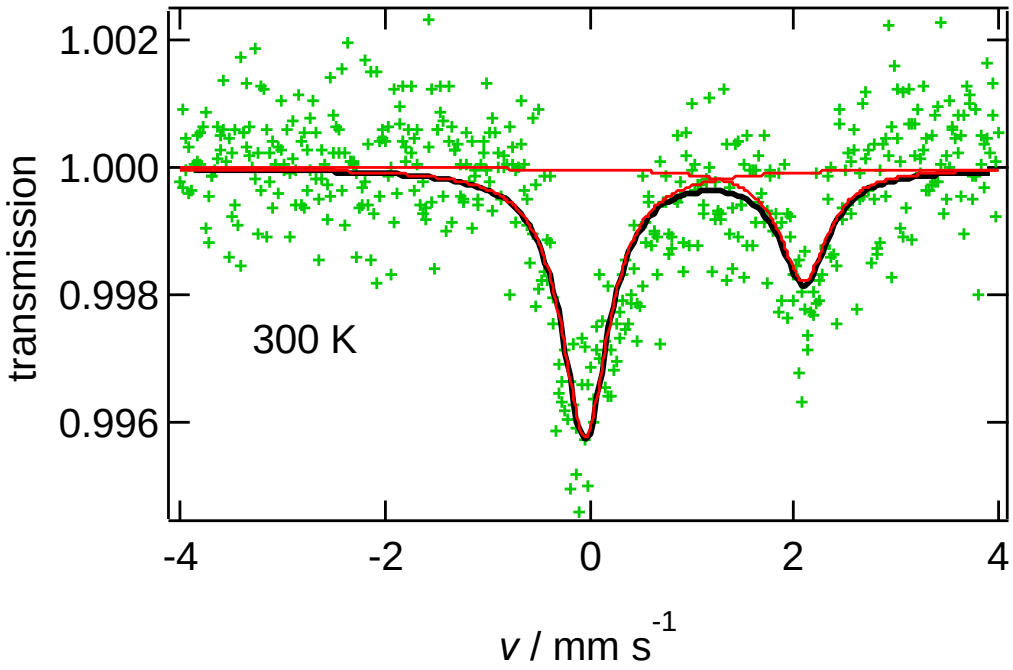

Figure 2.9: Mössbauer spectra of **2** at 300 K**.**

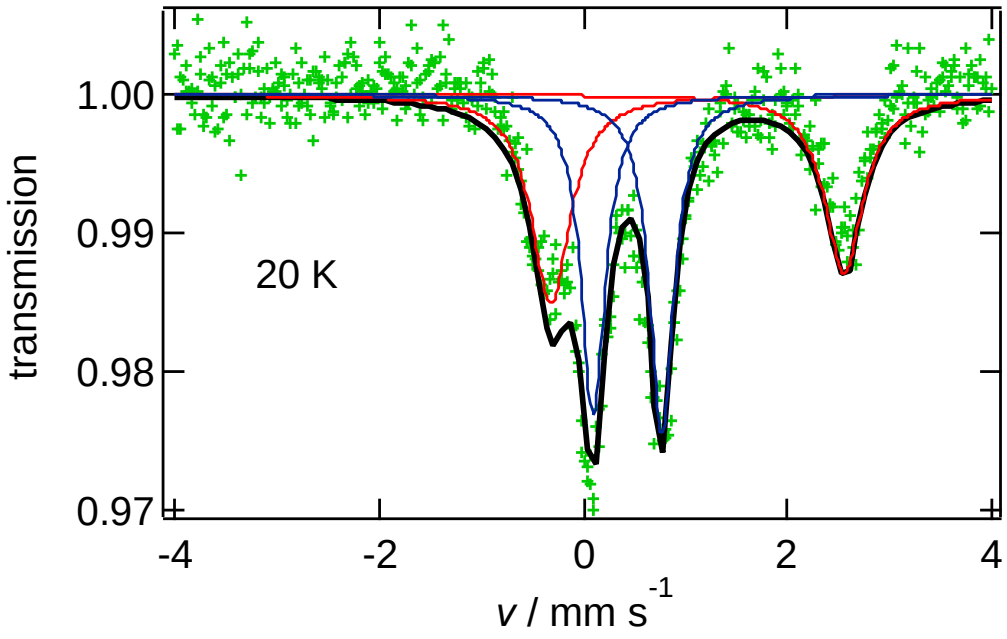

Figure 2.10: Mössbauer spectra of **2** at 20 K.

Table 2.5: Mössbauer parameters for **2** at 300 K.

δ_{IS} (mm / s)	ΔE_Q (mm / s)	Spin state
1.028	2.140	Fe(II) HS

Table 2.6: Mössbauer parameters for **2** at 20 K.

δ_{IS} (mm / s)	ΔE_Q (mm / s)	Spin state	Area fraction (%)
0.435	0.670	Fe(II) LS	51.0
1.119	2.870	Fe(II) HS	49.0

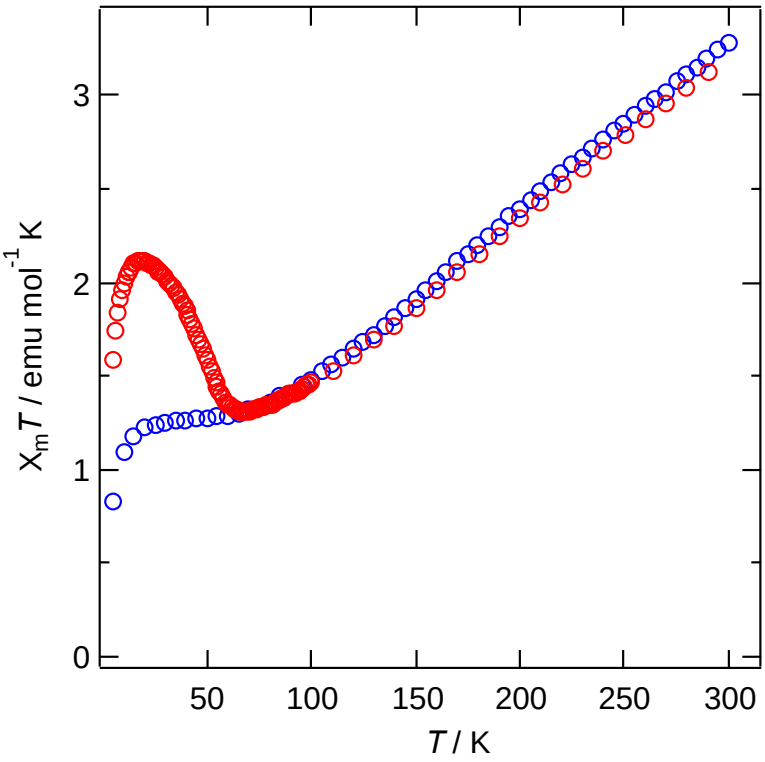

Figure 2.11: Green light induced magnetic susceptibility data collected for **2**. (Blue circle: before light irradiation, Red circle: after light irradiation)

2.4 Conclusion

Three Fe(II) complexes of the general formula $[Fe^{II}(H_2L^{1\text{-}4})_2](BF_4)_2 \cdot x(solv.)$, with different substituent groups, were synthesized and their electronic states were investigated. Complexes **1**, **2** and **3** show spin crossover behaviour, while **4** has a high-spin state in the temperature range of 1.8 - 300 K. The substituent groups affect the supramolecular packing of the molecular species. These structural perturbations are passed on to the coordination geometries of the iron ions, significantly influencing the spin states of the complexes. This insight into the design of modified asymmetric mononuclear SCO complexes will aid in the future fine design of bistable molecular systems.

References

[1] (a) W.R. Browne and B.L. Fringa, *Chimia*, **2010**, *64*, 398-403; (b) O. Sato, J. Tao and Y.-Z. Zhang, *Angew. Chem. Int. Ed.*, **2007**, *46*, 2152-2187; (c) Guillem Aromí, David Aguilá, Patrick Gamez, Fernado Luis, Olivier Roubeau, *Chem. Soc. Rev.* **2012**, *41*, 537-546; (d) O. Kahn, C. Jay Martinez, *Science*, **1998**, *279*, 44-48.

[2] (a) P. Gütlich and H.A. Goodwin Eds. *Spin Crossover in Transition Metal Compounds I, II, and III*, Springer-Verlag, Berlin, Germany, **2004**; (b) A. Bousseksou, G. Molnár, L. Salmon and W. Nicolazzi, *Chem. Soc. Rev.*, **2011**, *40*, 3313-3335; (c) M.A. Halcrow, *Chem. Soc. Rev.*, **2011**, *40*, 4119-4142; (d) J. Olguín and S. Brooker, *Coord. Chem. Rev.*, **2011**, *255*, 203-240; (e) P. Gütlich, Y. Garcia and H.A. Goodwin, *Chem. Soc. Rev.*, **2000**, *29*, 419-427; (f) D.J. Harding, P. Harding and W. Phonsri, *Coord. Chem. Rev.*, **2016**, *313*, 38-61; (g) P. Guionneau, *Dalton Trans.*, **2014**, *43*, 382-393; (h) P. Gamez, J.S. Costa, M. Quesada and G. Aromí, *Dalton Trans.*, **2009**, *38*, 7845-7853.

[3] (a) M. Yamada, H. Hagiwara, H. Torigoe, N. Matsumoto, M. Kojima, F. Dahan, J.P. Tuchagues, N. Re and S. Iijima, *Chem. Eur. J.*, **2006**, *12*, 4536-4549; (b) L.J.K. Cook, R. Kulmaczewski, R. Mohammed, S. Dudley, S.A. Barrett, M.A. Little, R.J. Deeth and M.A. Halcrow, *Angew. Chem. Int. Ed.*, **2016**, *55*, 4327-4331; (c) R.G. Miller and S. Brooker, *Chem. Sci.*, **2016**, *7*, 2501-2505; (d) S.A. Barrett and M.A. Halcrow, *RSC Adv.*, **2014**, *4*, 11240; (e) M. Fumanal, F. Jiménez-Grávalos, J. Ribas-Arino and S. Vela, *Inorg. Chem.*, **2017**, *56*, 4474-4483; (f) E. Coronado, M.Giménez-Marqués, G.M. Espallargas, F. Rey and I.J. Vitórica-Yrezábal, *J. Am. Chem. Soc.*, **2013**, *135*, 15986-15989; (g) G.J. Halder, C.J. Kepert, B. Moubaraki, K.S. Murray and J.D. Cashion, *Science*, **2002**, *298*, 1762-1765; (h) M.B. Bushuev, D.P. Pishchur, V.A. Logvinenko, Y.V. Gatilov, I.V. Korolkov, I.K. Shundrina, E.B. Nikolaenkova and V.P. Krivopalov, *Dalton Trans.*, **2016**, *45*, 107-120; (i) Ruth Pritchard, Colin A. Kilner, Malcom A. Halcrow, *Chem. Commun.,* **2007**, 577–579; (j) N.T. Madhu, Ivan Salitros, Frank Schramm, Svetlana Klyatskaya, Olaf Fuhr, Mario Ruben, *C .R. Chimie.* **2008**, *11*, 1166-1174; (k) Jérome Elhaïk, David Evans, Colin Kilner, Malcom A. Halcrow, *Dalton Trans.,* **2005**, 1693-1700.

[4] M. Yamada, M. Ooidemizu, Y. Ikuta, S. Osa, N. Matsumoto, S. Iijima, M. Kojima, F. Dahan and J.-P. Tuchagues, *Inorg. Chem.*, **2003**, *42*, 8406-8416.

[5] A. Galet, A.B. Gaspar, M.C. Munoz, J.A. Real, *Inorg. Chem.*, **2006**, *45*,4413-4422.

[6] (a) L.J.K. Cook, R. Mohammed, G. Sherborne, T.D. Roberts, S. Alvarez and M.A. Halcrow, *Coord. Chem. Rev.*, **2015**, *289-290*, 2-12; (b) M.A. Halcrow, *Coord. Chem. Rev.*, **2009**, *253*, 2493-2514; (c) G.A. Craig, O. Roubeau and G. Aromi, *Coord. Chem. Rev.*, **2014**, *269*, 13-31; (d) R.J. Deeth, M.A. Halcrow, L.J.K. Cook and P.R. Raithby, *Chem. Eur. J.*, **2018**, *24*, 5204-5212; (e) T.D. Roberts, F. Tuna, T.L. Malkin, C.A. Kilner and M.A. Halcrow, *Chem. Sci.*, **2012**, *3*, 349-354; (f) M.A. Halcrow, *New J. Chem.*, **2014**, *38*, 1868-1882.

[7] A. Kimura and T. Ishida, *Inorganics*, **2017**, *5*, 52.

[8] L.J.K. Cook, R.Kulmaczewski, R. Mohammed, S. Dudley, S.A. Barrett, M.A. Little, R.J. Deeth and M.A. Halcrow, *Angew. Chem. Int. Ed.*, **2016**, *55*, 4327-4331.

[9] W. Phonsri, D.S. Macedo, K.R. Vignesh, G. Rajaraman, C.G. Davies, G.N.L. Jameson, B. Moubaraki, J.S. Ward, P.E. Kruger, G. Chastanet and K.S. Murray, *Chem. Eur. J.*, **2017**, *23*, 7052-7065.

[10] Sheldrick, G. M. (1996).

[11] (a) M.B. Bushuev, D.P. Pishchur, V.A. logvinenko, Y.V. Gatilov, I.V. Korolkov, I.K. Shundrina, E.B. Nikolaenkova and V.P. Krivopalov, *Dalton Trans.*, **2016**, 45, 107-120; (b) S.Vela, J.J. Novoa and J. Ribas-Arino, *Phys. Chem. Chem. Phys.*, **2014**, *16*, 27012-27024; (c) M. Kepenekian, B.L. Guennic and V. Robert, *J. Am. Chem. Soc.*, **2009**, *131*, 11498-11502; S. (d) Vela and H. Paulsen, *Dalton*

Trans., Advance Article doi: 10.1039/C8DT04394A.

CHAPTER 3

Electronic State Conversions of Iron Complexes with Brønsted Acid and Base

3.1 Introduction

Next-generation intelligent molecular devices will rely on simple, nanoscale species possessing multiple distinct electronic states which can be reversibly switched under the application of external stimuli.[1] Amongst the most promising candidates capable of fulfilling these criteria are coordination complexes based on cheap, readily-available 1st row transition metals.[2] These have long been shown to exhibit an attractive variety of switchable magnetic, electronic and optical properties in response to temperature, light, pressure or guest absorption/desorption.[3] A key advantage of employing such species is their amenability to novel molecular design approaches which allows control over both their structure and composition, but also presents the potential for fine tuning of their electronic properties by modification of both the inner- (via ligand design).[4] and outer- (via hydrogen-bonding, anion or solvent interactions) coordination spheres.[5]

The modification of capping ligands allows manipulation of their binding strength and thus the tuning of reversible high-spin (HS) to low-spin (LS) state conversion in Fe^{II} or Fe^{III} spin crossover (SCO) complexes under thermal- or photo-excitation. Likewise, valence conversion – where an external stimulus is used to trigger an electron-transfer-coupled spin transition (ETCST) – can be achieved in poly-nuclear systems where strong electronic interactions between neighbouring metal centres are engineered by careful (or serendipitous) ligand selection/design.[6]

Outer-sphere coordination effects can be used to modify complex spin states upon exposure to chemical stimuli. For example, Coronado and Kepert have shown how the interaction of guest molecules with responsive coordination systems can be used to achieve spin state switching.[7] More recently, the development of pH-responsive systems has shown that multi-dentate ligands which retain an acidic proton – such as those containing free imidazole or pyrazole N-H moieties – allow the design of a new class of switchable complexes.[8] These “Brønsted ligands”, which can act simultaneously as both Brønsted acids and bases, strongly couple the properties of the complex to its environment, where protonation/deprotonation of the ligand dramatically modifies the redox behaviour and the ligand field of the coordinated metal cation(s). In addition, Brønsted ligand complexes typically form hydrogen-bonded networks through -N-H···N- donor-acceptor interactions, which can be influenced by the inclusion of complementary proton donors/acceptors.[9] The resultant formation of dynamic, supramolecular high-dimensional networks of SCO species can lead to enhancement of spin transition phenomena through cooperative interactions. Very few examples of direct, protonation-controlled state-switching in molecular species have been reported. Most recently, Lehn and co-workers showed how the SCO

behaviour of a polynuclear Fe_4 grid-type complex can be modified in response to pH by using protic, hydrazine-based ditopic ligand groups.[10] A more common approach has been to develop mononuclear Fe^{II}-complexes which reversibly respond to protonation/deprotonation, however in all cases, these systems show a binary response where the physical properties can be switched between just two discrete states.

In this work, a novel ligand design strategy employing an asymmetric Brønsted ligand can be used to isolate a mononuclear Fe-complex with five independently accessible physical states. To achieve multi-state switching in a structurally simple mononuclear complex, a new ligand design approach, obtaining the asymmetric tridentate ligand H_2L (this ligand is written as H_2L^1 in CHAPTER 2. In this CHAPTER 3, the ligand is described as H_2L for clarity.) was performed. H_2L possesses two distinct acidic protons on the benzimidazole and pyrazole moieties where the dissociation constants of each proton is different (imidazole pK_a = 19.8, pyrazole pK_a = 16.4). Considering the complex $[Fe^{II}(H_2L)_2]^{2+}$ (**1** in CHAPTER 2. In this CHAPTER 3, the complex is written as $\mathbf{1_A}$), the complexes have four Brønsted acid/base moieties. In addition, the iron ion is stabilized in two valence states, divalent and trivalent. Therefore it is considered that this complex can potentially stabilize 10 types of iron complexes by deprotonation/protonation and oxidation/reduction (Scheme 3.1). In this CHAPTER, five types of iron complexes $\mathbf{1_{A\text{-}E}}$ were isolated by stepwise deprotonation (Scheme 3.2) and their electronic states were determined.

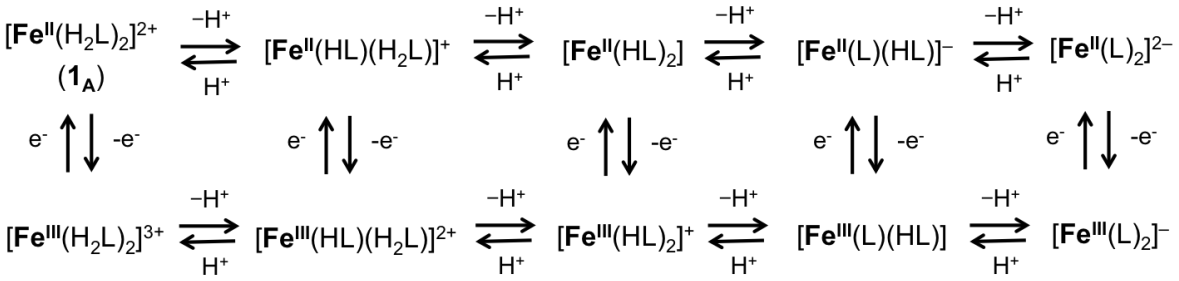

Scheme 3.1: 10 types of iron complexes.

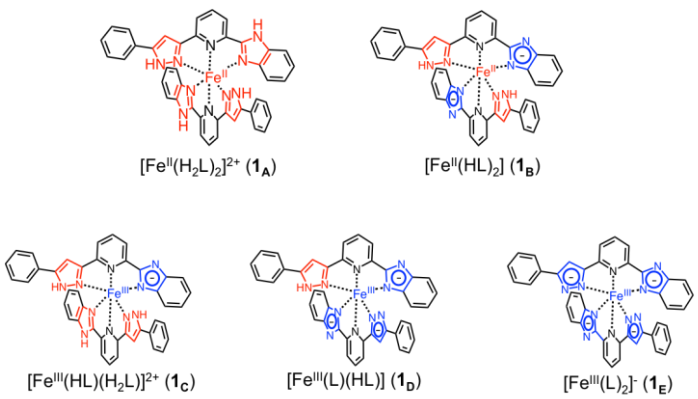

Scheme 3.2: The five isolated complexes presented in this chapter.

3.2 Experiments

Materials

All chemicals were used without further purification except when noted. Solvents and reagents were used as received from commercial suppliers.

SQUID Magnetometer Measurements

Variable-temperature magnetic susceptibility measurements were carried out on polycrystalline samples using a Quantum Design MPMS-XL SQUID magnetometer. Pascal's constants were used to determine the diamagnetic corrections.

X-ray Crystallography

Crystals were mounted on a glass capillary or a MiTeGen Dual-Thickness MicroMount, and data were collected at 100 K and 270 K (Bruker SMART APEXII diffractometer coupled with a CCD area detector with graphite monochromated Mo-$K\alpha$ (λ = 0.71073 Å) radiation). The structure was solved using direct methods and expanded using Fourier techniques within the SHELXTL program. Empirical absorption corrections by SADABS were carried out.[11] In the structure analyses, non-hydrogen atoms were refined with anisotropic thermal parameters. Hydrogen atoms were included in calculated positions and refined with isotropic thermal parameters riding on those of the parent atoms.

Mössbauer spectra

Mössbauer experiments were carried out using a ^{57}Co/Rh source in a constant-acceleration transmission spectrometer (Topologic Systems) equipped with an Iwatani HE05/CW404 cryostat. The spectrometer was calibrated using standard α-Fe foil.

Electrochemical measurements

Electrochemical measurements were carried out using a BAS 620A electrochemical analyzer. Cyclic voltammetry and differential pulse voltammetry measurements were carried out in a standard one-compartment cell under N_2 at 20 °C equipped with a platinum-wire counter electrode, a saturated calomel electrode (SCE) as the reference electrode, and a glassy carbon (GC) working electrode.

UV-Vis-NIR spectroscopy

UV-Vis-NIR absorption spectra were recorded on Agilent Technologies Cary 8454 UV-Vis spectrometer. The solid-state UV was measured on KBr pellet samples using the Shimadzu UV-3150 spectrometer equipped with a Unisoku USP-203-A cryostat.

Elemental analysis

Elemental analyses were performed using a Perkin Elmer 2400 element analyzer.

Synthetic Procedures

Syntheses of ligand H_2L and complex $[Fe^{II}(H_2L)](BF_4)_2$ (**1_A**) are listed in CHAPTER 2.

Synthesis of $[Fe^{II}(HL)_2]\cdot0.5(C_2H_4Cl_2)\cdot0.2(C_2H_5OH)\cdot0.3H_2O$ (1_B)

1_A (100 mg, 0.111 mmol) was dissolved into a mixed solution of ethanol and 1,2-dichroloethane (50 mL, v/v 1:2). Diluted NH_3 aq. solution (one drop of 28% ammonia solution in 50 mL of ethanol) was allowed to diffuse into the filtered red solution. After a few days, purple columnar crystals of $[Fe^{II}(HL)_2]\cdot5(C_2H_2Cl_2)$ (**1_B'**) suitable for single crystal X-ray structural analysis were obtained. Crystals were filtered, and air-dried samples of $[Fe^{II}(HL)_2]\cdot x$(solv.) (**1_B**) were used for physical measurements. (29.0 mg, yield 36 %) Anal. (calc.) for $C_{43.4}H_{31.8}N_{10}O_{0.5}ClFe$ (**1_B**$\cdot0.5(C_2H_4Cl_2)\cdot0.2(C_2H_5OH)\cdot0.3H_2O$) C: C,65.51 (65.76); H,3.78 (4.04); N,17.89 (17.67) %. FT-IR (KBr, cm^{-1}): 3201.8 (s, ν_{N-H}) 1602.9 (s, ν_{C-H}).

Synthesis of $[Fe^{III}(HL)(H_2L)](BF_4)Cl\cdot0.5CH_3OH\cdot1.8H_2O$ (1_C)

$FeCl_3\cdot6H_2O$ (26.0 mg, 0.1 mmol) in methanol (3 ml) was added to H_2L (66 mg, 0.2 mmol) in methanol (20 ml), and the mixture was stirred for 5 minutes at room temperature. The resulting orange solution was filtered and excess tetraethylammonium tetrafluoroborate was added to the filtrate. Orange block crystals of $[Fe^{III}(HL)(H_2L)](BF_4)Cl\cdot3(CH_3OH)$ (**1_C'**) suitable for structural analysis were obtained after diffusion of diisopropyl ether 3 days. (50 mg, yield 55 %) Orange crystals were collected by vacuo and air-dried affording $[Fe^{III}(HL)(H_2L)](BF_4)Cl\cdot0.5CH_3OH\cdot1.8H_2O$ (**1_C**) Anal. (calc.) for $C_{42.5}H_{34.6}N_{10}O_{2.3}BF_4ClFe$ (**1_C**$\cdot0.5CH_3OH\cdot1.8H_2O$): C,56.89 (56.70); H,4.12 (3.87); N,15.40 (15.56) %. FT-IR (KBr, cm^{-1}) 1610.6 (s, ν_{C-H}) , 1024.2 (s, ν_{B-F}).

Synthesis of complex $[Fe^{III}(L)(HL)]\cdot 4CH_3OH\cdot 3H_2O$ ($\mathbf{1_D}$)

$FeCl_3\cdot 6H_2O$ (26.0 mg, 0.1 mmol) in methanol (5 ml) was added to H_2L (66 mg, 0.2 mmol) in methanol (10 ml), and the reaction mixture was stirred for 5 minutes at room temperature. After stirring, triethylamine (27.3 μl, 0.2 mmol) was added to the solution and color changed from orange to green. After 3 minutes stirring, the green solution was filtered and allowed to stand without disturbing. The green plate crystals of $[Fe^{III}(L)(HL)]\cdot 4(CH_3OH)$ (**$\mathbf{1_D}$'**) were obtained by slow evaporation for 1 day. Crystals were collected by vacuo and air-dried, affording $[Fe^{III}(L)(HL)]\cdot CH_3OH\cdot 3(H_2O)$ (**$\mathbf{1_D}$**), which were used for physical measurements. (63 mg, yield 86 %) Anal. (calc.) for $C_{43}H_{37}N_{10}O_4Fe$ (**$\mathbf{1_D}$**$\cdot CH_3OH\cdot 3H_2O$): C, 63.47 (63.29); H, 4.58 (4.35); N, 17.21 (17.51) %. FT-IR (KBr, cm^{-1}) 1608.6 (s, $\nu_{C=N}$).

Synthesis of complex $(TEA)[Fe^{III}(L)_2]\cdot CH_3OH\cdot 3H_2O$ ($\mathbf{1_E}$)

$Fe(BF_4)_2\cdot 6H_2O$ (49 mg, 0.150 mmol) in methanol (5 ml) was added to H_2L (99 mg, 0.300 mmol) in methanol (20 ml), and the solution was stirred for 5 minutes at room temperature. After stirring, 1 M NaOH water (600 μl) was added to the solution and the color changed from red to blue. The blue solution was filtered and excess tetraethylammonium tetrafluoroborate ($TEABF_4$), was added. The blue plate crystals of $(TEA)[Fe^{III}(L)_2]\cdot 3(CH_3OH)\cdot 2(H_2O)$ (**$\mathbf{1_E}$'**) were obtained by slow evaporation for 1 day. Crystals were collected by vacuo and air-dried, affording $(TEA)[Fe^{III}(L)_2]\cdot CH_3OH\cdot 3(H_2O)$ (**$\mathbf{1_E}$**) for physical measurements. (78 mg, yield 59 %) Anal. (calc.) for $C_{51}H_{56}N_{11}O_4Fe$ (**$\mathbf{1_E}$**$\cdot CH_3OH\cdot 3H_2O$): C, 64.94 (64.78); H, 5.99 (5.92); N, 16.34 (16.20) %. FT-IR (KBr, cm^{-1}) 1600.4 (s, ν_{C-N}).

Table 3.1: Crystal parameters of **1_A'** and **1_B'**.

	1_A' (HS)	**1_A'** (LS)	**1_B'**
T / K	270	100	100
Instrument	APEX2	APEX2	APEX2
Formula	$C_{42}H_{30}B_2F_8FeN_{10}$	$C_{42}H_{30}B_2F_8FeN_{10}$	$C_{42}H_{28}FeN_{10}$
F.W.	904.23	904.23	728.59
Space Group	*C*2/c	*C*2/c	$P\bar{1}$
a / Å	23.590 (5)	23.06 (4)	12.6735 (14)
b / Å	12.299 (2)	12.49 (2)	13.3243 (15)
c / Å	19.719 (4)	19.42 (4)	14.0506 (16)
α / °	90	90	92.132 (2)
β / °	116.05 (3)	118.659 (18)	103.294 (2)
γ / °	90	90	103.6380 (10)
V / Å^3	5140 (2)	4908 (15)	2233.5 (4)
Z	4	4	2
μ / mm^{-1}	0.359	0.376	0.375
λ / Å	0.71073	0.71073	0.71073
*R*1 (> 2σ)	0.0643	0.0660	0.0515
*wR*2 (> 2σ)	0.1410	0.1382	0.1361

Table 3.2: Crystal parameters of **1_C'**, **1_D'**, and**1_E'**

	1_C'	**1_D'**	**1_E'**
T / K	100	100	100
Instrument	APEX2	APEX2	APEX2
Formula	$C_{45}H_{41}BClF_4FeN_{10}O_3$	$C_{46}H_{43}FeN_{10}O_4$	$C_{53}H_{62}FeN_{11}O_5$
F.W.	947.99	855.75	988.98
Space Group	$P2_1/n$	$P2_1/c$	$Pna2_1$
a / Å	15.446 (2)	12.1625 (16)	27.7460 (17)
b / Å	17.895 (3)	24.788 (3)	13.0276 (8)
c / Å	17.455 (3)	15.112 (2)	13.5959 (8)
α / °	90	90	90
β / °	115.311 (2)	108.274 (2)	90
γ / °	90	90	90
V / Å^3	4361.5 (12)	4326.3 (10)	13.5959 (8)
Z	4	4	4
μ / mm^{-1}	0.478	0.404	0.368
λ / Å	0.71073	0.71073	0.71073
*R*1 (> 2σ)	0.0743	0.0690	0.0401
*wR*2 (> 2σ)	0.1714	0.1846	0.0935

Table 3.3: Table of bond lengths (Å) and Σ values (^{O}) for five complexes.

1_A' (270 K)		**1_A'**(100 K)		**1_B'** (100 K)	
Fe-N1	2.134 (3)	Fe-N1	1.987 (5)	Fe-N1	1.972 (2)
Fe-N2	2.143 (3)	Fe-N2	1.911 (5)	Fe-N2	1.912 (3)
Fe-N3	2.182 (3)	Fe-N3	1.974 (5)	Fe-N3	1.977 (2)
Fe-N1	2.134 (3)	Fe-N4	1.987 (5)	Fe-N4	1.964 (2)
Fe-N2	2.143 (3)	Fe-N5	1.911 (5)	Fe-N5	1.921 (2)
Fe-N3	2.182 (3)	Fe-N6	1.974 (5)	Fe-N6	1.957 (3)
Ave.	2.150(3)	Ave.	1.957 (5)	Ave.	1.949 (3)
Σ(^{o})	142.1	Σ(^{o})	96.4	Σ(^{o})	90.1

1_C' (100 K)		**1_D'** (100 K)		**1_E'** (100 K)	
Fe-N1	2.237 (4)	Fe-N1	1.986 (3)	Fe-N1	1.953 (3)
Fe-N2	2.134 (4)	Fe-N2	1.911 (3)	Fe-N2	1.915 (3)
Fe-N3	2.172 (4)	Fe-N3	1.941 (3)	Fe-N3	1.969 (3)
Fe-N4	2.197 (4)	Fe-N4	1.923 (3)	Fe-N4	1.908 (3)
Fe-N5	2.123 (4)	Fe-N5	1.918 (3)	Fe-N5	1.914 (3)
Fe-N6	2.200 (4)	Fe-N6	1.947 (3)	Fe-N6	1.951 (3)
Ave.	2.18	Ave.	1.94	Ave.	1.94
Σ(^{o})	140.0	Σ(^{o})	80.9	Σ(^{o})	78.7

3.3. Results and Discussion

Structure of $\mathbf{1_A}$'

$\mathbf{1_A}$' is a mononuclear complex which is constructed from two ligands and one iron ion. At 100 K, the spin state is Fe(II) low spin. On the other hand, the spin state is Fe(II) high spin at 270 K. These results mean **$\mathbf{1_A}$'** is a spin crossover complex. (Details of **$\mathbf{1_A}$'** is written in CHAPTER 2.)

Cyclic voltammetry of $\mathbf{1_A}$

Cyclic voltammetry measurements of **$\mathbf{1_A}$**, carried out in acetonitrile at 293 K (Figure 3.1). The cyclic voltammogram showed one quasi-reversible redox process at $E_{1/2}$ = 0.86 V corresponding to the one-electron oxidation/reduction of the iron centres. This result suggested that the oxidized species was relatively stable in acetonitrile.

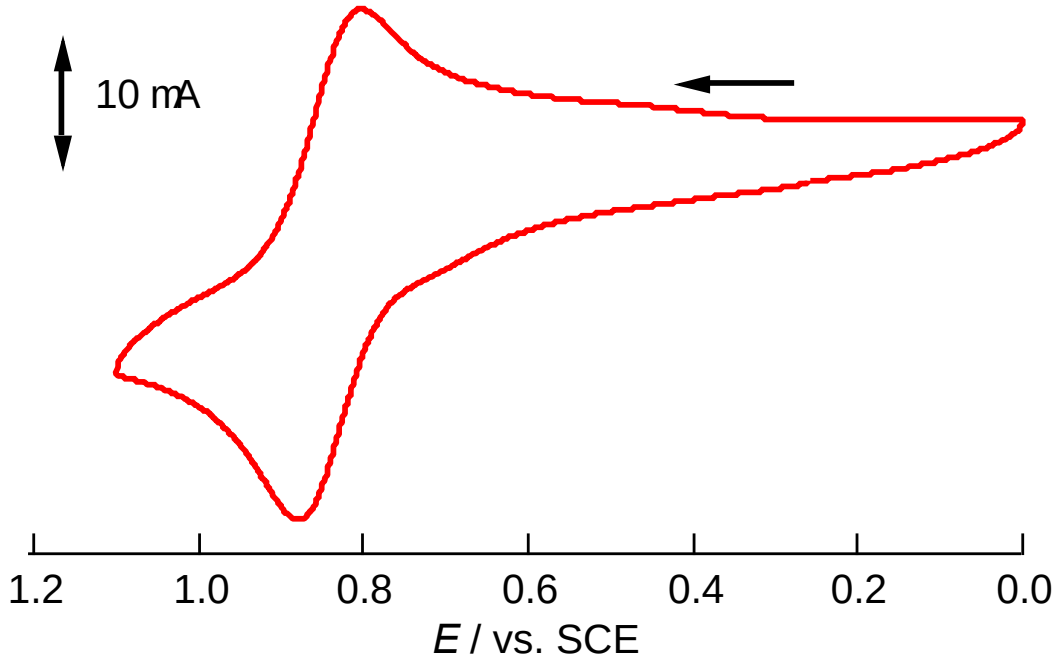

Figure 3.1: Cyclic voltammogram of **$\mathbf{1_A}$** in acetonitrile / 0.1 M *n*-Bu_4NPF_6.

Base addition cyclic voltammogram

Cyclic voltammograms were measured in an acetonitrile solution of **1**$_A$, before and after addition of 4 equivalents of 1,8-Diazabicyclo[5.4.0]undec-7-ene (DBU) under air. It is important to note that addition of fewer than four equivalents of base produced poor/uninterpretable data due to the insolubility of the partially deprotonated homologues whereas four equivalents of strong base was expected to lead to the complete deprotonation of the complex. Figure 3.2 shows the voltammogram of **1**$_A$ in which a quasi-reversible Fe(II) / Fe(III) redox couple appears, centred at +0.84 V vs. SCE. Subsequent addition of 4 equivalents of DBU causes the Fe-centred redox process to shift to –0.68 V vs. SCE, suggesting that the Fe(II) ion has been destabilized by ligand deprotonation and spontaneously oxidised to Fe(III).

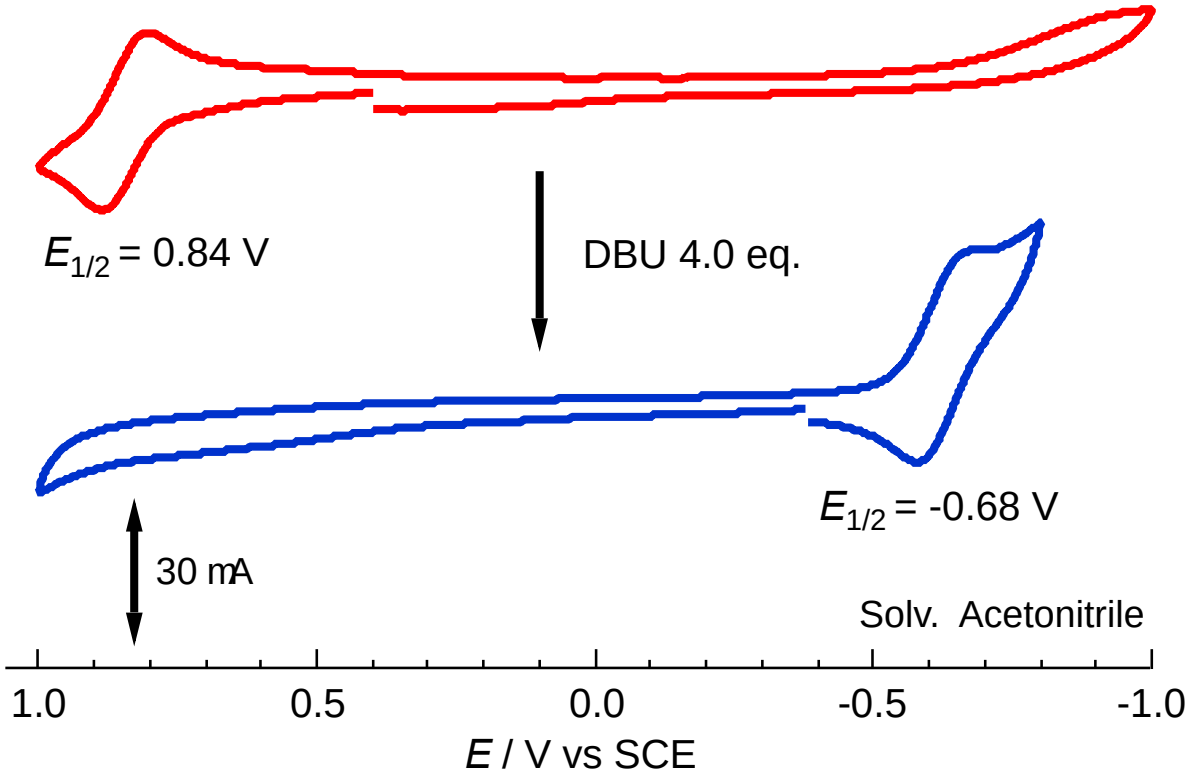

Figure 3.2: DBU titration cyclic voltammogram of **1**$_A$ in acetonitrile/ 0.1 M *n*-Bu_4NPF_6.

Base addition UV spectra

Figure 3.4 shows the effect on the UV-vis absorption spectrum of **1**$_A$ in acetonitrile upon the addition of 4 eq. DBU. At first, MLCT bands derived from **1**$_A$ were observed at 477 and 512 nm (Table 3.3). After DBU titration however, the band was red shifted and new peaks appeared at 586 and 720 nm. The new peaks can be identified as the LMCT bands of the deprotonated and oxidized **1**$_A$. From the CV and UV experiments, the stability of partially deprotonated complexes was suggested.

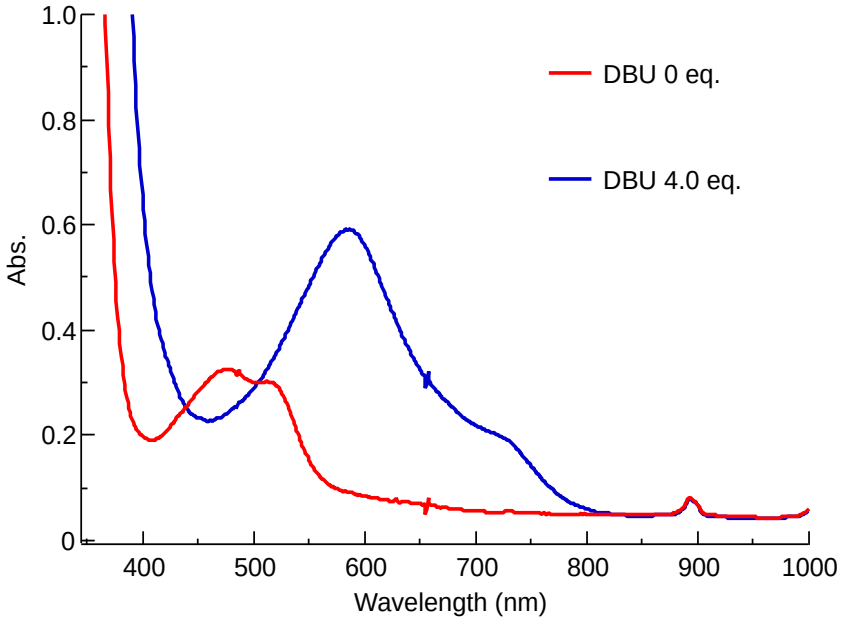

Figure 3.3: UV spectra of **1**$_A$ (red line: DBU 0 eq. blue line: DBU 4.0 eq.).

Table 3.4. Assignment of UV spectra.

	DBU 0 eq.		DBU 4.0 eq.	
Wavelength (nm)	477	512	586	720
Assignments	MLCT	MLCT	LMCT	LMCT

Synthesis of partially deprotonated complexes

To demonstrate the utility of the Brønsted ligands, isolation of partially (or totally) deprotonated complexes were performed. Synthesis methods are written in the Experimental section (CHAPTER 3.2).

The neutral divalent complex $[Fe^{II}(HL)_2]$ (**1_B'**) was isolated as purple crystals by the diffusion of ammonia to a solution of **1_A'**. Complex **1_B'** crystallizes in the triclinic space group $P\bar{1}$ (measured at 100 K). The structure is almost identical to that of **1_A'**, but the two deprotonated benzimidazole N atoms are no longer involved in hydrogen bonded interactions. In addition, there are no BF_4^- anions in the crystal lattice, supporting the assignment that **1_B'** is neutral. The average Fe-N bond length of 1.95 Å and Σ value of 90.1° are typical of a LS Fe(II) ion. π-π-stacking interactions and N-H···N hydrogen bonds between the protonated pyrazole and deprotonated benzimidazole moieties of neighbouring **1_B** units form a one-dimensional chain-like structure between complexes (Figure 3.4).

Complex $[Fe^{III}(HL)(H_2L)](BF_4)Cl$ (**1_C'**) was synthesized as orange needle crystals in the mixture of H_2L, $FeCl_3 \cdot 6H_2O$ and tetraethylammoniumtetrafluoroborate. **1_C'** crystallized in the $P2_1/n$ space group, and contained one BF_4^- and one Cl^- anion (Figure 3.5). Moreover, the average bond length between iron and nitrogen is 2.18 Å and the Σ value is 142.1°. This information indicated that the iron ion was in the ferric high spin state.

Complex $[Fe^{III}(L)(HL)]$ (**1_D'**) was synthesized as green block crystals from a mixture of H_2L, $FeCl_3 \cdot 6H_2O$ and triethylamine in methanol. **1_D'** crystallized in the $P2_1/c$ space group, and there were no counter ions. In addition, from the average bond length between iron ions and nitrogen atoms (1.94 Å) and the Σ value (80.9°), the Fe(III) LS state was indicated. This result was consistent with Mössbauer data. This complex is neutral, and three brønsted acid/base moieties are deprotonated (two benzimidazoles and pyrazole). As for the intermolecular interactions, the complex formed dimers through N-H···N hydrogen bonds between pyrazole and benzimidazole (Figure 3.6). The other Brønsted moieties form hydrogen bonds with methanol.

Complex $(TEA)[Fe^{III}(L)_2]$ (**1_E'**) was synthesized as blue-plate crystals from a mixture of H_2L, Fe(II) tetrafluoroborate and NaOH in methanol (Figure 3.7). **1_E'** crystallized in the $Pna2_1$ space group, and contained one tetraethylammonium cation. It means that **1_E'** is a totally deprotonated anionic complex. From the average bond length between the iron ion and nitrogen atoms (1.94 Å) and the Σ value (78.7°), the metal center was identified to be trivalent, in its low spin state.

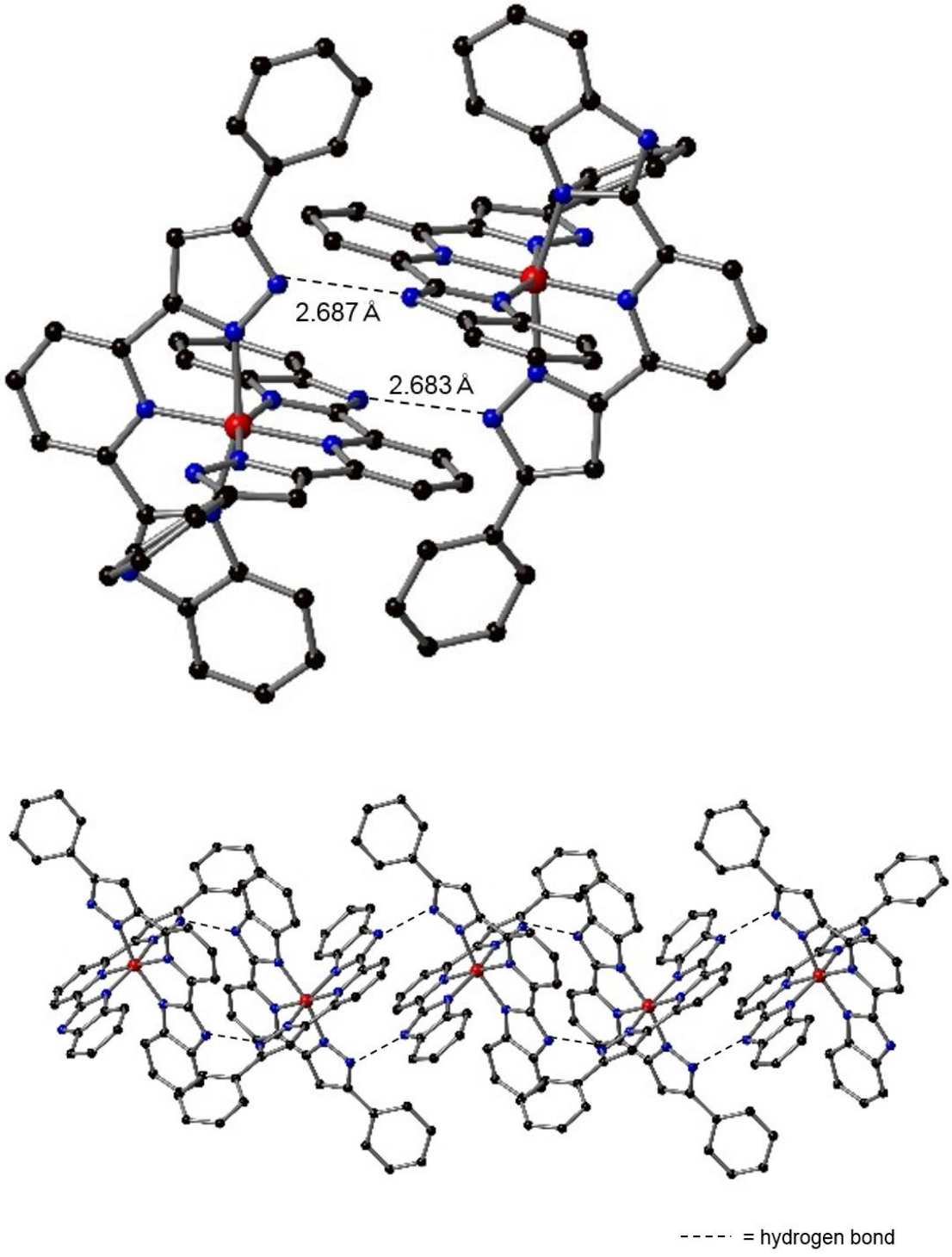

Figure 3.4: The molecular structure of **1_B'**, showing: intermolecular interactions between discrete molecules (top) and extended network structure (bottom).

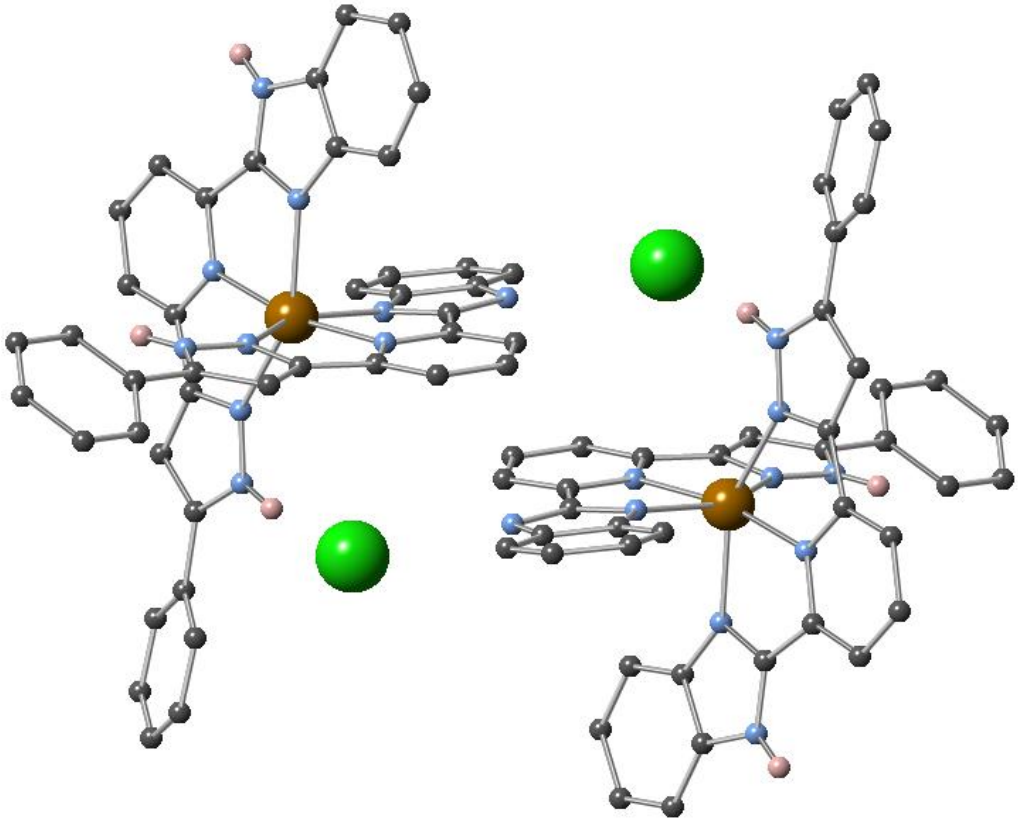

Figure 3.5: Ball and stick diagram showing the dimeric structure of **1_C'**.

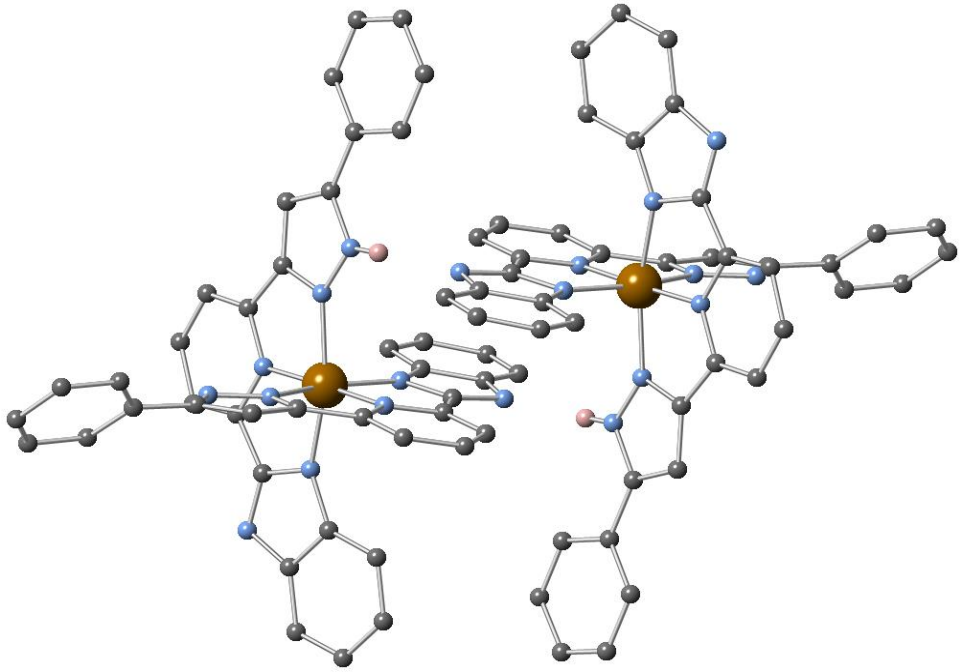

Figure 3.6: Ball and stick diagram showing the dimeric structure of **1_D'**.

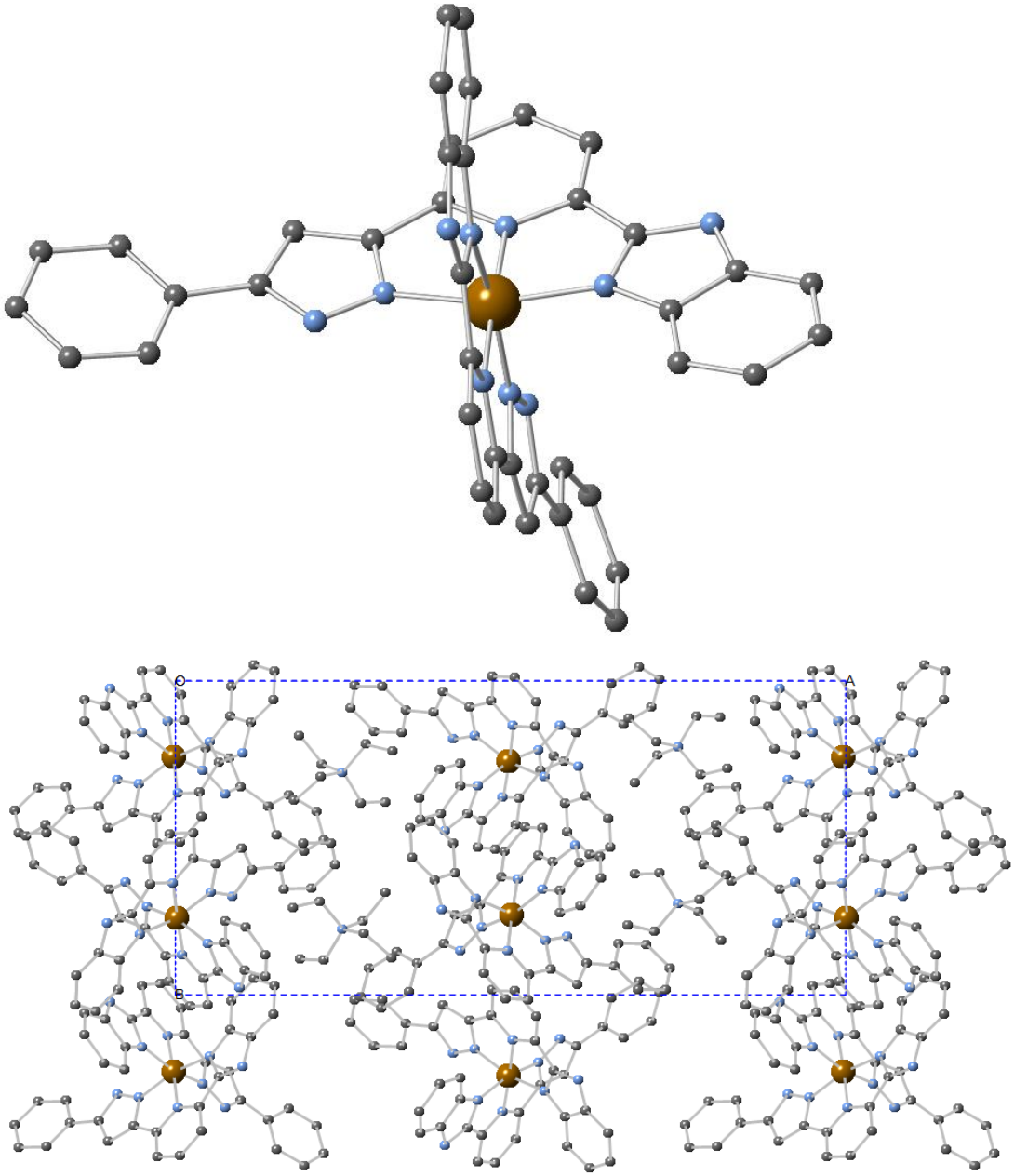

Figure 3.7: The molecular structure of **1_E**, showing: the discrete anion (top) the *b*-axis projection (bottom).

DC magnetic susceptibility and Mössbauer spectra

DC magnetic susceptibilities of crystalline samples of Fe complexes $\mathbf{1_A}$-$\mathbf{1_E}$ were measured under an applied magnetic field of 10000 Oe. Data are shown in Figure 3.8. $\mathbf{1_A}$ displays rapid spin conversion at $T_{1/2}$ = 260.5 K. From 300 K to 260 K, the $\chi_m T$ of $\mathbf{1_A}$ was constant at 3.33 emu mol^{-1} K, which is close to the spin only value expected for four unpaired electrons, S = 2 (3.0 emu mol^{-1} K), suggesting that all Fe(II) centres were in the HS state. High temperature single-crystal X-ray structural analysis and Mössbauer spectroscopy of $\mathbf{1_A}$ support this assignment (CHAPTER 2, Figure2. 7).

$\mathbf{1_B}$, on the other hand, appeared to be in the LS Fe(II) state below 350 K. At higher temperatures, however, the $\chi_m T$ value gradually changed from 0.140 emu mol^{-1} K at 320 K to 0.355 emu mol^{-1} K at 400 K, behaviour consistent with the partial HS-LS transition of Fe(II) ions. Mössbauer spectroscopy at 20 K, $\mathbf{1_B}$ is all Fe(II) LS state (Figure 3.10). These differences suggest that the spin transition temperature of SCO complexes can be raised by ligand deprotonation, due to the stabilization of the LS state in response to the increased ligand strength of the deprotonated moieties (arising through the increased negative charge on the coordinating N-atoms).

Temperature dependent magnetic data for $\mathbf{1_C}$, $\mathbf{1_D}$ and $\mathbf{1_E}$ are shown in Figure 3.9. At 300 K, the $\chi_m T$ value of $\mathbf{1_C}$ is 4.38 emu mol^{-1} K, which is close to 4.375 emu mol^{-1} K, the expected value for a high-spin Fe(III) species. On the other hand, $\mathbf{1_D}$ and $\mathbf{1_E}$ exhibit $\chi_m T$ values of 0.407 and 0.365 emu mol^{-1} K at 400 K respectively, consistent with low-spin Fe(III) ions. The spin states were also elucidated by Mössbauer spectra (Figure 3.11-13). As before, switching of the spin states of $\mathbf{1_C}$ (HS, S = 5/2) and $\mathbf{1_D}$ and $\mathbf{1_E}$ (LS, S = 1/2) arises from the increased ligand field strength upon deprotonation, due to greater σ-donation of the pyrazole and imidazole nitrogen atoms upon deprotonation.

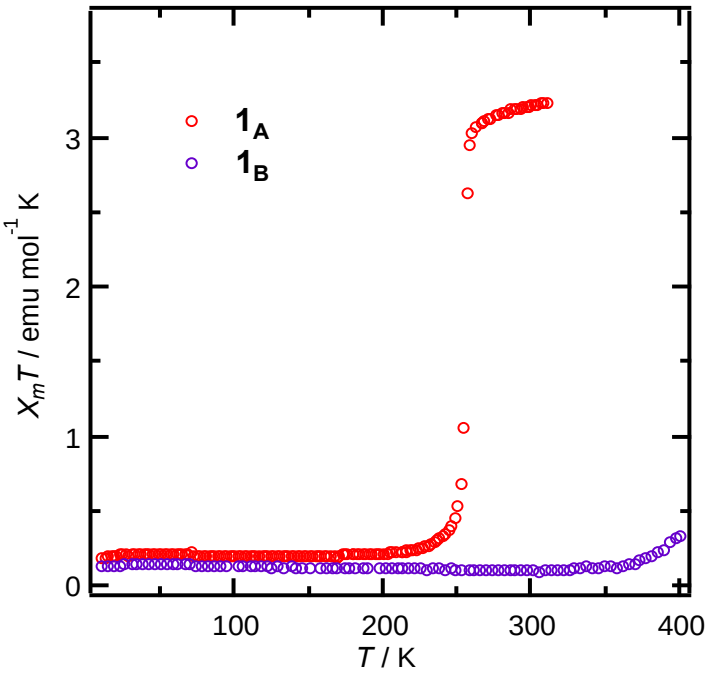

Figure 3.8: The thermal magnetic susceptibility data collected for $\mathbf{1_A}$ (red) and $\mathbf{1_B}$ (purple).

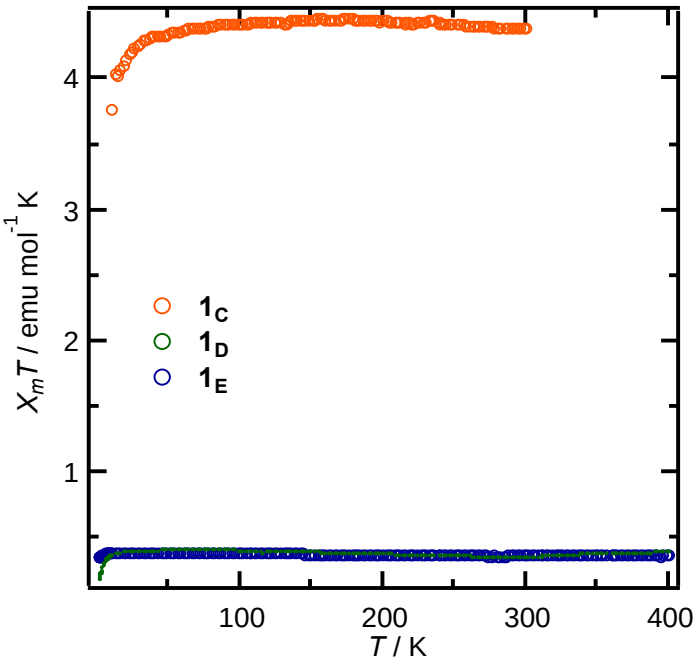

Figure 3.9: The thermal magnetic susceptibility data collected for $\mathbf{1_C}$ (orange), $\mathbf{1_D}$ (green) and $\mathbf{1_E}$ (blue).

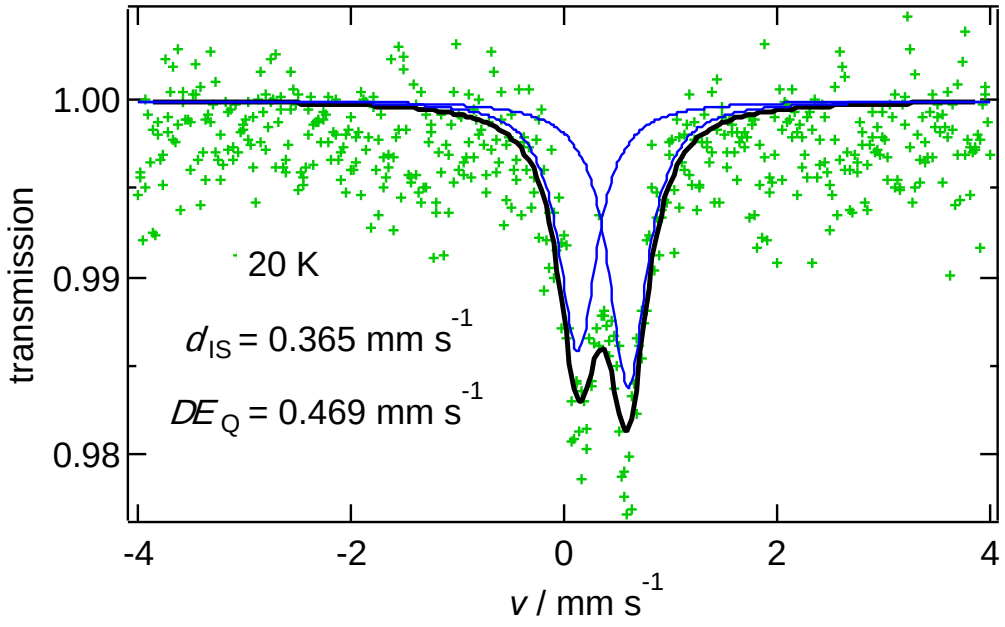

Figure 3.10: Mössbauer spectra of **1$_B$** at 20 K.

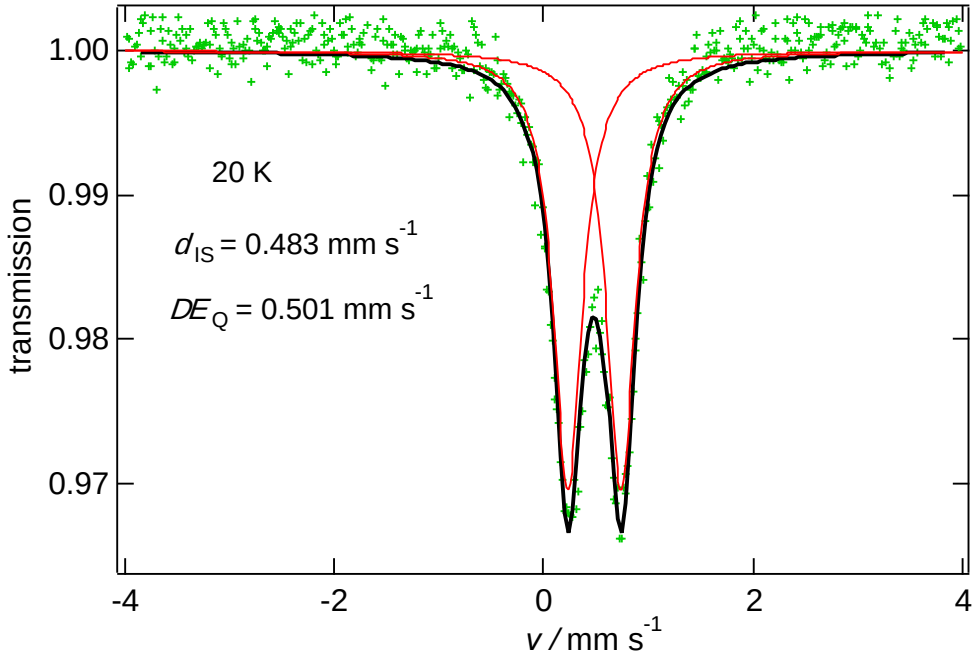

Figure 3.11: Mössbauer spectra of **1$_C$** at 20 K.

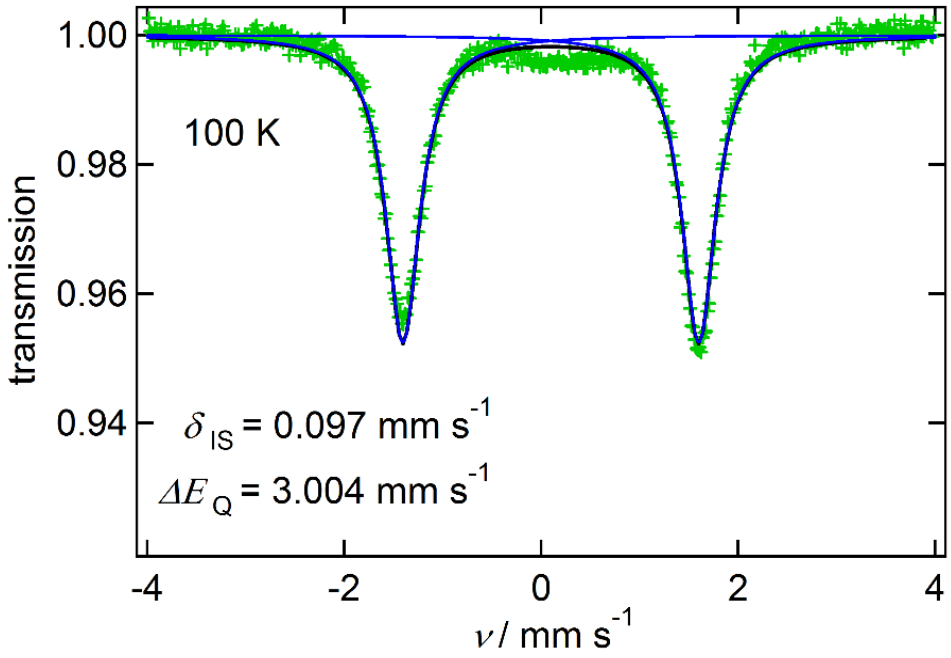

Figure 3.12: Mössbauer spectra of **1_D** at 100 K.

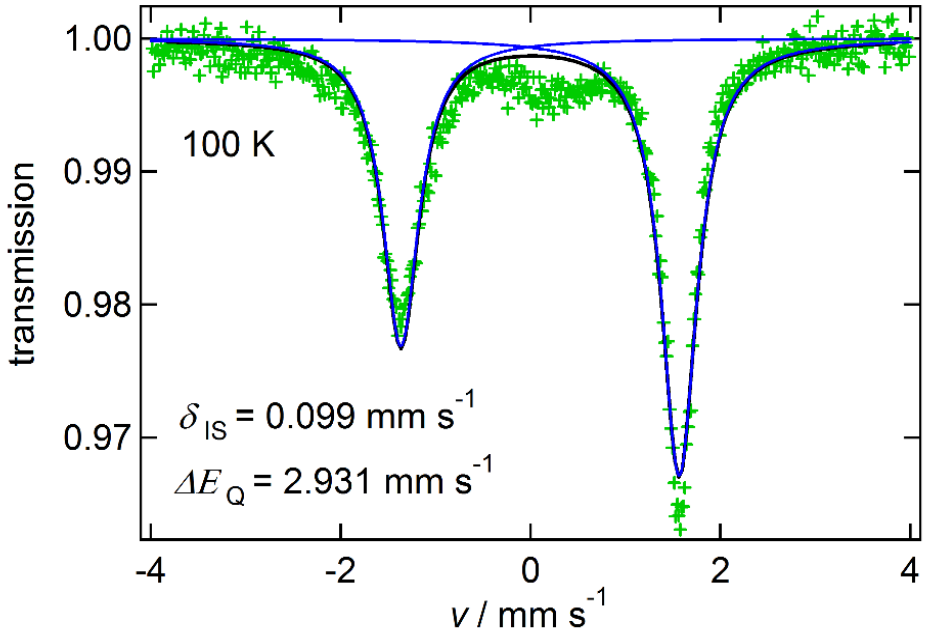

Figure 3.13: Mössbauer spectra of **1_E** at 100 K.

Table 3.5: Summary of Mössbauer spectra.

	T (K)	δ_{IS} (mm / s)	ΔE_Q (mm / s)	Spin state
$\mathbf{1_A}$	100	0.415	0.646	Fe(II) LS
$\mathbf{1_A}$	270	0.970	2.100	Fe(II) HS
$\mathbf{1_B}$	20	0.366	0.469	Fe(II) LS
$\mathbf{1_C}$	20	0.483	0.501	Fe(III) HS
$\mathbf{1_D}$	100	0.097	3.004	Fe(III) LS
$\mathbf{1_E}$	100	0.099	2.931	Fe(III) LS

Electrochemical properties

Cyclic voltammetry measurements of $\mathbf{1_C}$ and $\mathbf{1_E}$ were carried out in acetonitrile at 293 K. $\mathbf{1_C}$ showed one quasi-reversible redox process at $E_{1/2}$ = 0.44 V (Figure 3.14). The $E_{1/2}$ value is more negative than $\mathbf{1_A}$, suggesting that deprotonation stabilizes the higher oxidation state. The CV of $\mathbf{1_E}$ on the other hand, gave a single quasi-reversible redox process centred at $E_{1/2}$ = -0.68 V (Figure 3.15). The $E_{1/2}$ matches exactly with the base titration experiments conducted on $\mathbf{1_A}$ (+4.0 eq. DBU; Figure 3.2). This data revealed the conversion from $\mathbf{1_A}$ to $\mathbf{1_E}$ by ligand deprotonation.

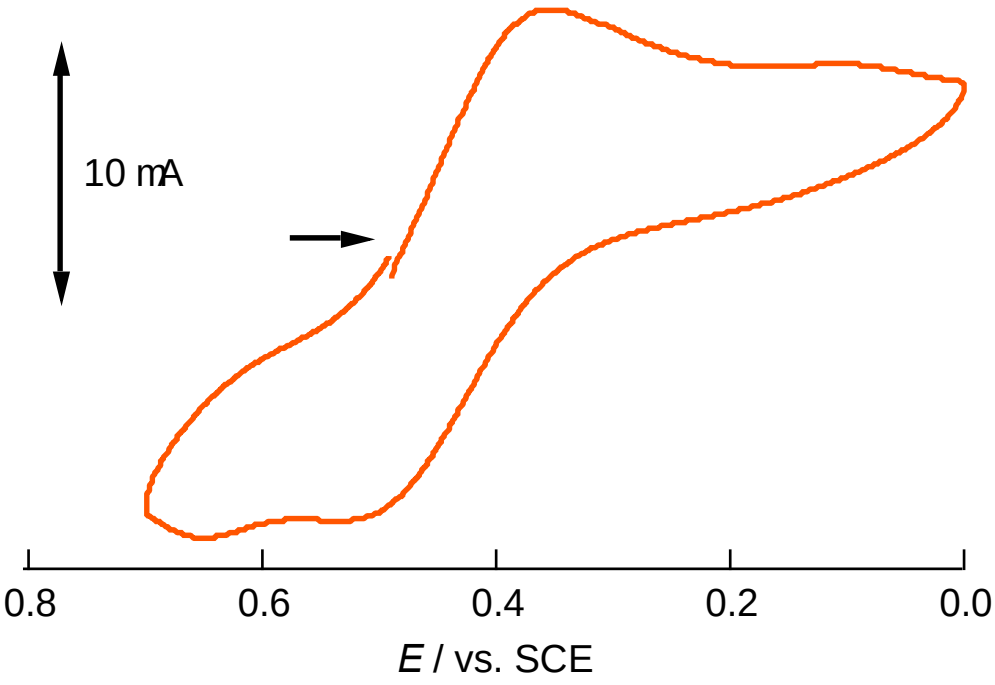

Figure 3.14: Cyclic voltammogram of $\mathbf{1_C}$ in acetonitrile/ 0.1 M n-Bu_4NPF_6.

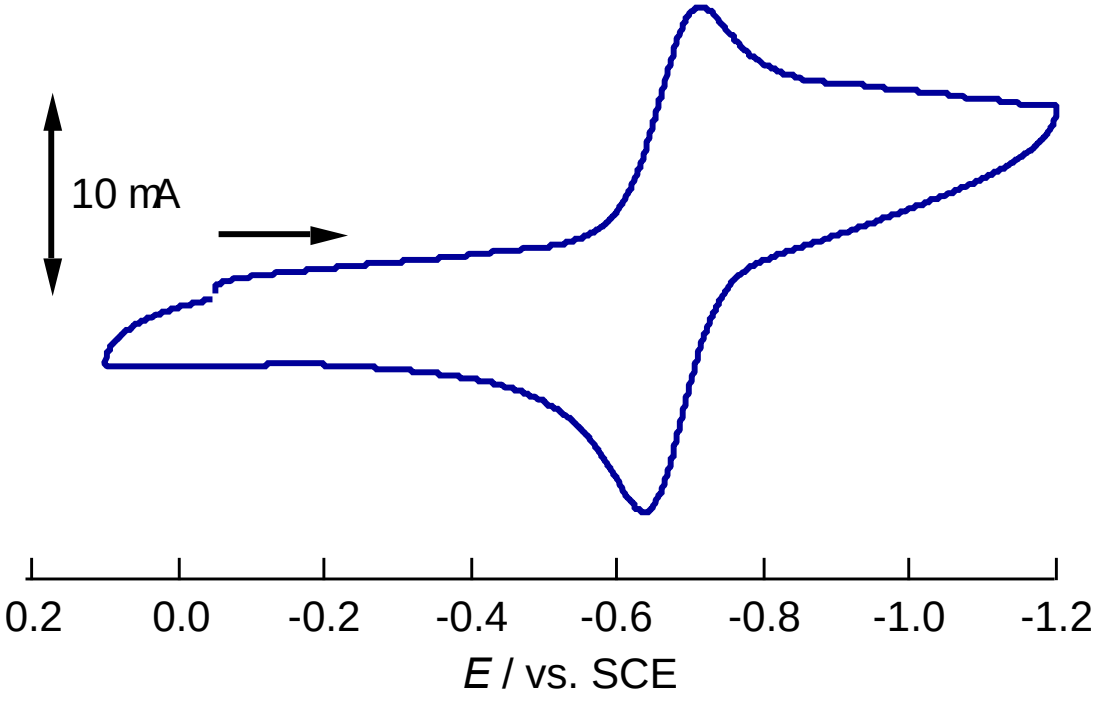

Figure 3.15: Cyclic voltammogram of $\mathbf{1_E}$ in acetonitrile/ 0.1 M *n*-Bu_4NPF_6.

Solid State UV spectra

Solid state UV spectra were measured at room temperature. All samples were prepared as KBr discs from single crystalline samples (Figure 3.16). The MLCT bands of $\mathbf{1_A}$ were observed at 487 and 534 nm, however, the MLCT band of $\mathbf{1_B}$ was red-shifted to 581 nm. It means that deprotonation of the ligand increased the energy level of both the iron ion d-orbitals and the ligand. As for the Fe(III) complexes, the LMCT band of $\mathbf{1_C}$ (540 nm) was red-shifted to $\mathbf{1_D}$ (632 nm) and $\mathbf{1_E}$ (598 nm), in the same manner as the Fe(II) complexes.

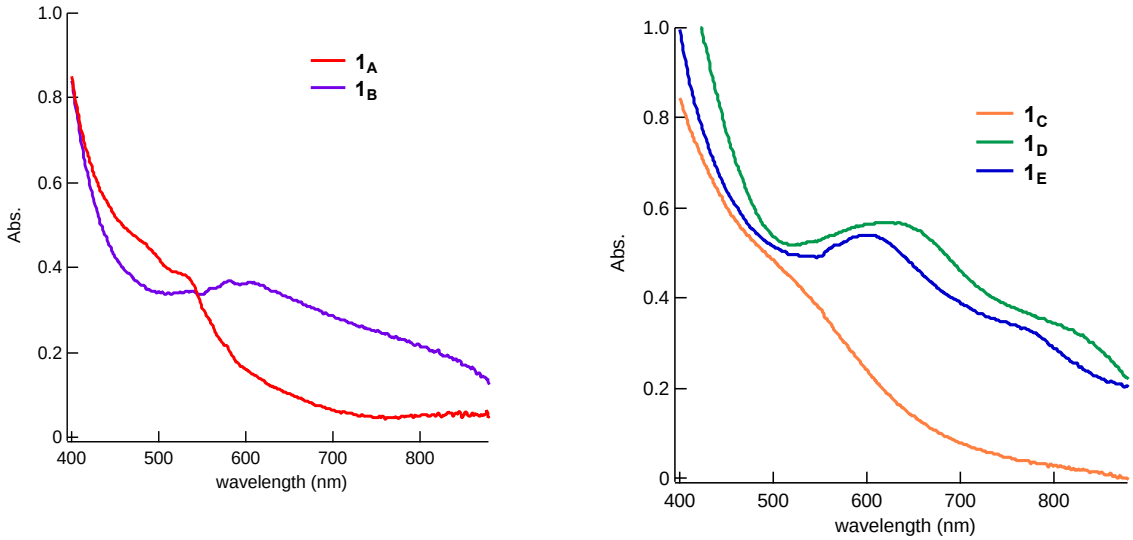

Figure 3.16: Solid state UV spectra of complexes $\mathbf{1_{A\text{-}E}}$. All spectra were collected on solid samples compressed into KBr pellets.

Base titration UV spectra of 1_A (acetonitrile solution)

To obtain detailed information on the stepwise deprotonation in solution state, DBU titration UV data for **1_A** were measured in acetonitrile solution (Figure 3.17). From DBU 0 eq to 4.0 eq., MLCT band derived from **1_A** decreased and new peaks were observed at 586 and 720 nm. This spectrum is exactly the same as that collected for **1_E** (Figure 3. 3). This indicates that deprotonation and oxidation of **1_A** was were simultaneously effected upon addition of the strong base under air. No isobestic point was observed, however, due to the insolubility of the neutral complex **1_B** in acetonitrile. To observe the conversion from **1_A** to **1_B** with accuracy, UV measurement in mixed solution was performed.

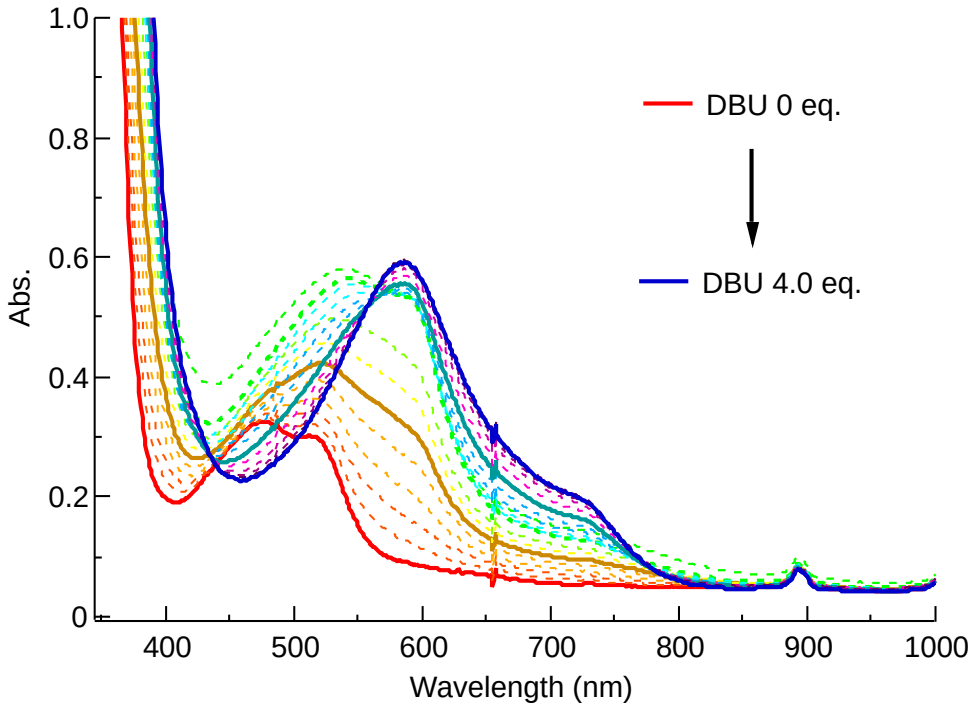

Figure 3.17: DBU titration UV spectra of **1_A** in acetonitrile solution

Base titration UV spectra of 1_A (mixture solution)

DBU titration UV data for **1_A** were measured in acetonitrile / N,N-dimethyformamide = 9 / 1 mixture solution (Figure 3.18). From DBU 0 eq. to 0.9 eq., the MLCT band was red-shifted with an isobestic point at 527 nm. The spectrum of **1_A** + 0.9 eq DBU (Figure 3.18 (left)) is almost the same as that of the solid-state spectrum of **1_B** (Figure 3.19). This suggests that stepwise deprotonation of **1_A** occurred in solution state. From DBU 0.9 eq. to 2.0 eq., the spectrum changes with no isobestic point (Figure 3.18 (center)). This process can be understood to involve deprotonation and iron oxidation reactions simultaneously. From DBU 2.0 eq. to 3.0 eq., the spectra were shifted with an isobestic point at 534 nm, and saturated (Figure 3.18 (right)). This process can be suggested to be conversion from **1_D** to **1_E**. These results indicate that complex **1_A** was deprotonated in a stepwise manner, and converted to **1_E** via intermediate states.

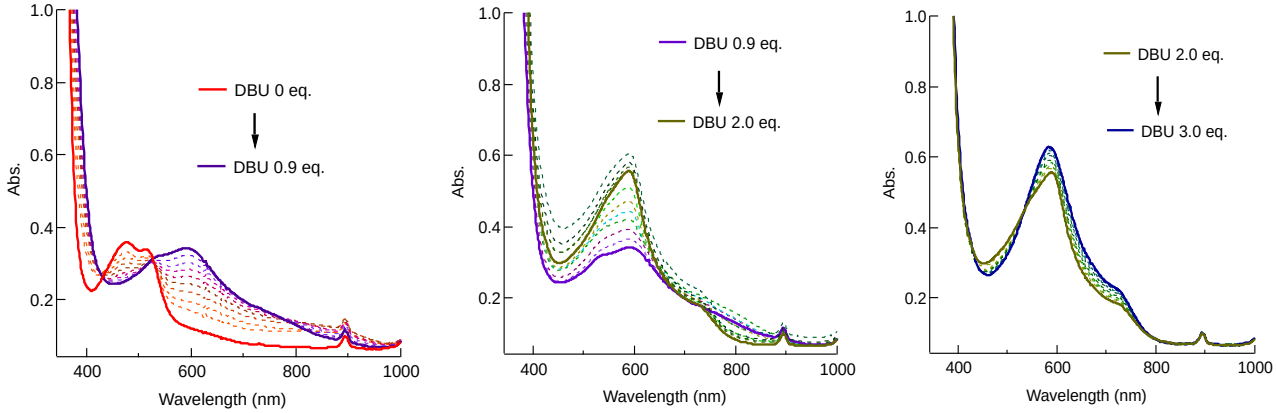

Figure 3.18: DBU titration UV spectra of **1_A**. in mixture solution (left: DBU 0 eq. to 0.9 eq., middle: DBU 0.9 eq. to 2.0 eq., right: 2.0 eq. to 3.0 eq.).

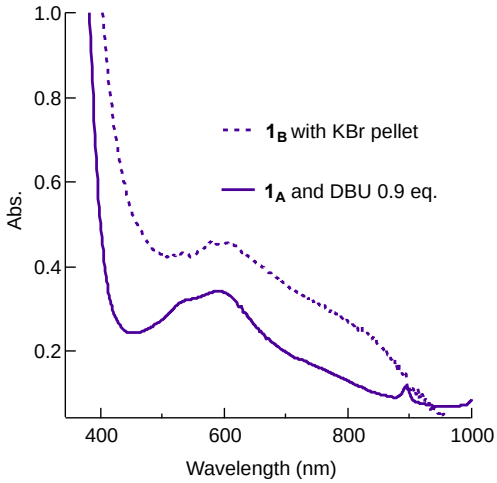

Figure 3.19: Comparison solid state UV of **1_B** and **1_A** with 0.9 eq. DBU.

Acid titration UV spectra of 1_E

Trifluoroacetic acid (TFA) titration UV data were measured for $\mathbf{1_E}$ in order to investigate protonation reactions. In acetonitrile solution, from TFA 0 eq. to 1.0 eq., the LMCT band decreased in intensity and a new peak appeared at longer wavelength (708 ~ 940 nm, Figure 3.20 (left)). This spectrum is almost same as that of the $\mathbf{1_D}$ solid state spectrum (Figure 3.21 (light)), suggesting that a single protonation has occurred. The solubility of $\mathbf{1_D}$ is not good, so no isobestic point was observed. From TFA 1.0 eq. to 2.0 eq., the peaks decreased in intensity with no isobestic point (Figure 3.20 (center)). This process corresponds to the protonation of complex $\mathbf{1_D}$. From TFA 2.0 eq. to 3.3 eq., a new peak was observed at 445 nm (Figure 3.20 (right)). From the comparison with the solid state UV, this spectrum is derived from the triply-protonated $\mathbf{1_C}$ or the quadruply-protonated complex (Figure 3.21 (right)). These results suggested that complex $\mathbf{1_E}$ was protonated in a stepwise manner in solution with no reduction.

Figure 3.20: TFA titration UV spectra of $\mathbf{1_E}$. (left: TFA 0 eq. to 1.0 eq., middle: TFA 1.0 eq. to 2.0 eq., right: TFA 2.0 eq. to 3.3 eq.

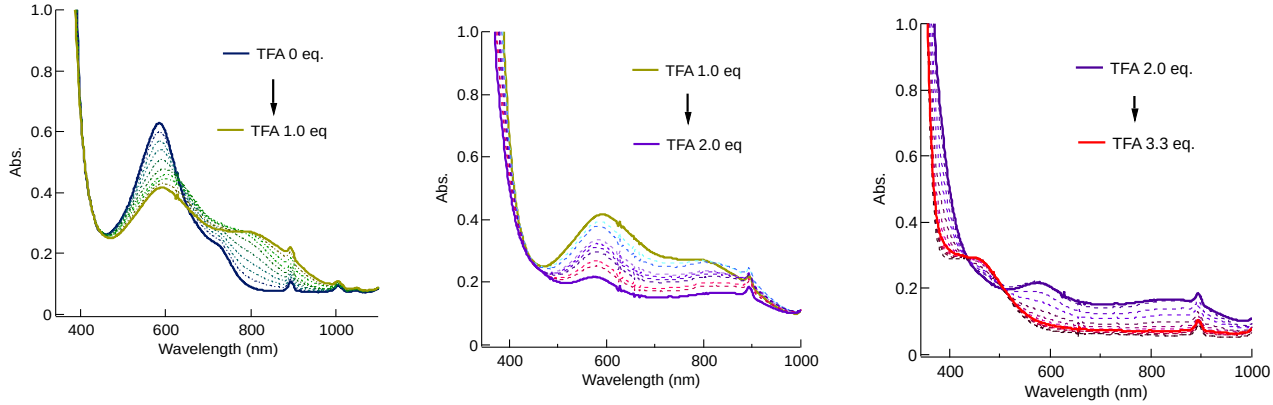

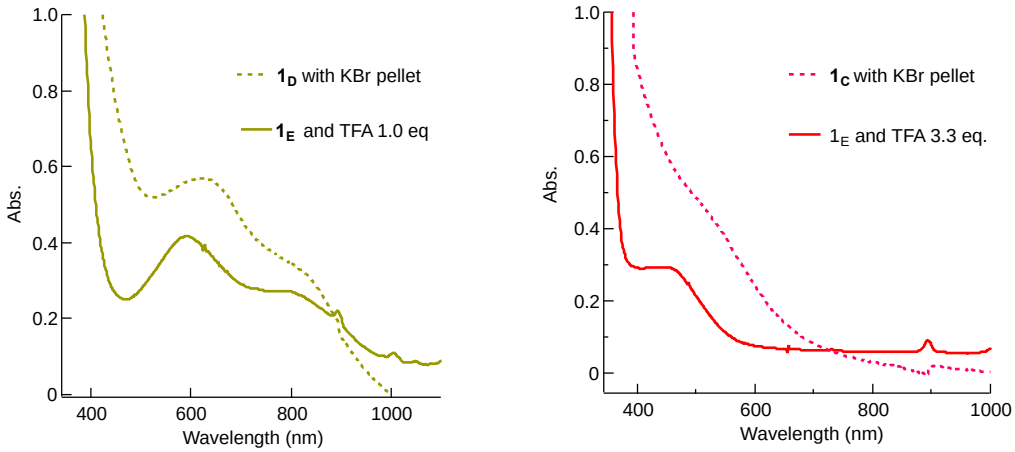

Figure 3.21: Comparison between solid state and solution-state TFA titration absorption spectra (left: $\mathbf{1_D}$ and $\mathbf{1_E}$ with 1.0 eq. TFA. right: $\mathbf{1_C}$ and $\mathbf{1_E}$ with 3.3 eq. TFA)

Vapor absorption induced electronic state conversion of $\mathbf{1_E}$

To explore the potential to effect protonation/deprotonation driven electronic state conversion in the solid-state, acid (or base) vapor absorption experiments were performed on complex $\mathbf{1_E}$. A powder sample of $\mathbf{1_E}$ was exposed to trifluoroacetic acid (TFA) vapor for 30 seconds and the color of the solid changed from blue to red (Figure 3.22 bottom). In addition, an increase in the magnetic moment was observed after exposure to acid. From comparing the normalized $\chi_m T$ values before and after exposure (Figure 3.22 top), that of the red powder ($\chi_m T$ = 3.830 emu K mol^{-1}) was about ten times as large as that of $\mathbf{1_E}$ ($\chi_m T$ = 0.366 emu K mol^{-1}). The difference corresponds to the conversion from Fe(III) LS state (calculated value of 0.375 emu K mol^{-1}) to HS state (calculated value of 4.375 emu K mol^{-1}). Namely, $\mathbf{1_E}$ converted to $\mathbf{1_C}$**'** by protonation and its spin state was changed. Moreover, exposure of the resultant HS sample $\mathbf{1_C}$**'** to ammonia vapor for one minute led a color change from red to green (Figure 3.22 bottom). The normalized $\chi_m T$ value decreased from 3.830 to 0.175 emu K mol^{-1}. This indicates that $\mathbf{1_C}$**'** (Fe(III) HS) was converted to $\mathbf{1_D}$**'** (Fe(III) LS). These results suggest that the Brønsted ligands allow the spin states of the iron complexes to be switched upon protonation/deprotonation even the solid-state.

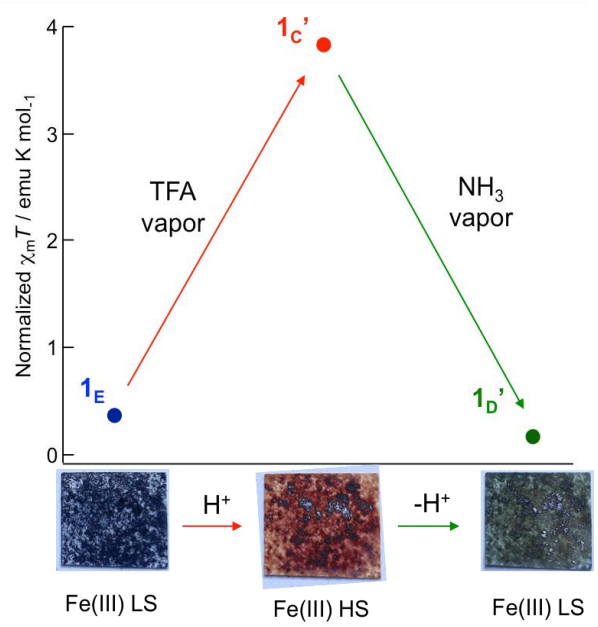

Figure 3.22: Normalized $\chi_m T$ values of vapor deposition experiment $\mathbf{1_E}$ (top) and color change of powder sample $\mathbf{1_E}$.

Electronic state conversion scheme of $\mathbf{1}_{A\text{-}E}$

Scheme 3.3 is a summary of the electronic state conversions achievable in a single mononuclear iron complex with Brønsted ligands. $\mathbf{1}_A$ can be deprotonated and converted to $\mathbf{1}_B$ by base. Both complexes showed SCO behavior, but the $T_{1/2}$ are different due to the modification of the ligand field upon deprotonation. The ferric complex $\mathbf{1}_C$ can be deprotonated with base in a stepwise manner, and converted to $\mathbf{1}_D$ or $\mathbf{1}_E$. $\mathbf{1}_C$ exists in the Fe(III) HS state at all temperature, while $\mathbf{1}_D$ and $\mathbf{1}_E$ exist only in the LS state. The interconversion between Fe(III) complexes is reversible in solution, and moreover, even in the solid-state, $\mathbf{1}_E$ was converted to $\mathbf{1}_C$ by exposure to acid vapor. When strong base was added in $\mathbf{1}_A$ solution, both oxidation and deprotonation occurred and caused conversion to $\mathbf{1}_E$, indicating that ligand deprotonation stabilized the high oxidation state of iron.

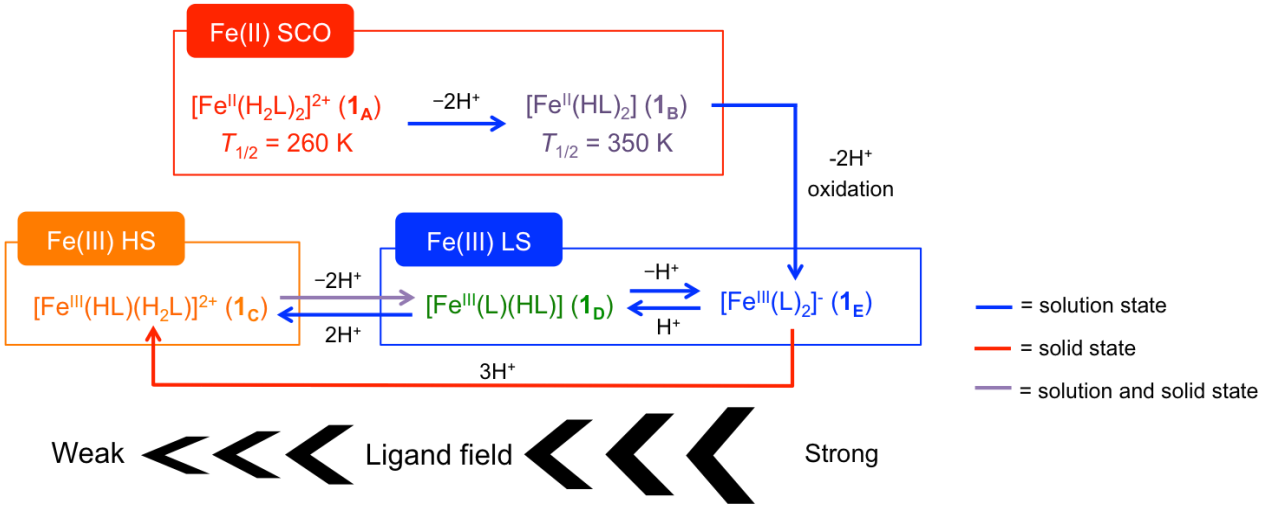

Scheme 3.3: Summary of electronic state conversions.

3.4 Conclusion

We have demonstrated that a novel ligand design strategy employing an asymmetric, tridentate, Brønsted ligand permits multi-state switching behaviour in a simple mononuclear coordination complex. Unlike in the handful of previous examples of protonation-triggered switching in mononuclear metal complexes, which show exclusively binary switching responses, we have demonstrated that five distinct electronic states can be accessed, all of which show differing colorimetric, electrochemical and/or magnetic properties. This unique multi-step switching response is due to the asymmetric design of the Brønsted ligand groups, allowing the ligand field of the central Fe ion to be carefully tuned by sequential deprotonation steps as a result of the different pK_a values of the incorporated pyrazole and benzimidazole moieties. The asymmetric ligand design strategy employed here should be broadly applicable across a wide range of different coordination complexes and could also be used in the design of novel supramolecular assemblies or sensors based on molecular recognition through dynamic H-bonding interactions. Multi-responsive, proton-coupled systems based on this strategy will represent an important next-step in the development of smart molecular devices with switchable physical and electronic states.

References

[1] (a)Bousseksou, A., Molnár, G., Demont, P. & Menegotto, J. *J. Mater. Chem.* **2003**, *13*, 2069–2071; (b) O. Kahn, C. J. Martinez, *Science* **1998**, *279*, 44-48; (c) G. Aromí, D. Aguilà, P. Gamez, F. Luis, O. Roubeau, *Chem. Soc. Rev.* **2012**, *41*, 537-546; (d) O. Sato, *Nature Chem.* **2016**, *8*, 644.

[2] (a) Halepto, D. M., Holt, D. G. L., Larkworthy, L. F. Leigh, G. L. Povey, D.C. & Smith, G. W. *J. Chem. Soc., Chem. Commum.* **1989**,1322; (b) Sim, P. G. & Sinn, E. *J. Am. Chem. Soc.* 1981, **103**, 241-243; (c) Hayami, S., Komatsu, Y., Shimizu, T., Kamihata, H. & Lee, Y. H. *Coord. Chem. Rev.* **2011**, *255*, 1981-1990.

[3] (a) Halder, G., Kepert, C. J., Moubaraki, B., Murray, K. S. & Cashion, J. D., *Science,* **2002**, *298*, 1762-1765; (b) J.-F. Létard, J. A. Real, N. Moliner, A. B. Gaspar, L. Capes, O. Cador, O. Kahn, *J. Am. Chem. Soc.* **1999**, *121*, 10630-10631; (c) I. A. Gass, S. R. Batten, C. M. Forsyth, B. Moubaraki, C. J. Schneider, K. S. Murray, *Coord. Chem. Rev.* **2011**, *255*, 2058-2067; (d) M. C. Muñoz, J. A. Real, *Coord. Chem. Rev.* **2011**, *255*, 2068-2093; (e) M. G. Cowan, J. Olguín, S. Narayanaswamy, J. L. Tallon, S. Brooker, *J. Am. Chem. Soc.* **2012**, *134*, 2892-2894; (f) T. Matsumoto, G. N. Newton, T. Shiga, S. Hayami, Y. Matsui, H. Okamoto, R. Kumai, Y. Murakami, H. Oshio, *Nature Commun.* **2014**, *5*, 3865.

[4] (a) J. A. Kitchen, J. Olguín, R. Kulmaczewski, N. G. White, V. A. Milway, G. N. L. Jameson, J. L. Tallon, S. Brooker, *Inorg. Chem.* **2013**, *52*, 11185-11199; (b) M. Seredyuk, K. O. Znovjyak, J. Kusz, M. Nowak, M. C. Muñoz, J. A. Real, *Dalton Trans.* **2014**, *43*, 16387-16394; (c) D. Müller, C. Knoll, M. Seifried, J. M. Welch, G. Giester, M. Reissner, P. Weinberger, *Chem. Eur. J.* **2018**, *24*, 5271-5280.

[5] (a) M. Yamada, E. Fukumoto, M. Ooidemizu, N. Bréfuel, N. Matsumoto, S. Iijima, M. Kojima, N. Re, F. Dahan, J.-P. Tuchagues, *Inorg. Chem.* **2005**, *44*, 6967-6974; (b) Y. Sekine, M. Nihei, H. Oshio, *Chem. Eur. J.* **2017**, *23*, 5193-5197.

[6] (a) C. P. Berlinguette, A. Dragulescu-Andrasi, A. Sieber, J. R. Galán-Mascarós, H.-U. Güdel, C. Achim, K. R. Dunbar, *J. Am. Chem. Soc.* **2004**, *126*, 6222-6223; (b) D. Li, R. Clérac, O. Roubeau, E. Harté, C. Mathonière, R. Le Bris, S. M. Holmes, *J. Am. Chem. Soc.* **2008**, *130*, 252-258.

[7] (a) E. Coronado, M. Giménez-Marqués, G. Mínguez Espallargas, F. Rey, I. J. Vitórica-Yrezábal, *J. Am. Chem. Soc.* **2013**, *135*, 15986-15989; (b) M. J. Murphy, K. A. Zenere, F. Ragon, P. D. Southon, C. J. Kepert, S. M. Neville, *J. Am. Chem. Soc.* **2017**, *139*, 1330-1335.

[8] (a) F. Lambert, C. Policar, S. Durot, M. Cesario, L. Yuwei, H. Korri-Youssoufi, B. Keita, L. Nadjo, *Inorg. Chem.* **2004**, *43*, 4178-4188; (b) Y.-H. Luo, M. Nihei, G.-J. Wen, B.-W. Sun, H. Oshio, *Inorg. Chem.* **2016**, *55*, 8147-8152.

[9] (a) K. Sugiyarto, D. Craig, A. Rae, H. Goodwin, *Aust. J. Chem.* **1994**, *47*, 869-890; (b) Y. Sunatsuki, Y. Ikuta, N. Matsumoto, H. Ohta, M. Kojima, S. Iijima, S. Hayami, Y. Maeda, S. Kaizaki, F. Dahan, J.-P. Tuchagues, *Angew. Chem. Int. Ed.* **2003**, *42*, 1614-1618; (c) G. Brewer, L. J. Alvarado, C. T. Brewer, R. J. Butcher, J. Cipressi, C. Viragh, P. Y. Zavalij, *Inorg. Chim. Acta* **2014**, *421*, 100-109.

[10] S. Dhers, A. Mondal, D. Aguilà, J. Ramírez, S. Vela, P. Dechambenoit, M. Rouzières, J. R. Nitschke, R. Clérac, J.-M. Lehn, *J. Am. Chem. Soc.* **2018**, *140*, 8218-8227.

[11] Sheldrick, G. M. (1996).

CHAPTER 4

An Antiferromagnetically Coupled Heterometal Cu_6Fe Wheel

4.1 Introduction

Polynuclear complexes exhibit physical properties and functions derived from the electronic and magnetic interactions between their constituent transition metal ions, and the search for new compounds with novel properties and functions continues to be an important area of research.[1] In the field of biomolecular chemistry, several enzyme models with polynuclear active sites have been investigated.[2] It is thus critical to find effective synthetic methods for polynuclear clusters in order to better understand the reaction mechanisms of these active sites.

A range of alkoxo bridged polynuclear metal clusters, such as homometal [Mn_{13}] clusters,[3] [Fe_7][4] and [Mn_7][5] wheels, and heterometal [Mn_8Cu_{12}][6] and [Mn_5Ln_6] species[7] were investigated. In addition, various self-assembled clusters, rings, grids, and helices were synthesized by using polypyridine-type ligands.[8] The archetypical polynuclear complexes based on *β*-diketone-type ligands are antiferromagnetic rings. Caneschi *et al*. reported a [Fe_{10}] ring, which shows stepwise magnetization originating from the level-crossing of spin ground states at low temperature.[9] [$NaFe_6$][10] and [$LiFe_6$],[11] wheel-type complexes also show quantum magnetization steps. Note that research into heterometal rings and wheel complexes has been limited due to the difficulty of their syntheses.

In addition, some polynuclear complexes have acidic N-H parts as Brønsted acid/base moieties. These parts enable tuning of the physical properties of complexes by deprotonation (or protonation). Physical property conversion has two types, one is spin state conversion, and the other is arrangement conversion by deprotonation. In 2018, Clérac *et al*. synthesized tetranuclear iron (II) grid $[Fe^{II}_4(H_2L)_4](BF_4)_8$, ($H_2L$ = Pyridine-2-carboxaldehyde [2-(3,4,5-Trimethoxyphenyl)pyrimidine-4,6-diyl]dihydrazone), and it showed both stepwise deprotonation and SCO behavior conversion.[12] Ligand deprotonation is a useful method to change complex spin state, not only in mononuclear complexes but also in polynuclear cluster. At present, however, examples of this are very rare. The synthesis of multinuclear complexes with has Brønsted acid/base moieties is therefore important research from the viewpoint of catalyst design and the fabrication of new switchable materials.

In this work, we focus on the asymmetric multidentate bridging ligand, 1-(2-pyridine)-3-(2-pyrrole)acetylacetone (H_2L^5, scheme 4.1), and its complexation reactions with copper and iron sources have been investigated. This ligand has one pyrrole moiety which has acidic proton (pK_a = 23.0). This part can act as a metal coordination site when deprotonated. So H_2L^5 is a useful building block for the synthesis of metal clusters.[13] In addition, the pyrrole moiety part can act as a Brønsted acid/base too. Hydrogen bonded interaction between clusters can therefore be considered very likely. Herein, the synthesis, structure, magnetic properties, and proton response in solution of the obtained heptanuclear Cu_6Fe wheel complex are reported.

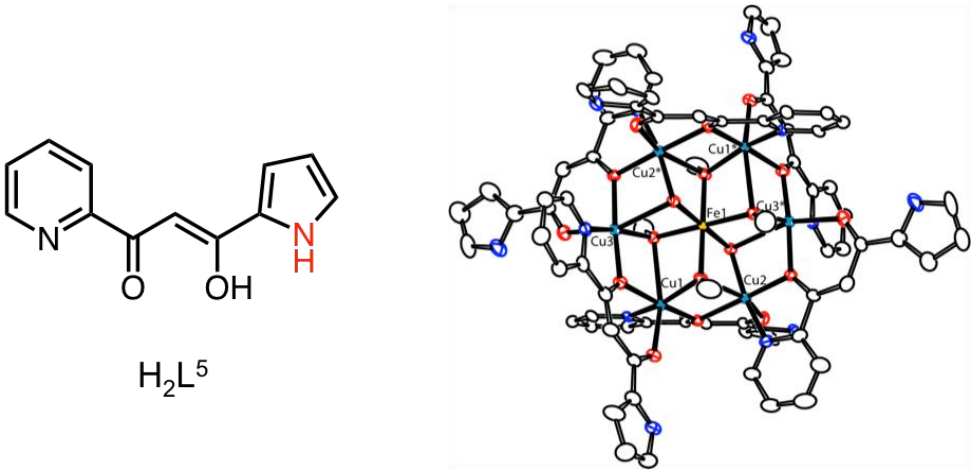

H_2L^5

Scheme 4.1 Structure of H_2L_{py} and ORTEP diagrams of Cu_6Fe wheel complex.

4.2 Experiments

Materials

All chemicals were used without further purification except when noted. Solvents and reagents were used as received from commercial suppliers.

SQUID Magnetometer Measurements

Variable-temperature magnetic susceptibility measurements were carried out on polycrystalline samples using a Quantum Design MPMS-XL SQUID magnetometer. Pascal's constants were used to determine the diamagnetic corrections.

X-ray Crystallography

Crystals were mounted on a glass capillary or a MiTeGen Dual-Thickness MicroMount, and data were collected at 100 K (Bruker SMART APEXII diffractometer coupled with a CCD area detector with graphite monochromated Mo-$K\alpha$ (λ = 0.71073 Å) radiation). The structure was solved using direct methods and expanded using Fourier techniques within the SHELXTL program. Empirical absorption corrections by SADABS[14] were carried out. In the structure analyses, non-hydrogen atoms were refined with anisotropic thermal parameters. Hydrogen atoms were included in calculated positions and refined with isotropic thermal parameters riding on those of the parent atoms.

Mössbauer spectra

Mössbauer experiments were carried out using a ^{57}Co/Rh source in a constant-acceleration transmission spectrometer (Topologic Systems) equipped with an Iwatani HE05/CW404 cryostat. The spectrometer was calibrated using standard α-Fe foil.

Electrochemical measurements

Electrochemical measurements were carried out using a BAS 620A electrochemical analyzer. Cyclic voltammetry and differential pulse voltammetry measurements were carried out in a standard one-compartment cell under N_2 at 20 °C equipped with a platinum-wire counter electrode, a saturated calomel electrode (SCE) as the reference electrode, and a glassy carbon (GC) working electrode.

UV-Vis-NIR spectroscopy

UV-Vis-NIR absorption spectra were recorded on Agilent Technologies Cary 8454 UV-Vis spectrometer.

Elemental analysis

Elemental analyses were performed using a Perkin Elmer 2400 element analyzer.

Synthesis Procedures

Synthesis of 1-(2-pyridine)-3-(2-pyrrole)acetylacetone (H_2L^5)

A solution of sodium ethoxide prepared by sodium (2.46 g, 107 mmol), 2-acetylpyrrole (12.5 g, 82.7 mmol) and picolinic acid ethyl ester (9.025 g, 82.7 mmol) in 150 ml of diethylether was refluxed for 4 hours under a nitrogen atmosphere. The resulting yellow solid was filtered and aqueous acetic acid (15 % (v/v)) was added to the residue. The resulting light-yellow solid was filtered, and dried in a vacuum desiccator. Recrystallization from methanol yielded light yellow microcrystals (3.48 g). Yield 20 %. ^{1}H NMR (400 MHz, $CDCl_3$): δ 9.25 (s, 1H, pyrrole NH), 8.69 (d, 1H, py), 8.05 (d, 1H, py), 7.83 (t, 1H, py), 7.39 (t, 1H, py), 7.24 (d, 1H, pyrrole), 7.10 (d, 1H, pyrrole), 6.35 (s, 1H, pyrrole). Selected IR (KBr): 1628(s), 1580(s), 1566(s), 1541(s), 1441(s), 1138(s), 1124(s), 787(s), 746(s) cm^{-1}. Anal. (Calc). for $C_{12}H_{10}N_2O_2$: C, 67.28 (67.37); H, 4.71 (4.87); N, 13.08 (13.06).

Synthesis of $[Cu^{II}_6Fe^{III}(HL^5)_6(OH)_2(OCH_3)_4](NO_3)_3 \cdot 6H_2O$ ($[Cu_6Fe] \cdot 6H_2O$)

To a methanol solution (15 mL) of $Cu(NO_3)_2 \cdot 3H_2O$ (24.2 mg, 0.1 mmol) was added a methanol solution (10 mL) of H_2L^5 (21.4 mg, 0.1 mmol) with trimethylamine (27.6 μL, 0.2 mmol). The resulting brown solution was stirred and a methanol solution (5 mL) of $Fe(NO_3)_3 \cdot H_2O$ (6.7 mg, 0.0167 mmol) was added. The reaction mixture was slowly evaporated for one week allowing yellow plates of the heptanuclear Cu_6Fe complex, $[Cu^{II}_6Fe^{III}(HL^5)_6(OH)_2(OCH_3)_4](NO_3)_3 \cdot 6H_2O$ (**$[Cu_6Fe] \cdot 6H_2O$**), to be obtained. The crystals were filtered and air dried, affording **$[Cu_6Fe] \cdot 6H_2O$** (12.1mg, yield 34%) C, 42.09 (42.25); H, 3.72 (3.78); N, 9.69% (9.88). ICP data suggests ratio of Cu:Fe is 6:0.93. IR (KBr): 1385, 1472, 1528, 1595, 1609 cm^{-1}. Anal. Calcd. (found) for $C_{76}H_{80}N_{15}O_{33}Cu_6Fe$: C, 42.09 (42.25); H, 3.72 (3.78); N, 9.69 (9.88).

Table 4.1: Crystal parameters of **[Cu_6Fe]**.

	[Cu_6Fe]
T / K	100
Instrument	APEX2
Formula	$C_{76}H_{84}N_{15}O_{35}Cu_6Fe$
F.W.	2204.68
Space Group	*C*2/c
a / Å	18.487 (2)
b / Å	18.231 (3)
c / Å	29.363 (4)
α / °	90
β / °	108.090 (2)
γ / °	90
V / Å^3	9467 (2)
Z	4
*R*1 (> 2σ)	0.0711
*wR*2 (> 2σ)	0.1121

4.3 Results and Discussion

Structure

X-ray structural analyses reveal that the heptanuclear complex consists of six singly-protonated ligands HL^5, six copper ions on the rim of the wheel and one iron ion at the centre of the wheel, bridged by four alkoxo and two hydroxo ions (Figure 4.1). Each ligand acts as a bridging ligand between two metal centers on the rim, with the *β*-diketone and the pyridine-enol sites acting as bidentate chelating ligands. The copper ions have N1O5 octahedral coordination environments and are coordinated by both *β*-diketone and pyridine-enol sites. All copper ions exhibit Jahn-Teller distortions toward oxygen atoms belonging to methoxo/hydroxo and ketone moiety (represented in Figure 4.2: O2-Cu1-O9, O4-Cu2-O7, and O6-Cu3-O8). The iron ion located at the centre of the wheel molecule has an O6 octahedral coordination geometry with four methoxo and two hydroxo groups. Considering charge balance and bond valence sum calculations, the valence of the iron ion was estimated as trivalent. The wheel molecule has an inversion centre on the iron ion and there are three nitrate ions in the crystal lattice per wheel molecule.

Mössbuer spectra

To determine the spin state of the iron ion, Mössbauer spectra was collected (Figure 4.3). Parameters are listed in table 4.2. This data indicates that the compound included an Fe(III) high spin species, of which the doublet has Mössbauer parameters δ_{IS} = 0.20 mm s^{-1} and ΔE_Q = 0.40 mm s^{-1}, typical for a high spin Fe(III) ion.

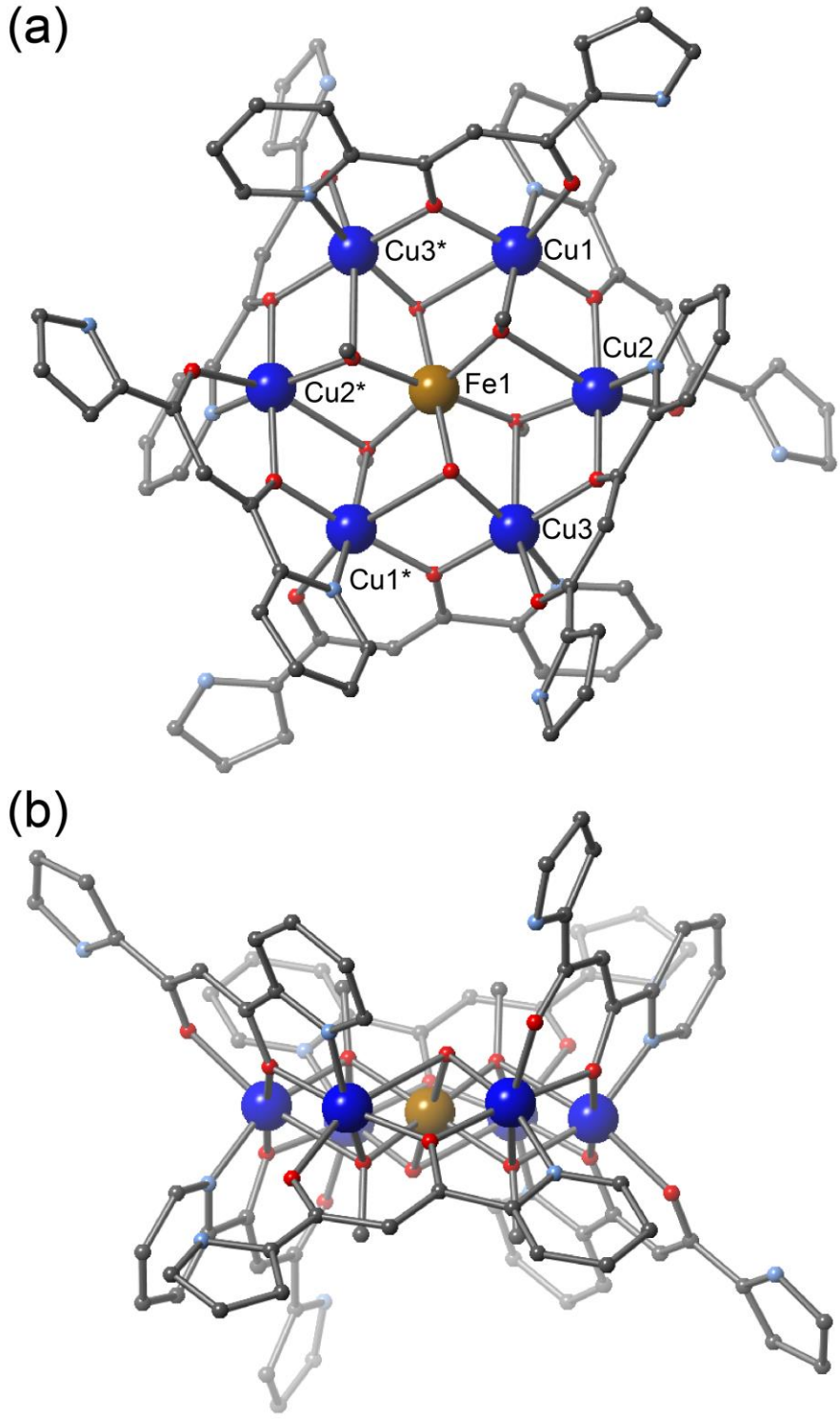

Figure 4.1; Molecular structure of **[Cu_6Fe]** determined at 100K. (a) top view and (b) side view. Hydrogen atoms, solvent molecules, and counter anions are omitted for clarity.

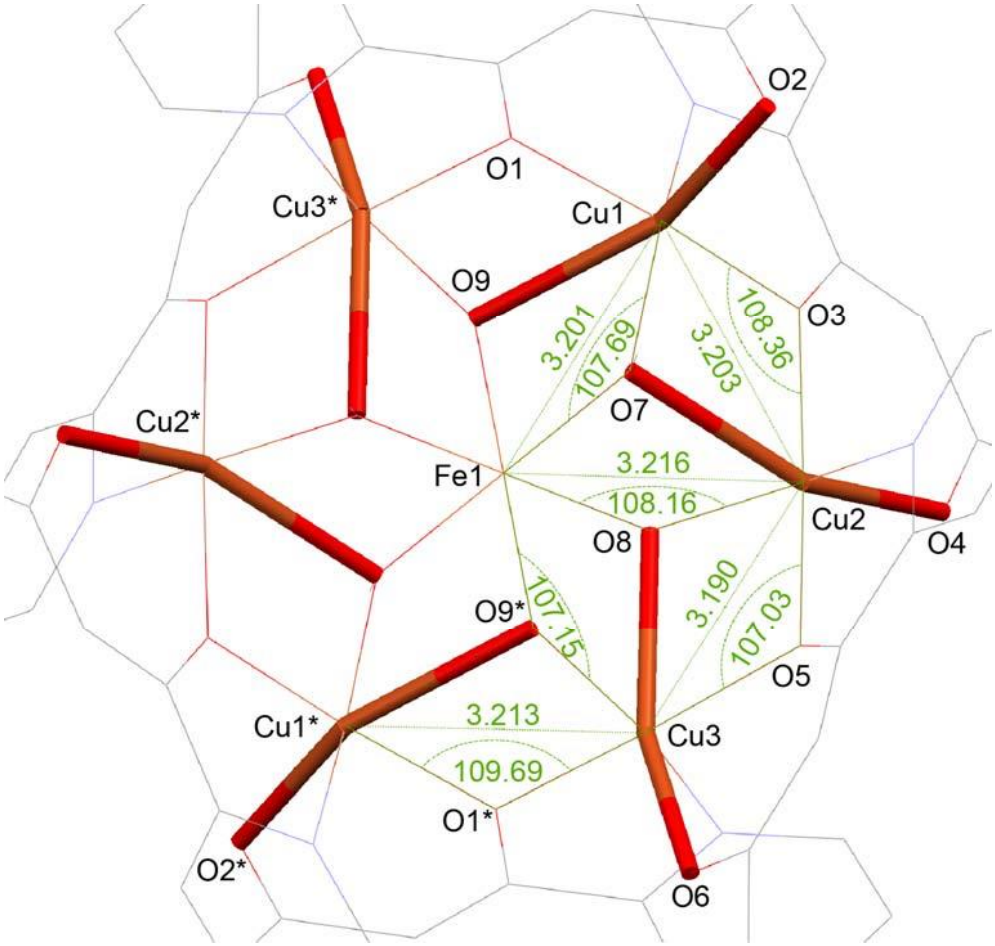

Figure 4.2: Core structure of **[Cu_6Fe]** and selected geometrical information. This figure represents details of the core structure of the Cu_6Fe wheel. Atomic bonds depicted as capped sticks represent Jahn-Teller axes. Selected intermetallic separations and bridging angles related to effective magnetic paths are shown in green text.

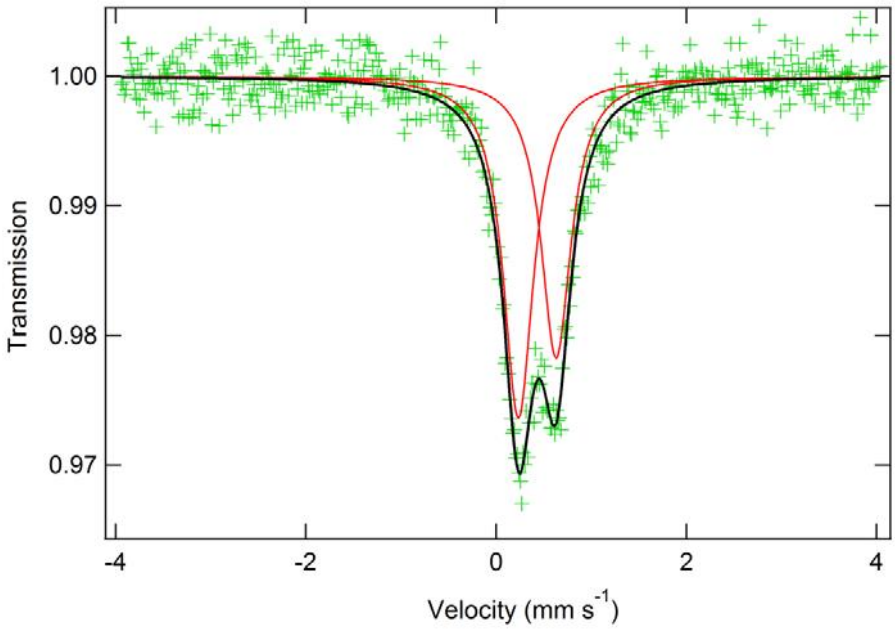

Figure 4.3: Mössbauer spectra of **[Cu_6Fe]** at 20 K.

Table 4.2: Mössbauer parameters of **[Cu_6Fe]** at 20 K.

δ_{IS} (mm / s)	ΔE_Q (mm / s)	Spin state
0.20	0.40	Fe(II) HS

DC magnetic susceptibility.

Cryomagnetic studies reveal that antiferromagnetic interactions are operative between metal ions (Figure 4.4). The $\chi_m T$ value at 300 K is 5.34 emu mol^{-1} K, which is smaller than the expected value, 6.625 emu mol^{-1} K, for six magnetically isolated Cu(II) ions (S = 1/2) and one high spin Fe(III) ion (S = 5/2). As temperature decreased, so did the $\chi_m T$ values, reaching 0.800 emu mol^{-1} K at 1.8 K. In field dependent magnetization measurements, the magnetization saturation value at 1.8 K is 1.5 $N\beta$, indicating an S = 1/2 spin ground state. According to the molecular structure, a spin model with two kinds of magnetic exchange pathways can be applied to the magnetic analyses (Figure 4.4 inset), corresponding to the following spin Hamiltonian.

$$\begin{aligned} H = & -2J_{\mathrm{Cu–Cu}}(S_{\mathrm{Cu1}}\cdot S_{\mathrm{Cu2}} + S_{\mathrm{Cu2}}\cdot S_{\mathrm{Cu3}} + S_{\mathrm{Cu3}}\cdot S_{\mathrm{Cu1}*} \\ & + S_{\mathrm{Cu1}*}\cdot S_{\mathrm{Cu2}*} + S_{\mathrm{Cu2}*}\cdot S_{\mathrm{Cu3}*} + S_{\mathrm{Cu3}*}\cdot S_{\mathrm{Cu1}}) \\ & - 2J_{\mathrm{Fe–Cu}}(S_{\mathrm{Fe1}}\cdot S_{\mathrm{Cu1}} + S_{\mathrm{Fe1}}\cdot S_{\mathrm{Cu2}} + S_{\mathrm{Fe1}}\cdot S_{\mathrm{Cu3}} \\ & + S_{\mathrm{Fe1}}\cdot S_{\mathrm{Cu1}*} + S_{\mathrm{Fe1}}\cdot S_{\mathrm{Cu2}*} + S_{\mathrm{Fe1}}\cdot S_{\mathrm{Cu3}*}) \end{aligned}$$

Using the PHI program, the following parameters were obtained, g_{Cu} = 2.15, g_{Fe} = 2.00, $J_{Cu\text{-}Cu}$ = -12.0 cm^{-1}, and $J_{Fe\text{-}Cu}$ = -116.0 cm^{-1}. The $d_{x2\text{-}y2}$ magnetic orbitals on the Jahn-Teller axis of the peripheral copper ions can overlap through enolate oxygen atoms (O1, O3, and O5) and the bridging angles were found to be between 107.03-109.69 degrees, mediating antiferromagnetic interactions. On the other hand, magnetic interactions between iron and copper ions will operate through the μ_3-methoxo/hydroxo bridges (O7, O8, and O9), in which the bridging angles range from 107.15 to 108.16 degrees. As the intermetallic separations are not especially long (as represented in Figure 4.2), these bridging conditions will likewise favor antiferromagnetic interactions due to the significant overlap of magnetic orbitals between the iron and copper ions.

Field-dependent magnetization data is shown in Figure 4.5. The data was compared with the theoretical curve simulated by the same parameters for temperature-dependent magnetic susceptibilities, suggesting an S = 1/2 spin ground state in the low temperature region. If strong antiferromagnetic interactions between copper ions are assumed, a spin ground state of S = 5/2 originating from the high spin Fe(III) ion can be justified in this spin model. However, saturated magnetization is close to S =1/2 ground state, which is derived from strong antiferromagnetic interactions between copper and iron ions. This situation is consistent with analysis of magnetic susceptibilities by the above mentioned spin model. The generation of fully reliable fitting parameters would necessitate synthesis of an isostructural Cu_6Zn wheel with a diamagnetic central zinc ion.

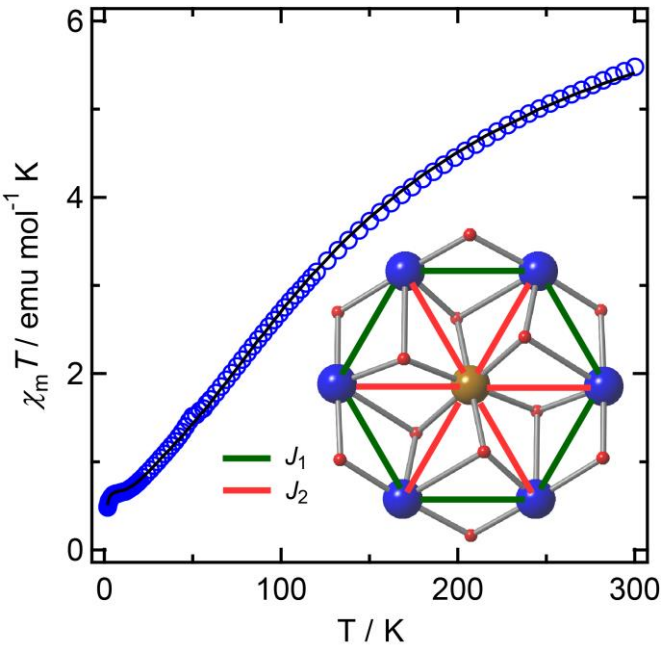

Figure 4.4: The $\chi_m T$ versus T plot for **[Cu_6Fe]**. The solid line represents the best fit (see text). Shown inset are the coupling interactions modeled in the magnetic analysis.

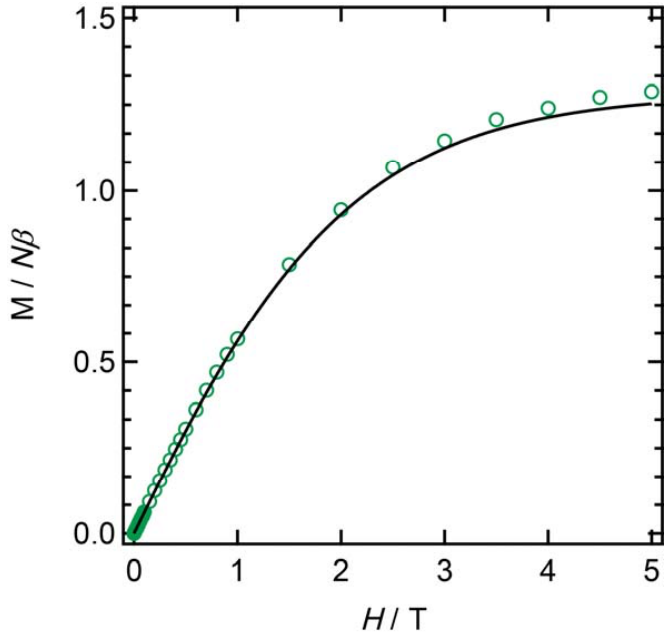

Figure 4.5: Magnetization curve of **[Cu_6Fe]** at 1.8 K. Solid line indicates theoretical magnetization curve analyzed by spin model described inset.

Base titration electrochemical properties

Electrochemical data obtained in acetonitrile are shown in Figure 4.6. At first, reduction waves were observed at -0.75, -1.13, and -1.57 V versus SCE but each of these waves were irreversible. The data suggest that the complex **[Cu_6Fe]** is not stable during redox processes. After 1,8-Diazabicyclo [5.4.0] undec-7-ene (DBU) addition, a new peak appeared at -0.87 V, however, stepwise change was not observed. This peak was likely derived from decomposed **[Cu_6Fe]**.

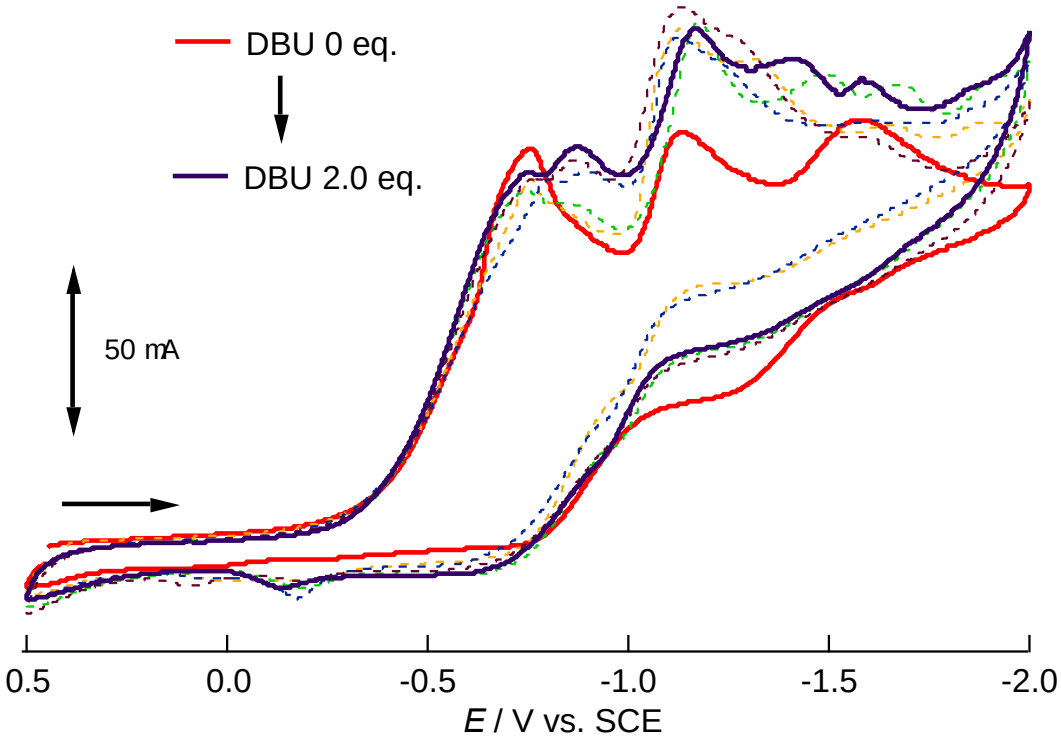

Figure 4.6: DBU titration cyclic voltammogram of **[Cu_6Fe]** in acetonitrile / 0.1M *n*-Bu_4NPF_6

Base titration UV absorption spectra

Absorption spectra of **[Cu$_6$Fe]** in acetonitrile at room temperature were shown in figure 4.7. The complex shows an absorption maximum at 378 nm, which is assigned to the LMCT band from bridging μ_3-methoxo/hydroxo groups to the Fe(III) ion. Upon addition of 1,8-Diazabicyclo [5.4.0] undec-7-ene (DBU), the LMCT band shifted to 412 nm and saturated at 3.0 eq. DBU. It suggests that ligand deprotonation caused some change of **[Cu$_6$Fe]**. **[Cu$_6$Fe]** has six protonated parts, so it is reasonable to suggest that that half of the Brønsted acid/base parts were deprotonated. In basic solution, **[Cu$_6$Fe]** may exist as the deprotonated cluster, or undergo dimerization, or decomposition. In order to determine the nature of the deprotonated species, crystallization and ESI-MS measurements after base titration will be required.

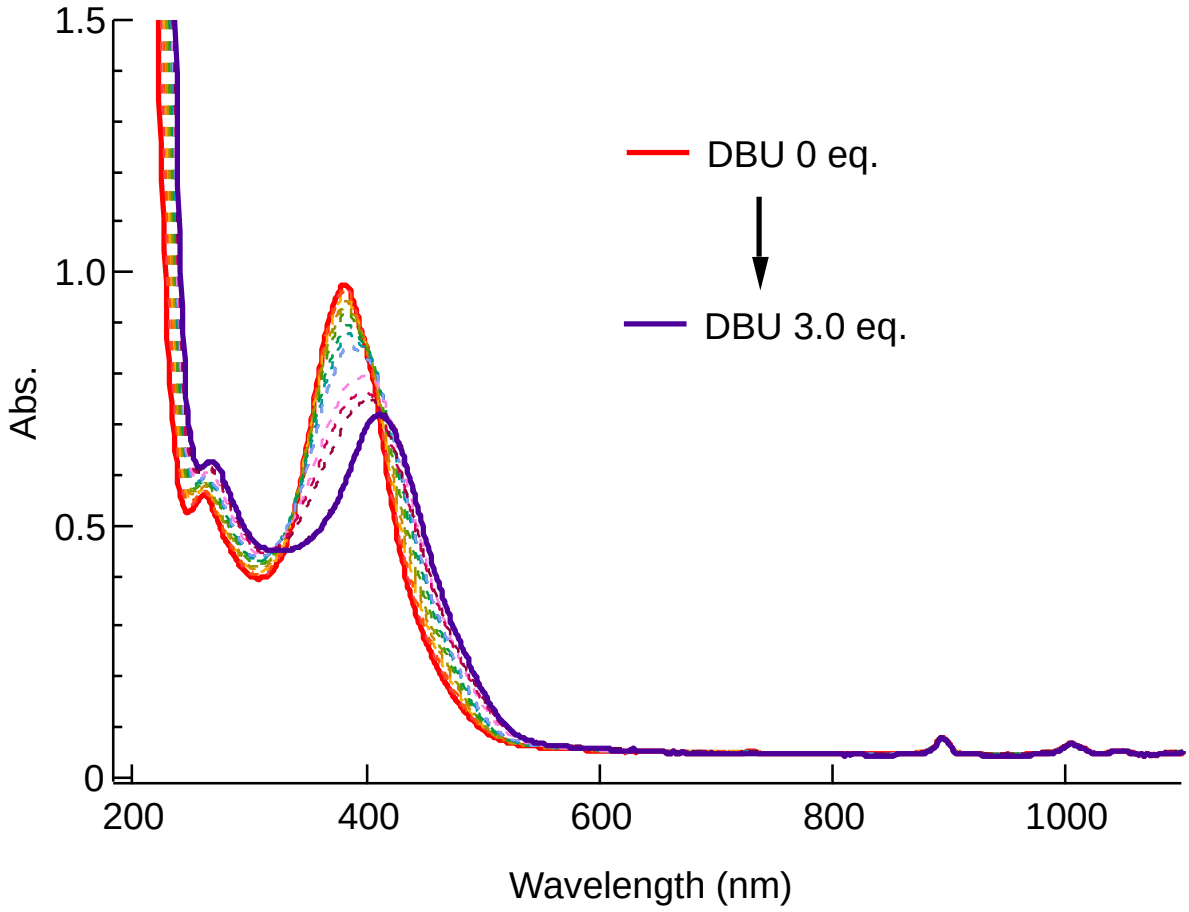

Figure 4.7: DBU titration UV spectra of **[Cu$_6$Fe]** in acetonitrile.

4.4 Conclusion

A heterometal wheel complex **[Cu_6Fe]** with Brønsted acid/base ligands was synthesized by the one-pot reaction of an asymmetric *β*-diketone-type ligand H_2L^5 with copper and iron sources. The magnetic properties and physical properties in solution were investigated. From measurement of UV and CV, **[Cu_6Fe]** was shown to convert to another cluster in basic solution. These results suggested that **[Cu_6Fe]** showed proton response. The synthesis proton responsive multinuclear clusters is an important research goal from the viewpoint of catalyst development and responsive magnetic material fabrication. These results will provide useful information to aid in the development of new functional materials.

References

[1] (a) P. Chaudhuri, *Coord. Chem. Rev*. **2003**, *243*, 143; (b) K. Takanashi, A. Fujii, R. Nakajima, H. Chiba, M. Higuchi, Y. Einaga, K. Yamamoto, *Bull. Chem. Soc. Jpn*. **2007**, *80*, 1563; (c) P. Vairaprakash, H. Ueki, K. Tashiro, O. M. Yaghi, *J. Am. Chem. Soc*. **2011**, *133*, 759; (d) Kyle W. Galloway, Alexander M. Whyte, Wolfgang Wernsdorfer, Javier Sanchez-Benitez, Konstantin V. Kamenev, Andrew Parkin, Robert D. Peacock, Mark Murrie, *Inorg. Chem*. **2008**, *47*, 7438; (e) A. J. Tasiopoulos, A. Vinslava, W. Wernsdorfer, K. A. Abboud and G. Christou, *Angew. Chem., Int. Ed*., **2004**, *43*, 2117; (f) G. A. Timco, T. B. Faust, F. Tuna, R. E. P. Winpenny, *Chem. Soc. Rev*. **2011**, *40*, 3067. (g) E. J. L. McInnes, S. Piligkos, G. A. Timco, R. E. P. Winpenny, *Coord. Chem. Rev*. **2005**, *249*, 2577.

[2] P. Buchwalter, J. Rosé, P. Braunstein, *Chem. Rev.* **2015**, *115*, 28.

[3] G. N. Newton, S. Yamashita, K. Hasumi, J. Matsuno, N. Yoshida, M. Nihei, T. Shiga, M. Nakano, H. Nojiri, W. Wernsdorfer, H. Oshio, *Angew. Chem., Int. Ed*. **2011**, *50*, 5716.

[4] N. Hoshino, A. M. Ako, A. K. Powell, H. Oshio, *Inorg. Chem*. **2009**, *48*, 3396.

[5] S. Koizumi, M. Nihei, T. Shiga, M. Nakano, H. Nojiri, R. Bircher, O. Waldmann, S. T. Ochsenbein, H. U. Güdel, F. Fernandez-Alonso, H. Oshio, *Chem.-Eur. J*. **2007**, *13*, 8445.

[6] S. Yamashita, T. Shiga, M. Kurashina, M. Nihei, H. Nojiri, H. Sawa, T. Kakiuchi, H. Oshio, *Inorg. Chem*. **2007**, *46*, 3810.

[7] T. Shiga, T. Onuki, T. Matsumoto, H. Nojiri, G. N. Newton, N. Hoshino, H. Oshio, *Chem. Commun*. **2009**, 3568.

[8] H. Sato, M. Yamaguchi, T. Onuki, M. Noguchi, G. N. Newton, T. Shiga, H. Oshio, *Eur. J. Inorg. Chem*. **2015**, 2193.

[9] M. Affronte, J. C. Lasjaunias, A. Cornia, A. Caneschi, *Phys. Rev. B* **1999**, *60*, 1161.

[10] A. Caneschi, A. Cornia, A. C. Fabretti, S. Foner, D. Gatteschi, R. Grandi, L. Schenetti, *Chem.-Eur. J.* **1996**, *2*, 1379.

[11] M. Affronte, J. C. Lasjaunias, A. Cornia, *Eur. Phys. J. B*, **2000**, *15*, 633.

[12] Sébastien Dhers, Abhishake Mondal, David Aguilá, Juan Ramírez, Sergi Vela, Pierre Dechambenoit, Mathieu Rouziéres, Jonathan R. Nitschke, Rodophe Clérac, Jean-Marie Lehn, *J. Am. Chem. Soc.* **2018**, *140*, 8218–8227.

[13] M. Yamaguchi, Mathter Thesis, University of Tsukuba, 2015.

[14] Sheldrick, G. M. (1996).

CHAPTER 5

General Conclusion

Multi-bistable materials are useful for next generation memory devices, because these compounds can be converted between more than three states upon exposure to external stimuli. To make multi-bistable materials, synthesis of multinuclear complex or co-crystallization of bistable molecules are common methods. However, these can rely on complicated synthetic pathways. It is therefore an important goal to develop multi-step state switchable systems based on simple materials. The use of Brønsted acid/base groups as capping ligands for metal complexes is one method that stimuli-responsiveness can be introduced without the need for particularly challenging synthesis. Brønsted acid/base ligand can allow multiple states to exist in the same system upon deprotonation. Therefore, the combination of metal ions and Brønsted acid/base ligand has the potential to facilitate multistep spin state conversion. In this thesis, the author developed new iron complexes that have Brønsted acid/base ligands and investigated their electronic state conversions. These complexes exhibit spin states that can be switched upon ligand deprotonation (or protonation),

In CHAPTER 2, four types of Brønsted acid/base ligand were prepared: $H_2L^{1\text{-}4}$ ((2-[5-(R-phenyl)-1*H*-pyrazole-3-yl] 6-benzimidazole pyridine); H_2L^1: R =phenyl; H_2L^2: R = 4-methylphenyl; H_2L^3: R = 2,4,6-trimethylphenyl; H_2L^4: R = 2,3,4,5,6-pentamethylphenyl), and used to form iron complexes $[Fe^{II}(H_2L^{1\text{-}4})_2](BF_4)_2$, the magnetic properties of which were investigated. From the SQUID measurements, $[Fe^{II}(H_2L^1)_2](BF_4)_2$, $[Fe^{II}(H_2L^2)_2](BF_4)_2$, and $[Fe^{II}(H_2L^3)_2](BF_4)_2$, showed SCO behavior, while $[Fe^{II}(H_2L^4)_2](BF_4)_2$, has a high-spin state at all studied temperatures.

In CHAPTER 3, stepwise deprotonation of complex $[Fe^{II}(H_2L)_2](BF_4)_2$ was performed, and its partially or totally deprotonated analogs were isolated. $[Fe^{II}(H_2L)_2]^{2+}$ converted to $[Fe^{III}(L)_2]^-$ by DBU addition and the deprotonated species $[Fe^{III}(L)_2]^-$ was isolated and characterized. This result means deprotonation stabilizes the high oxidation state. Three partially deprotonated complexes were also isolated, $[Fe^{II}(HL)_2]$, $[Fe^{III}(HL)(H_2L)]^{2+}$ and $[Fe^{III}(L)(HL)]$, by controlled base addition. SQUID measurements revealed that deprotonation caused an increase of ligand strength, shifting the SCO

temperature of the Fe(II) complexes to higher temperature. In addition, the conversion between high spin state and low spin state was observed for the Fe(III) complexes in the solution- and solid state.

In CHAPTER 4, a new heterometal wheel type complex $[Cu^{II}_6Fe^{III}(HL^5)_6(OH)_2(OCH_3)_4](NO_3)_3$ was synthesized by using 1-(2-pyridine)-3-(2-pyrrole)acetylacetone (H_2L^5), which includes one pyrrole moiety. The pyrrole group can act as both coordination site and a Brønsted acid/base part. From the SQUID measurement, strong antiferromagnetic interactions between copper ions are observed. In addition, base titration UV measurements reveal conversion of cluster molecules by deprotonation of the pyrrole moieties.

List of Publications

CHAPTER 2

Ryo Saiki, Haruka Miyamoto, Hajime Sagayama, Reiji Kumai, Graham N. Newton, Takuya Shiga, and Hiroki Oshio, Substituent dependence on the spin crossover behaviour of mononuclear Fe(II) complexes with asymmetric tridentate ligands, *Dalton Trans,* submitted.

CHAPTER 3

Takuya Shiga, Ryo Saiki, Lisa Akiyama, Reiji Kumai, Dominik Natke, Franz Renz, Jamie M. Cameron, Graham N. Newton, and Hiroki Oshio, A Brønsted ligand molecular switch with five accessible states, *Angew. Chem. Int. Ed.*, submitted.

CHAPTER 4

Ryo Saiki, Norifumi Yoshida, Norihisa Hoshino, Graham N.Newton, Takuya Shiga, and Hiroki Oshio, An Antiferromagnetically Coupled Heterometal Cu_6Fe Wheel, *Chem. Lett.*, **2017**, *46*, 1197-1199.

Other Publication

Takahiro Sakurai, Ryo Saiki, R.J. Wei, Graham. N. Newton, Takuya Shiga, and Hiroki Oshio, Oxalate-bridged heterometallic chains with monocationic dabco derivatives, *Dalton Trans.*, **2016**, *45*,16182-16189.

Acknowledgement

The author is very grateful to Professor Hiroki Oshio, Dr. Masayuki Nihei, Dr. Takuya Shiga, and Dr. Graham Neil Newton for their kind advices and valuable discussion throughout this study. The author is grateful to Professor Takahiko Kojima, Kazuya Saito, and Masayuki Takeuchi for reviewing for this thesis and for the valuable discussion. The author deeply thanks Prof. Youichi Murakami and Prof. Reiji Kumai (High Energy Accelerator Research Organization) for the structural analyses on the synchrotron. The author would like to thank all member of Oshio's laboratory.

Thanks are also due to my parents for their kind encouragements and support.